PAULIUS KARPAVIČIUS

RESEARCH AND DEVELOPMENT OF A UNIVERSAL WIRELESS SENSOR FOR CUTTING TOOL CONDITION MONITORING

DOCTORAL DISSERTATION

Kaunas
2021

KAUNAS UNIVERSTY OF TECHNOLOGY

PAULIUS KARPAVIČIUS

RESEARCH AND DEVELOPMENT OF A UNIVERSAL WIRELESS SENSOR FOR CUTTING TOOL CONDITION MONITORING

Doctoral dissertation
Technological Sciences, Mechanical Engineering (T 009)

2021, Kaunas

This dissertation was prepared at Kaunas University of Technology, Institute of Mechatronics, during the period 2016–2020.

Scientific Supervisor:

Prof. Habil. Dr. Vytautas OSTAŠEVIČIUS, (Kaunas University of Technology, Technological Sciences, Mechanical Engineering, T 009).

Doctoral dissertation has been published in:
http://ktu.edu

Editor:

Brigita Brasienė (Publishing Office "Technologija")

KAUNO TECHNOLOGIJOS UNIVERSITETAS

PAULIUS KARPAVIČIUS

UNIVERSALAUS BEVIELIO JUTIKLIO SKIRTO PJOVIMO ĮRANKIO BŪKLĖS STEBĖJIMUI TYRIMAI IR KŪRIMAS

Daktaro disertacija
Technologijos mokslai, Mechanikos Inžinerija (T 009)

2021, Kaunas

Disertacija rengta 2016-2020 metais Kauno technologijos universitete, Mechatronikos institute.

Mokslinis vadovas:

Prof. habil. dr. Vytautas OSTAŠEVIČIUS, (Kauno technologijos universitetas, technologijos mokslai, mechanikos inžinerija, T 009).

Interneto svetainės, kurioje skelbiama disertacija, adresas:
http://ktu.edu

Redagavo:

Brigita Brasienė (leidykla "Technologija")

TABLE OF CONTENTS

LIST OF ABBREVIATIONS

AE – Acoustic emission,
CAD – Computer aided design,
CAE – Computer aided engineering,
CNC – Computer numerical control,
FEM – Finite element method,
GDP – Gross domestic product,
HSS – High speed steel,
IaaS – Infrastructure as a service,
iOS – iPhone operating system,
IoT – Internet of things,
L&T – Longitudinal and torsional,
LAN – Local area network,
M2M – Machine to machine,
MCU – Microcontroller,
NdFeB – Neodymium magnet,
OTA – Over the air,
PaaS – Platform as a service,
PAN – Personal area network,
PCB – Printed circuit board,
PCBA – Printed circuit board assembly,
PZT – Lead zirconate titanate piezo ceramic,
R&D – Research and development,
RF – Radio frequency,
SaaS – Software as a service,
SVM – Support vector machine,
TCM – Tool condition monitoring,
Wi-Fi – Wireless fidelity,
WSN – Wireless sensor network,
XaaS – Everything as a service,
5G – Fifth generation.

INTRODUCTION

Importance of the topic

"Industry 4.0" is a new industrial revolution, which is centred on such concepts as connectivity, Big Data and Cloud computing. The adoption of this new concept offers enormous opportunities to deliver the initiatives of the Circular Economy Action Plan for a cleaner and more competitive Europe, while promising to improve the quality, flexibility and efficiency of any production process that implements these concepts. This research work is dedicated to R&D, one of the key milestones in "Industry 4.0", where digital and physical devices for monitoring the cutting process are developed by using the cyber-physical components.

Another indispensable aspect of "Industry 4.0", which is the Internet of Things (IoT), enables machine-to-machine connectivity and communication by creating networks that overcome geographical constraints and barriers, allowing dynamic and efficient use of available manufacturing resources. Therefore, this research develops a web-based wireless monitoring system for technological processes with distributed cloud-based Big data applications.

Combining the strengths of IoT platform and Artificial intelligence enabled rapid access to the real-world data and its processing, thus providing a virtual view of the real technological process. Product quality, a key factor in smart manufacturing, is pursued through the research of the tool-workpiece interaction dynamics and innovation of self-powering wireless monitoring of the milling process. The research on the dynamics of tool-workpiece interaction and innovation of the self-powering wireless monitoring of the milling process ensures that the product quality, a key factor in smart manufacturing, is achieved.

The R&D results that are presented in this research will be accessible to the developers of Future Smart Factories; furthermore, it will facilitate the supply of the required products under critical conditions imposed by the Globalization processes.

Aim and objectives of the research

The aim of this research is to analyse and develop a universal self-powering wireless IoT sensor system for rotating shank-type tool condition monitoring.

The following objectives are set in order to reach the defined research aim:

1. To theoretically investigate and develop a universal self-powering wireless sensor node based on the L&T vibrational mode generation;
2. To experimentally validate and adapt the developed self-powering wireless sensor node energy generation and data transmission properties;
3. To adapt the machine learning algorithm for tool wear prediction.

Research methods

Both theoretical and experimental studies were carried out during the research work that is presented in this dissertation. The theory of vibration was applied in the numerical simulation, which was carried out by means of the finite element method

with the commercial software COMSOL Multiphysics 5.1. Design, and 3D models were developed by using the commercial software package Solidworks 2018. A piezoelectric transducer, a 3D scanning laser Doppler vibrometer (Polytec Inc.) and a web-based wireless monitoring system for technological processes were utilized during the research. A Leadwell V-20 milling centre was used to carry out milling operations. PicoScope hardware and software were used to acquire and process the signals obtained during the research. The theoretical findings were verified by an experimental study carried out at Kaunas University of Technology, Institute of Mechatronics and Department of Mechanical Engineering.

Defended statements

1. The use of a rotating shank-type tool holder with helical slots increases the amplitudes of vibrations of the piezoelectric transducer during the cutting process, providing sufficient electricity to activate the wireless sensor node.
2. The assessment of change in electricity that was harvested during tool wear can be used to monitor the cutting tool condition.

Scientific novelty

1. A numerical model of a horn-type waveguide with uniformly distributed helical slots, enabling the transformation of torsional vibrations into longitudinal vibrations, which are transmitted to deform a piezoelectric transducer, was developed;
2. A universal self-powered sensor wirelessly transmitting data for monitoring and controlling of technological process was developed.

Practical significance

1. The developed universal self-powering wireless sensor is suitable for monitoring material cutting processes by employing rotating shank-type tools.
2. The developed universal self-powered wireless sensor design was patented and manufactured.

Research approbation

The research presented in the dissertation has been published in various journals and conferences: two articles in “Web of Science” indexed international journals with high impact (journal “The International Journal of Advanced Manufacturing Technology” (IF2.96); journal “Sensors” (IF3.275), and two articles in indexed international journal “Mechanika” (IF0.5) and IEEE proceedings.

The results have been presented in the following international conferences:

- Proceedings of the 22nd International Scientific Conference “Mechanika” 2017, Kaunas.
- Proceedings of the 23rd International Scientific Conference “Mechanika” 2018, Kaunas.

- Proceedings of the 24th International Scientific Conference "Mechanika" 2019, Kaunas.
- 15th International Conference "Mechatronic Systems and Materials" 2020, Poland.
- "9th Junior Scientist Conference" 2019, Lithuania.
- Proceedings of the 26th International Scientific Conference "Mechanika" 2021, Kaunas.

Patent application:

1. Ostasevicius V, Jurenas V, Karpavicius P, Bubulis A, Eidukynas D, Cesnavicius R, Cepenas M. Wireless sensor to assess the quality of rotating tools. Patent Application number LT2009:553.

Structure of the dissertation

This dissertation consists of an introduction, main part, which is split into four chapters, conclusions, references and the list of publications. The prepared dissertation consists of:

- 110 pages,
- 81 figures,
- 28 tables.

The first chapter of the dissertation reviews the research literature on "Industry 4.0", its concept and key components: connectivity, Cloud manufacturing, Big Data and how on-line and real-time machining process monitoring based on self-powering wireless sensor networks fits in with "Industry 4.0". The literature, concerning ambient energy harvesters, with the main focus on vibrational energy harvesting with piezoelectric transducers, has been reviewed. The application of horn-type waveguide resonators in machining environments with shank-type rotating tools has been investigated.

The second chapter presents the theoretical investigation and modelling of horn-type tool holder for the generation of the L&T mode coupling and energy harvesting from vibrations, excited in the tool, during milling operation.

The third chapter of the dissertation is concerned with the design of self-powering, wireless sensor node. The development of an embedded system used in the device is presented and discussed in detail. The architecture for using the sensor as a monitoring device for condition of rotating shank-type tools has been presented.

In the fourth chapter, the results of the theoretical investigation are verified by the performed experimental studies and application of machine learning models.

Conclusions present the results that were obtained during the theoretical and experimental investigations.

1. LITERATURE REVIEW

Introduction

With the rapid advancements of industry technology, many new concepts have emerged in manufacturing. The next generation of industry, defined by a far-sighted term “Industry 4.0”, highlights a new industrial revolution. This new paradigm shift, utilizing Big Data application and connectivity, promises to increase the manufacturing flexibility combined with the mass customization, allowing to achieve better quality and higher productivity of the manufacturing process as a whole. This new manufacturing paradigm is at the core of IoT (Internet of Things) and smart manufacturing, at the centre of which is M2M (Machine-to-machine) communication, connecting factory devices and enabling to achieve dynamic, efficient, real-time process communication.

This embedded factory wide communication can be achieved by adapting wireless sensor networks (WSN), consisting of low cost and low power wireless sensor nodes, enabling continuous environmental monitoring and process control over a large area. Such sensor nodes, distributed in a manufacturing environment, enable the measurement of various process parameters, such as remaining machining tool life or its condition.

However, the sensor nodes that constitute WSNs have limited energy in their primary power storage unit, leading to their inability to operate over long periods of time, thus requiring significant maintenance effort. Due to these limitations, ambient energy harvesting from the immediate surroundings of the deployed sensors has received a significant interest from the researchers.

1.1. “Industry 4.0”

The real and virtual worlds are growing fast and rapidly merging into the Internet of Things. This evolution of technology has led the scientific communities, together with business communities and governments, to direct this growth trajectory towards the fourth industrial revolution called “Industry 4.0”. “Industry 4.0” is a new industrial era with high flexibility in production volume, product customization and high level of integration between customers, companies and suppliers (Fig. 1.1.), while as well ensuring sustainability [1]. The 4^{th} industrial revolution is created on the basis of digitalization of factories and in combination with other emerging technologies such as IoT and smart machines, enabling modular, efficient and eco-friendly manufacturing systems, where individualized products control their own manufacturing process, enabling manufacturing in small production volumes, while still maintaining economic conditions and benefits, provided by the mass production [2].

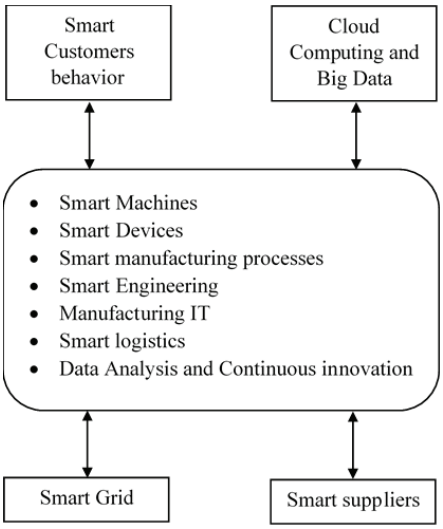

Fig. 1.1. Reference architecture of IoT based smart factory [1]

Thus, "Industry 4.0" is an interdisciplinary branch of science that is situated at the interface of electrical engineering, business administration, computer science, business and information systems engineering as well as mechanical engineering, as it requires adaptation of new technologies as well as the introduction of new business models to make this leap (Fig. 1.2.). In general, the next generation of industry, i.e., "Industry 4.0", has promised to increase the flexibility combined with mass customization, providing better quality and higher productivity of the manufacturing process by utilizing Big Data applications and M2M connectivity [3].

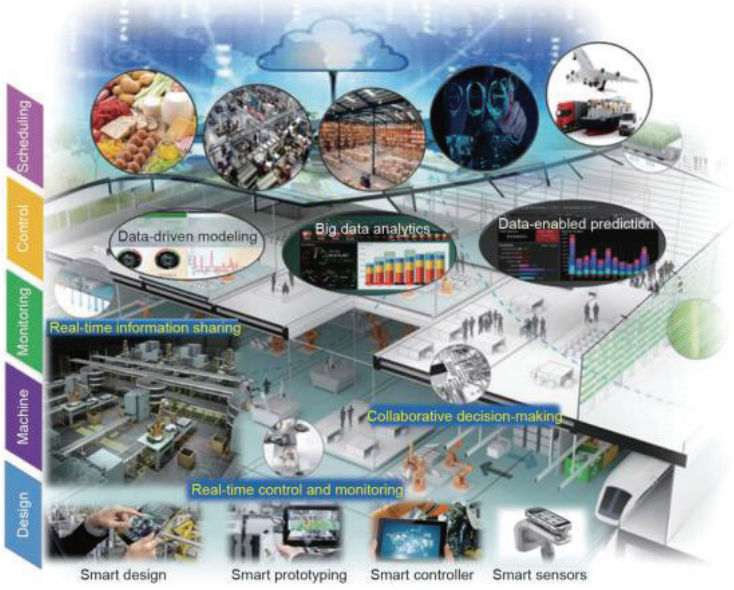

Fig. 1.2. The framework of "Industry 4.0" concept [3]

The framework of "Industry 4.0" research topics as presented in Fig.1.2. can be categorized into the following:

- Smart design,
- Smart machines,
- Smart monitoring,
- Smart control,
- Smart scheduling.

As it can be seen, the key aspect of "Industry 4.0" is the interconnectivity and computerization of the traditional industries, making the factories smart enough in terms of adaptability and resource efficiency, enabling the coordination between disparate devices or cyber physical objects that may be physically placed in distant geographical locations. Thus, one can expect that wireless communication technologies such as Wi-Fi, Bluetooth, 5G and others will play a key role due to their ease of deployment and scalability [4].

It is estimated that industry accounts for about 17% of the created GDP in the European Union countries as well creating approximately 32 million jobs [5]. This explains the importance and impact of understanding the "Industry 4.0" technology and what effect its implementation roadmap can have on the countries' economies and social wellbeing of their respective populations. However, this paradigm shift is expected to affect the manufacturing model and the employees in the factory, whose tasks and requirements will change as well. As the most flexible entity in the cyber-physical production systems, workers can expect to be faced with a large variety of jobs, ranging from the specification and monitoring to the verification of the production strategies, and each individual worker will do a wide range of tasks, depending on which production system he or she is working [6]. Furthermore, the workers will have to take on the roles of creative problem solvers, when confronted with complex problems, as the last instance in the cyber-physical structure (Fig.1.3.).

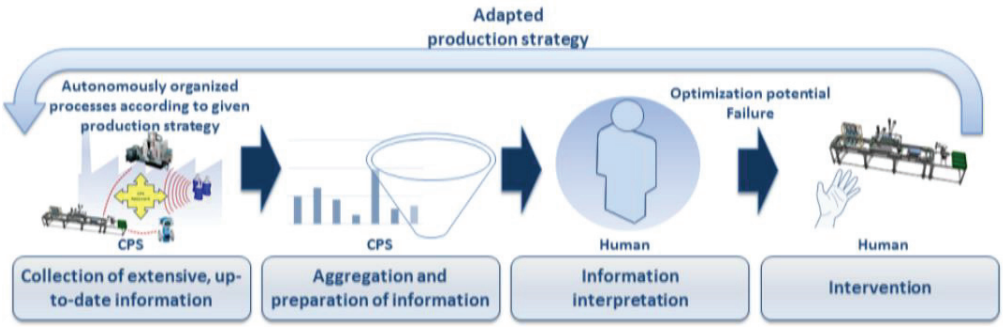

Fig. 1.3. The user as a monitor of the production strategy and the last instance in the decision-making process [6]

1.2. Cloud manufacturing and Big Data

The concept of cloud computing enables the adaptation of pay-as-you-go business models, is able to dynamically scale up and down the required IT resources, according to the changes in demand, ensuring service flexibility [7]. In general, Cloud computing is regarded as the sum of four fundamental service models: IaaS (infrastructure as a service), PaaS (platform as a service), SaaS (service as a service) and XaaS (everything as a service), where cloud manufacturing is the sum of all of them. These services define a layered system structure as provided in Fig. 1.4.

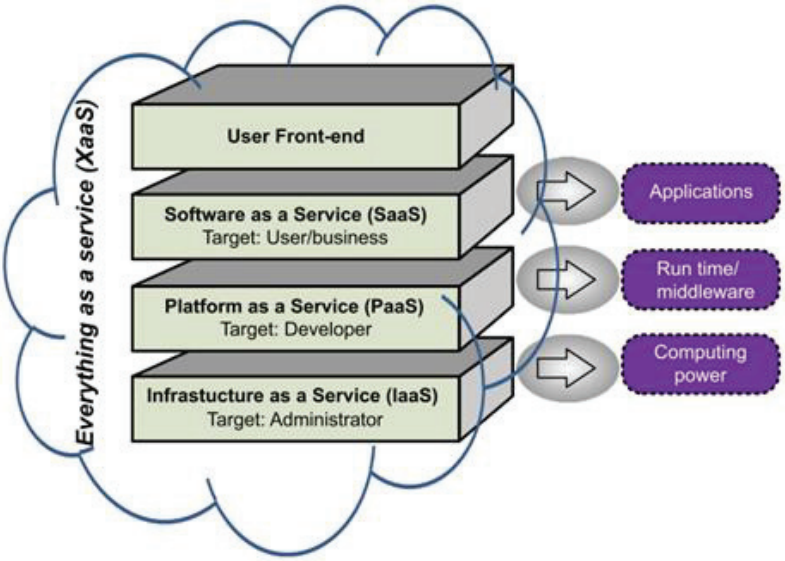

Fig. 1.4. Cloud computing: everything as a service [7]

• Infrastructure as a service (IaaS): provides customers with pay-as-you-go option for hardware resources.

• Platform as a service (PaaS): provides customers a platform with all the systems and environments required for development, testing, running and deploying of applications.

• Software as a service (SaaS): is a software licensing and delivery model in which software is licensed on a subscription basis.

From the technological side, cloud manufacturing is enabled by the adaptation of different technologies, such as networked manufacturing, virtual manufacturing, IoT (internet of things) and, of course, cloud computing, fused together within the system framework architecture. In Fig. 1.5., "Manufacturing Resource Layer" encompasses the resources that are required during the product development life cycle. "Virtual Service Layer" identifies manufacturing resources, virtualizes them and packages as cloud services. "Global Service Layer" takes full responsibility of the entire cloud operational activity, and "Application Layer" is the interface between the user and manufacturing cloud resources.

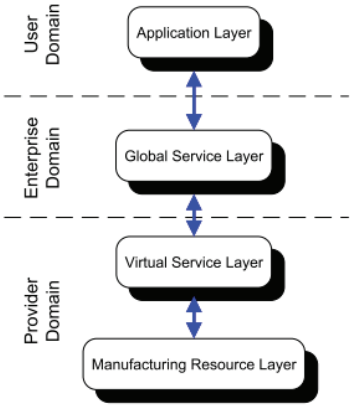

Fig. 1.5. Layered architecture of a cloud manufacturing system [7]

At the manufacturing, intelligent sensors of the "Resource Layer", specifically wireless sensor networks (WSN), provide the ability to perceive, gather and transmit valuable manufacturing and product related data during the manufacturing process, providing possibility to link the physical manufacturing facility to the virtual world of the internet application [8]. These intelligent sensors enable the collection and processing of product and equipment relevant data, providing the right information for the right purpose at the right time that can be used for real-time informed decision-making and implementation of predictive manufacturing [9].

From a practical point of view, the services can be classified into two basic types [10], i.e., OnCloud services, which are running entirely on a cloud platform, and OffCloud services, which need additional operations by an operator of a cloud platform (Fig. 1.6.).

Fig. 1.6. Capability services for the whole life cycle of the product [10]

Other existing interpretation of cloud manufacturing denotes: it is the cloud computing technology that is applied to the manufacturing area and is considered as an innovation of the existing manufacturing paradigm, similar to smart manufacturing, i.e., decentralized, distributed, networked composition of autonomous systems [11]. Nevertheless, as stated by the definition, one of the key features of cloud manufacturing is the smart connectivity and ubiquitous sensing and the data collection of the distributed resources, where these resources are classified into two categories, i.e., hard resources, such as manufacturing cell, or soft resources, such as software and data. Thus, the adaptation of cloud technologies in manufacturing enables the centralization of operation management of services and direct access to the individual manufacturing equipment and resources.

Big data is usually characterized based on the 3Vs theory, which is the following: volume, variety and velocity, meaning that big data consists of a large amount of multi-source heterogeneous and real time data, which in manufacturing enterprise is generated during R&D, manufacturing operation and maintenance stages [12]. The benefits of the collection and evaluation of this big data from sensors result in better decision-support for management and operations, together with the improvement in understanding of the predicting service patterns for manufacturing equipment and products alike. As IoT and smart sensors are evolving and becoming more frequently applicable in various industries, more data are generated and collected, which requires smooth processing, such as scalable and flexible cloud computing.

The purpose to perform analytics on big data is to provide the real-time statistical results to the users of the system, enabling supervisory control and system configuration, in other words, providing problem solving in real-time. In between the physical world, where the traditional manufacturing system is located, and the cyber world, where the Internet connectivity resides and computing in the cloud is performed, there is a layer of cyber-physical devices [13], such as sensors and actuators, local area networks, and the application and cybersecurity software that complete the cyber-physical system model that is depicted in Fig.1.7.

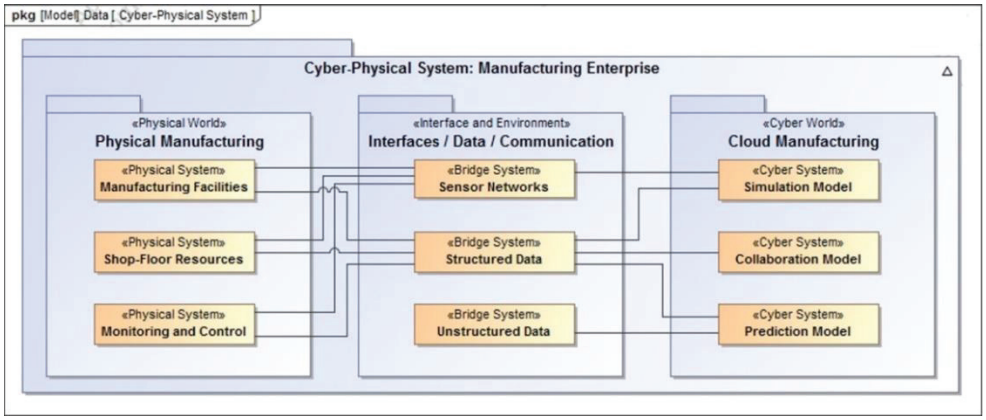

Fig. 1.7. The proposed manufacturing cyber-physical system [13]

As these requirements are satisfied, the big data can be successfully utilized in a manufacturing environment as one of the core technologies, enabling Cloud manufacturing.

1.3. Machining process monitoring

During the milling operation, the following physical signals are generated and can be observed in order to determine the tool condition and tool life: cutting forces, torque, vibration, acoustic emission, current and power, sound and temperature. Each of these physical signals, individually or in combination, can be measured by applying direct or indirect sensoric systems that are used for the detection of tool wear [14–16].

The milling process is a very versatile machining process that is capable of producing flat or curved surfaces and complex geometry parts by intermittent material removal, which is performed when feeding the workpiece past the rotating multi-toothed cutter. Due to the interactions that are happening between the tool and the workpiece, the sharp edge of the tool undergoes deformation and damage, which results in wear. The implementation of TCM (Tool Condition Monitoring) systems can ensure an early detection of tool wear and maintain machining accuracy. The general framework of TCM is provided in Fig.1.8., where it consists of sensors, signal processing, classification and tool condition detection [14].

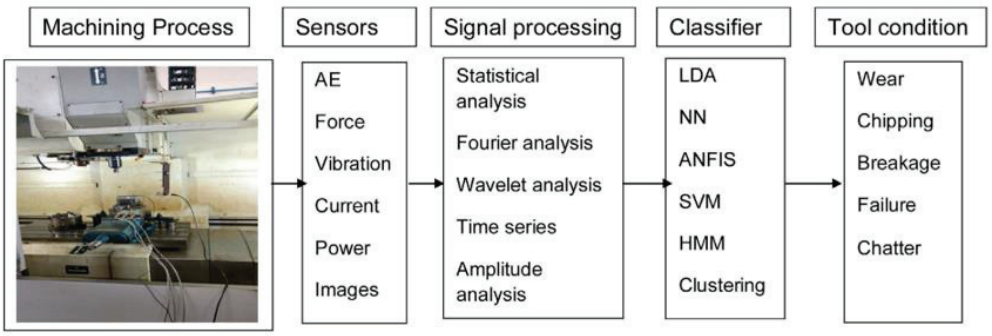

Fig. 1.8. Reference architecture of a TCM system that is deployed in smart factory [14]

As mentioned before, during the machining process, the severe wear of a cutting tool can lead to the degradation in the workpiece quality or the tool breakage, resulting in unexpected equipment downtime, damage to the machine or even injury to the operator [15].

According to the available statistics, more than 75% of the equipment failures in the production process are caused by the tool wear and failure, which contribute up to 6.8% of the machining process downtime, where from 3% to 12% of the production cost are related to the conditions of the cutting tools and their replacement. The implementation of a TCM system is expected to generate 10–50% cutting speed increment, 75% downtime reduction and 30% maintenance saving; thus, the economic incentive for the implementation of tool monitoring systems has risen, and a

significant amount of the research is being performed in order to develop such systems that are robust and reliable enough to be deployed in the industrial environments [16].

The application of sensors to measure the above-described physical signals can provide significant information about the actual tool condition in real-time, such as wear, chatter or breakage or be used for closed loop control autoresonant systems implemented for ultrasonic assisted machining applications [17]. Although any sensor application should follow and comply with the industry requirements that are as follows: low cost, small size, robustness, reliability and non-invasive installation. Such compliant sensors can be integrated inside a cloud manufacturing framework, realizing on-line smart machining process monitoring, based on the cloud computing service TCM systems that are able to learn from the sensorial data, thus realizing a cyber-physical system [18, 19].

Such implemented smart tool condition monitoring systems can significantly increase the machining productivity and reduce the tool costs by optimizing their life, implementing condition-based tool replacement strategies instead of time-based tool replacement, which is especially important for high precision, high speed and complex functional machining processes.

Such smart process monitoring systems are implemented by utilizing physical and virtual monitoring, big data analytics and sensor fusion through a distributed network. The virtually assisted on-line milling process control and monitoring system are discussed in article [19], where simulated machining states are accessed by the real time monitoring system, which detects the tool failure and adaptively adjusts the feed by predicting the forces from the feed and the spindle drive motor currents that are supplied by a CNC. With the real-time acquisition of the CNC process data, it realizes the low delay, high-precision simulation and visualization of the three-dimensional machining process. The system interface is shown in Fig. 1.9.

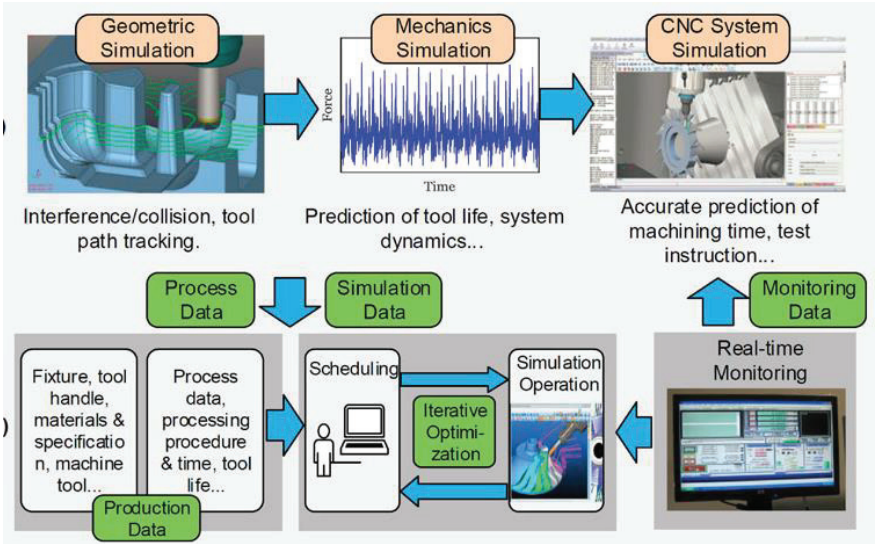

Fig. 1.9. The fusion of physical and virtual machining process modeling [19]

1.4. Wireless self-powered sensor node networks

Wireless sensor networks (WSNs) are becoming more and more integrated into industrial and domestic systems. In general, WSNs consist of distributed, autonomous, wireless networked sensor nodes that can be employed for monitoring a physical space. In the past decade, wireless sensor networks have gained attention by the researchers and users, because of their ability for remote monitoring and data gathering tasks in diverse environments. Though the energy limitations of wireless sensor nodes are a significant issue, as such, the devices are usually distributed in the environment with limited or difficult access, thus complicating any kind of maintenance work and retaining the requirement for operation over the extended period of time. Therefore, the idea to harvest and use the ambient energy from the immediate surrounding for the purpose of recharging the batteries of a device or directly powering the sensor node has lately gained significant traction. The authors of the article [20], which is dedicated to reviewing advancements in energy-harvesting wireless sensor networks, define the sensor node as consisting of a wireless transceiver, a microcontroller, memory and a battery with a capability to capture and use small amounts of energy from heat, light, sound, vibration or movement within immediate environment, thus enabling to extend its lifetime. The wireless sensor node architecture consists of one or multiple sensing units, a wireless communication transceiver, a data processing unit, an energy harvester, one or more energy storage units and a power management system as described visually in Fig. 1.10.

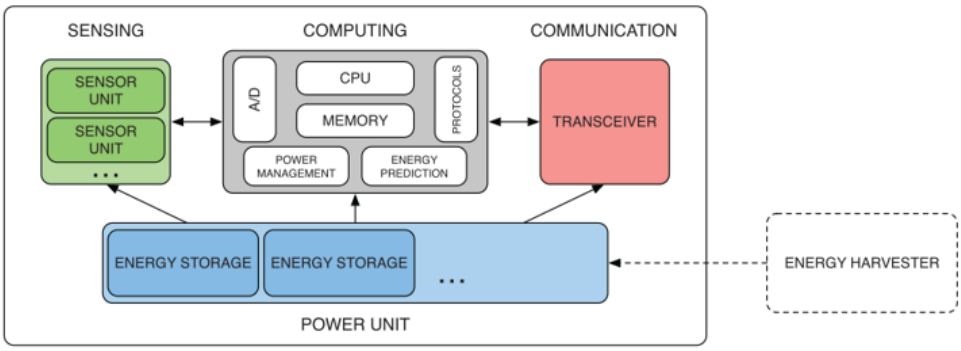

Fig. 1.10. Wireless sensor node architecture [20]

Other definitions of wireless sensor networks describe a sensor node as consisting of four main subsystems: a sensing subsystem to acquire data, a processing subsystem for local data processing, a wireless communication subsystem for data reception or transmission and a power source [21].

Energy harvesting can be described as a mechanism that is used to generate energy from its ambient surroundings, providing an uninterrupted power supply from multiple ambient or external sources, depending on the environmental application of the sensor network. These sources include the energy harvested from the ambient environment, such as radio frequency, solar, thermal, flow-based and wind-based

energy, or from the external sources, such as mechanical vibrations, pressure and stress-strain or human activity, and a single system can combine multiple types of energy that has been harvested depending on the demand. It is important to understand that power densities vary depending on the available energy source. In order to work uninterrupted in most cases, the sensor nodes require a continuous power supply, whether that supply is in an active mode to transmit and process data or an inactive mode, when sensor nodes are brought to sleep, as shown in Fig. 1.11.

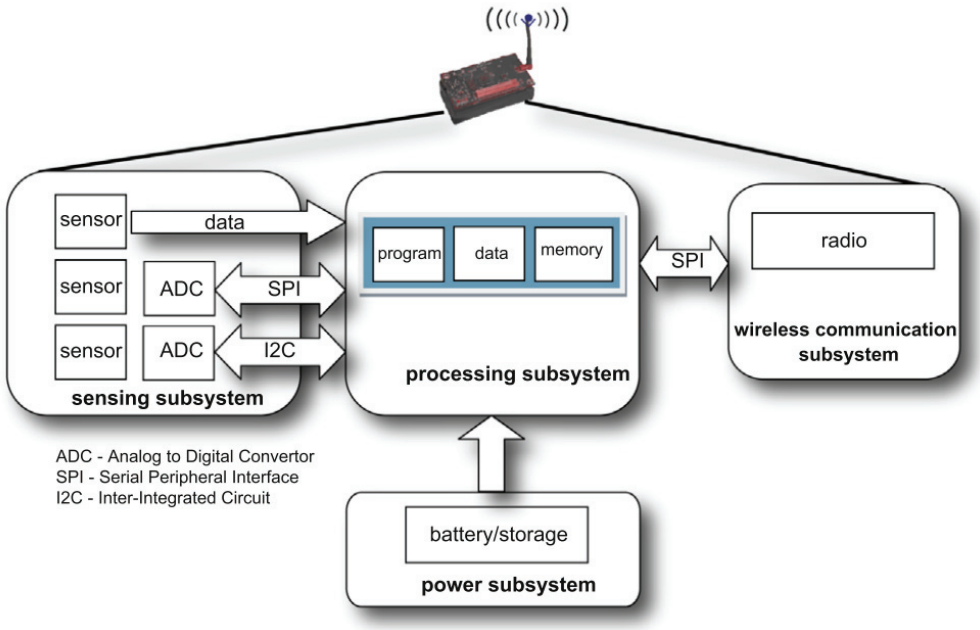

Fig. 1.11. Sensor node architecture with battery as the main source [21]

Article [22] provides the overview of power management schemes, which if implemented, provide efficient utilization of the harvested energy in application with the wireless sensor nodes, which are divided into three main groups, enabling duty cycling, transmission control or energy balancing. The duty cycling control can be subdivided into further energy management schemes based on sleep/wakeup or maximum/minimum duty cycles with transmission policies that are following such strategies: fixed transmission power, variable transmission power and probability distribution.

Wireless sensor nodes perform three basic tasks: sampling of a physical quantity from the surrounding environment, processing and storing of the obtained data and transferring the sensed data wirelessly to a collection point that is called a base station or sink node [23]. Generally, almost half of the energy used by a sensor node is devoted for the communication purposes; thus, a wireless sensor network has to be designed with a focus on maximizing the channel throughput, while minimizing node exploitation. Thus, it is very important to implement energy efficient protocols that maximize the lifetime of the network, while ensuring the required connectivity,

coverage as well as fault tolerance of the wireless sensor network. The data aggregation protocols are split into structure-free flat networks and structured hierarchical networks. The flat network protocols are SPIN, DAA+RW, SFEB, MADA, and the hierarchical network protocols are cluster-based, chain-based, tree-based, grid-based. Each can be selected based on the design requirements of the wireless sensor network to be deployed for the specific application.

Another important challenge, concerning wireless sensor nodes, is their deployment strategy inside the predefined location or environment, which highly affects WSNs coverage, connectivity, energy efficiency and lifetime. The deployment mechanisms can be classified into deterministic and nondeterministic [24]. Deterministic deployment is where sensors are placed to monitor physical conditions, according to the pre-defined scheme; the deterministic methods use static deployment sensors to achieve full coverage, increasing the sensing effectiveness of coverage with a lesser number of sensors. Non-deterministic deployment is dropping of sensors in such a way as it would be expected to be used in a disaster area, which can be random or grid-based, where the sensors are usually scattered, resulting in randomized distribution of sensor with their density being controlled to an extent.

1.5. Ambient energy harvesting

As battery-powered wireless devices have low lifetime due to the limited capacity of the power supply, the sensor nodes and the network as a whole are not robust. As a solution, the energy harvesting from the existing energy sources in the surroundings, such as solar, thermal, mechanical and electromagnetic waves, have emerged.

The radio frequency (RF) energy harvesting is obtained from the electromagnetic waves that are radiating in the range between 3 kHz and 300 GHz frequency in the environment. The power density of RF energy varies between 0.2nW/cm2 and 1μW/cm2 [25]. The main benefit of harvesting this energy type is that electromagnetic waves of the RF energy sources that are radiating in different frequency bands are ubiquitous and available in even inaccessible places, covering a wide area. For this reason, RF energy is considered as a viable source for wireless sensor network and IoT applications, utilizing low power source. Typically, An RF energy harvester consists of an antenna to capture the RF signal, an impedance matching circuit to ensure the maximum power transfer, a rectifier to convert RF power to DC, a voltage multiplier to increase the DC voltage level, and an energy storage device to capture the harvested energy for future use. Figure 1.12. provides a block diagram of an RF energy harvesting system architecture.

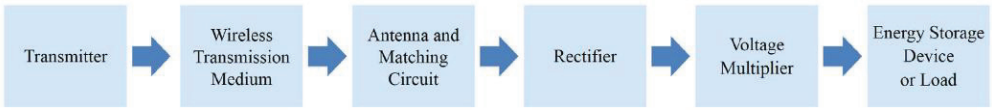

Fig. 1.12. Radio frequency energy harvester architecture block diagram [25]

RF power conversion efficiency is highly dependent on the distance from the energy source, frequency band, operation voltage, antenna gain, number of antennas, matching topology, rectification method, diode type, voltage multiplier topology, multiplier voltage, stage number, power management algorithm, energy storage device type and load impedance.

Heat constitutes a huge cost-effective energy resource, converting heat into the electrical power source [26]. Low-grade thermal energy harvesting technologies are currently based on the thermoelectric, pyroelectric, thermomagnetic and thermoelastic effects (Fig. 1.13.).

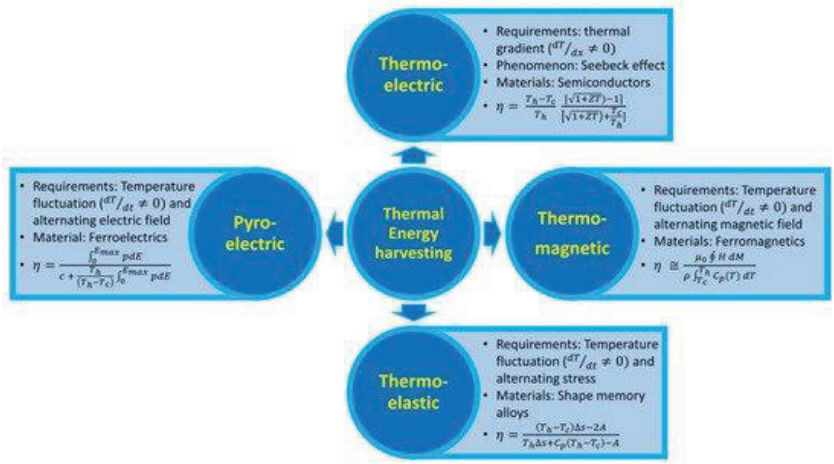

Fig. 1.13. Relevant thermal energy harvesting technologies: thermoelectricity, pyroelectricity, thermomagneticity and thermoelasticity [26]

The waste heat is further split into three groups based on the source temperatures: high grade (649 °C and higher), medium grade (from 232 °C to 649 °C) and low grade (323 °C or lower), which constituted over 50% of the total waste heat. For high and medium thermal energy recovery, a steam turbine is typically employed, while for low-grade thermal energy harvesting, thermoelectric, pyroelectric, thermomagnetic and thermoelastic effect-based technologies are used with thermoelectric energy harvesting being the most popular.

Since the early 2000s, the photovoltaics has been used to harvest solar energy, converting it to the electrical power as a viable alternative source to fossil fuels. Solar powered devices, such as low power electronics or remote-powered sensors, are able to harvest solar energy, store that energy and provide electrical power [27]. Solar-powered standalone devices are interesting in applications, when wired electricity networks are not available, such as in IoT or “Industry 4.0” applications. Outdoors, the solar energy harvesting is the most reasonable energy source for self-powered systems, leveraging the 0.1 W/cm2 solar energy flux with efficiencies ranging from 3–30%; though indoors, their surface power density drops to the level of 10–100μW/cm2 [28]. Other drawbacks of solar energy include its dependence on the weather conditions and the fact that no power can be generated during the night time.

Vibrational energy harvesting is the technique used to scavenge energy from unwanted vibrations that are present in the environment. The common principles for vibration energy harvesting and conversion to the electrical power are as follows: electromagnetic, piezoelectric, electrostatic and magnetostrictive [29]. These principles are further broken down into subcategories of moving coil type, moving magnet type, resonant type for electromagnetic harvesters, electret-free and electret-based for electrostatic harvesters and axial type or bending type for magnetostrictive harvesters.

Electromagnetic energy harvesting is based on Faradays law [30], where a permanent magnet has movement inside the conductive coil. The use of electromagnetic method for energy harvesting includes a simple resonator construction for low-frequency conversion, enabling higher conversion efficiency and not requiring an external voltage source. However, these benefits are significantly negatively affected when downsizing the harvester. A simple electromagnetic harvester configuration is provided in Fig. 1.14.

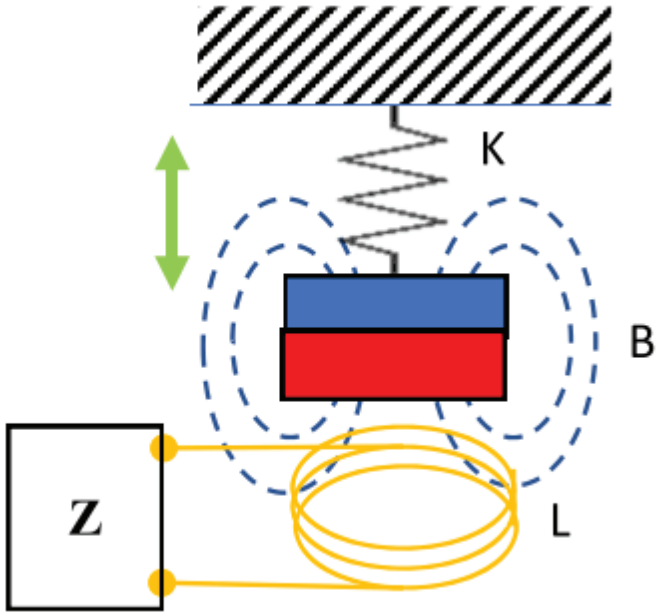

Fig. 1.14. Configuration of a simple electromagnetic energy harvester [30]

The piezoelectric generators produce electricity when experiencing mechanical stress or strain, resulting in the deformation of the material's structure [31]. The piezoelectric materials are defined by their type: one is direct type, where, due to the mechanical deformations, an electric field across the material is generated, while another is converse effect type, where applied electric field induces deformations in the material (Fig. 1.15.).

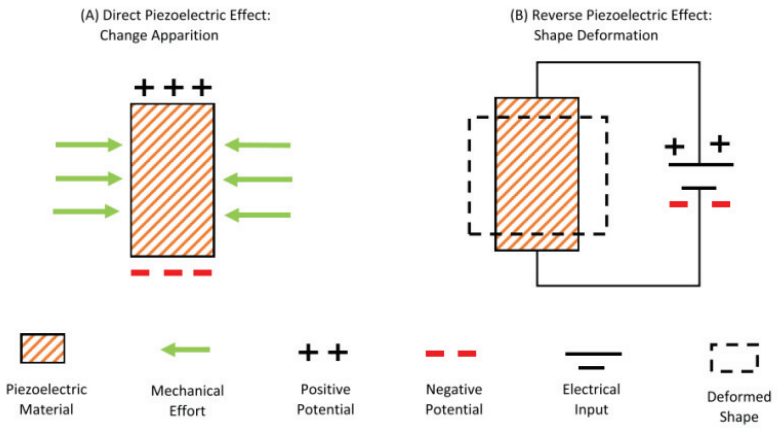

Fig. 1.15. Electromechanical conversion of piezoelectric phenomena [31]

The most commonly used piezoelectric energy harvester is the PZT generator in the form of an anamorphic or multi-layered cantilever beam, although other different geometrical arrangements, such as a diaphragm plate, a ring or a more complex one, such as an elongated hexagon, can be used depending on the application.

1.6. Piezoelectric energy harvesting

In case of energy harvesting application, the most important material properties of piezoelectric materials are its piezoelectric strain constant d, piezoelectric voltage constant g, electromechanical coupling factor k, mechanical quality factor Q and dielectric constant ε [32].

In addition to cantilevers, the energy harvesters with circular shapes are as well being used for vibrational energy harvesting, such as cymbal transducers (Fig. 1.16.).

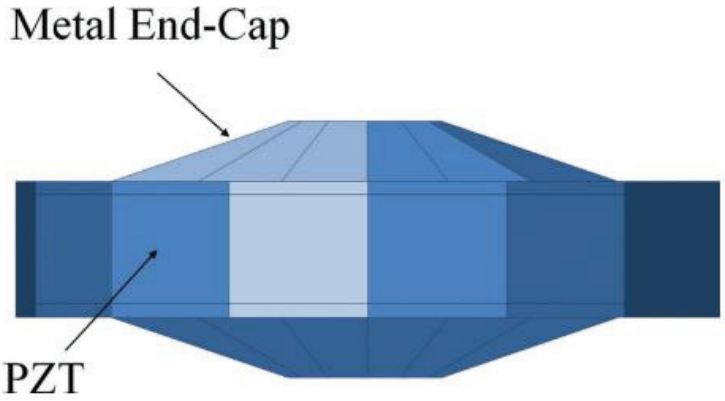

Fig. 1.16. Schematic of a piezoelectric "cymbal" transducer [32]

Piezoelectric coefficient d_{ij} is the ratio of the strain in the j axis to the electric field, applied along the i axis, while all external stresses are constant. Electromechanical coupling coefficient k_{ij} represents the ability of the piezoelectric material to transform electrical energy into mechanical and vice versa, and the piezoelectric voltage constant g_{ij} signifies the electric field that has been developed along the i-th axis, when the material is stressed along the j axis [33].

The most common piezoelectric materials that are used for the energy harvesting application are piezoceramics due to their large electromechanical coupling constants and the ability to provide high energy conversion rate [34]. Piezoelectric ceramic transducers are mostly utilized in the energy harvesting of the mechanical vibrations, focusing on the low energy levels from microwatts to milliwatts. As compared to the other transducers, used for vibrational energy harvesting, piezoelectric transducers allow high voltage output, fast and simple mechanical to electrical energy conversion, overall high system efficiency and comparably good durability [35].

Cantilever type structure is one of the most used structures in piezoelectric energy harvesting, especially for mechanical energy harvesting from vibrations, as a large mechanical strain can be produced within such structure piezoelectric material during the excitation [36]. Moreover, the resonance frequency of the fundamental flexural modes of a straight cantilever either in bimorph or unimorph configuration is much lower than those of other configurations. The most common d_{31} mode bimorph cantilever device consists of two separate interconnected piezoelectric sheets with an electrode between them Fig. 1.17.

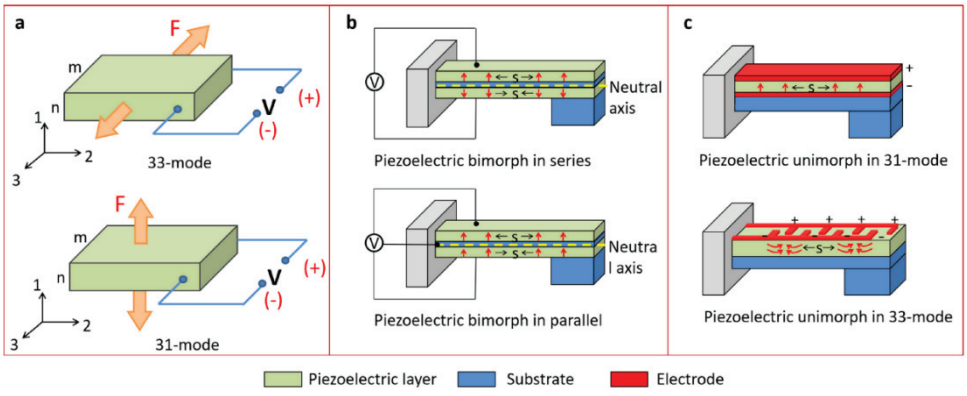

Fig. 1.17. (a) Piezoelectric material used in d_{33} mode and the d_{31} mode, (b) d_{31} bimorph cantilever in series and parallel connections, (c) d_{31} mode and d_{33} mode unimorph cantilever configuration [36]

Such structure is designed to operate in the bending mode, where the top layer of the elements is in tension, and the bottom layer in compression or vice versa and generates an electrical charge based on the piezoelectric effect.

Ring type PZT transducers have been developed for the applications that have high impact forces, consisting of a piezoelectric ceramic disc and a metal end cap on each side, which converts and amplifies the applied axial stress to the radial stress on

the PZT ring, therefore, combining both d_{33} and d_{31} modes, providing higher energy output, as compared to the cantilever energy harvesters.

1.7. Horn-type waveguides and their areas of application

Ultrasonic step horn type waveguide is used to obtain longitudinal-torsional vibrations, where the introduction of diagonal slits ring on the horn leads to the longitudinal and torsional mode coupling. In ultrasonic systems, horn-type waveguides are implemented for L&T vibration mode coupling or degeneration purpose. Such horn devices, able to provide longitudinal-torsional motion, are used in a variety of ultrasonic applications, such as motors, ultrasonic welding, machining or rock-cutting operations. The longitudinal-torsional ultrasonic vibration machining process has found a popular application in the machining of hard and brittle materials, such as various composites and ceramics that are used in aerospace, military and other industrial sectors, as it allows reducing the cutting forces and the friction between the tool and the workpiece, thus lowering the cutting temperatures, improving tool life and the precision, quality and the cutting capacity of the tools [37]. A sandwiched type piezoelectric ultrasonic transducer is presented in Fig. 1.18., consisting of coaxially segmented, longitudinally and tangentially polarized piezoelectric ceramic ring groups, positioned on the exponential shape solid metal horn and back-metal cylinder, pressed from the back side [38].

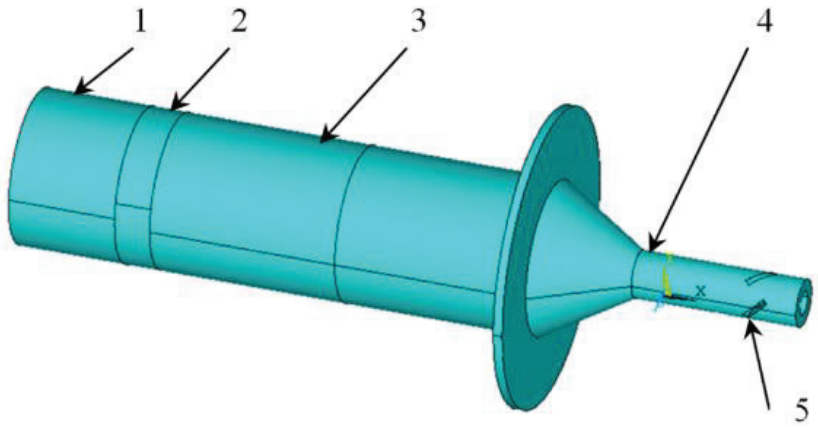

Fig. 1.18. Structure diagram of the longitudinal-torsional composite vibrator: 1 – rear cover, 2 – piezoelectric ceramic sheets, 3 – front cover, 4 – horn, 5 – diagonal slits [38]

A new way to achieve longitudinal-torsional complex vibrations by the conical compound horn, consisting of a cone and a circular cylinder, has been proposed by Jiaxin Zheng [39]. This was achieved by selecting the appropriate cone structure dimensions that are allowing to approximate longitudinal and torsional vibration resonant modes, establishing wave and frequency equations of these vibrations, based on one dimensional wave theory.

Longitudinal and torsional mode generation and degeneration dependence on the introduction of helical shape flutes in the stem section of a versatile horn-type waveguide allow for the torsionality of the horn to be adjusted according to the requirements of a specific application by altering the depth and the helix angle of these flutes [40]. There, the torsionality is used to compare the degree of coupling between the longitudinal and torsional responses by evaluating the ratio of tangential to longitudinal vibration amplitude at the edge of the horn tip. The proposed sandwich-type transducer design consists of two oppositely polarized d_{33} mode PZT-4 piezoelectric ceramics that are placed between the front and the back covers, where the latter is introduced to allow a more efficient transfer of the ultrasonic energy in a forward direction. The investigated relationship of the longitudinal-torsional resonance frequency and the amplitude versus dimensions of the diagonal slits show that torsional vibration amplitude can be adjusted by changing the length of the cylinder, thus allowing to prepare the vibration system for use, according to the application requirements. The researchers in the article [41] present a study, realizing a longitudinal-torsional vibration by the introduction of multiple diagonal slits on the surface of a stepped horn, where its resonant frequency was adjusted by a varying angle and structure parameters of the slits.

A sandwiched composite ultrasonic vibrator is designed to be driven by axially polled PZT stack in order to generate the longitudinal-torsional motion used in wire drawing application [42]. The L&T motion is achieved by introducing grooves that are machined either along the thread curves or as a straight line along the surface of the transducers' front mass. The made observations show that thread grooves have a higher effect than straight grooves for the mode degeneration, resulting in significantly higher torsional response amplitude of the transducer's output surface.

A longitudinal-torsional (L&T) hybrid vibrator that is driven by the two longitudinal ultrasonic transducers for the ultrasonic-assisted wire drawing is proposed by the researchers in [43]. The design of the device (Fig. 1.19.) consists of two identical transducers that are installed vertically on the two side surface of a transformer with an offset distance and stagger angle between their axes, allowing the transformer to synthesize and amplify the vibration of the two transducers, producing L&T composite vibration of 19.597 kHz, longitudinal amplitude of 17 μm and tangential and torsional displacements of 3.92 μm, 0.15°, when driven by a voltage of 400 Vp-p.

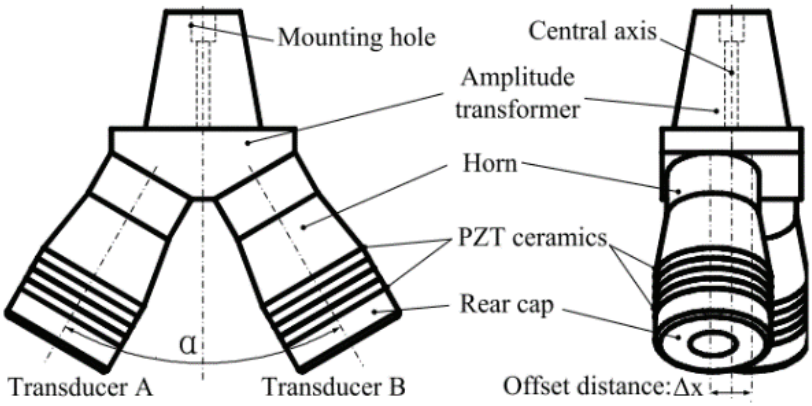

Fig. 1.19. The structure and composition of the skew-typed composite vibrator [43]

An ultrasonic step horn with spiral slots using the principle of mode conversion has been designed realizing L-T vibration [44]. The ultrasonic transducers with appropriate torsional longitudinal vibration amplitude ratios were designed, manufactured and implemented in a milling glass plane, where the experimental results show cutting force reduction by 48–78%, implementing the L&T mode when compared to the traditional methods.

1.8. Ambient energy harvesting during machining process

Machine tool chatter is a self-excited vibration problem, occurring in large rates of material removal, resulting from the unavoidable flexibility between the cutting tool and the workpiece. It is important to mention the turning process and the turning tool, which is a flexible structure, vibrating during the cutting process at several natural modes. In order to evaluate the possibility of energy harvesting from the rotating tool, the angular vibrations of the milling tool holder were measured directly on the rotating tool. A pronounced periodicity was present in the acceleration measurements that were carried out during the milling operations [45]. This periodicity can be directly associated with the harmonics of the tool structure, the number of cutting edges as well as the spindle speed. Increasing the cutting depth resulted in increasing the cutting forces, and thus, in greater excitation levels as well. When changing the feed speed (feed rate), no significant changes were observed, although a small increase in the vibration level with increasing speed has been noticed. Milling can be described as an interrupted cutting process, because during each revolution of the cutter, its teeth enter and exit the workpiece, and in this way, they are subjected to an impact force cycle. The frequency of approximately 150 Hz dominates due to the collision between the cutter tooth and the workpiece material. The amplitudes of the vibrations between the interrupted cutting periods are considerably lower than during the impact. They are characterized by lowered amplitudes until the new tooth comes in contact with the workpiece. These amplitudes are not sufficient for the energy generation, and the most favourable are vibro-impact accelerations, whose sequence intervals depend on the cutting regimes. This means

that higher effectiveness is demonstrated by the rotating cutting tool accelerations, mostly related to the tool speed and the number of cutting edges, rather than the cutting tool vibration modes.

It is as well claimed that the energy harvesters for rotating and non-rotating cutting tools should be designed by using a few different types of piezoelectric transducers, whose natural frequencies differ by more than 10 times. In such a case, due to the force resulting from any changes in the acceleration or motion, the mass squeezes the piezoelectric material, and it, in turn, generates an electrical charge, corresponding to the force it was affected. The initial conditions for energy harvester design are related to the necessity to find an appropriately shaped piezoelectric transducer for high and sufficiently low frequencies. Fig. 1.20. shows the proposed architecture of such energy harvester.

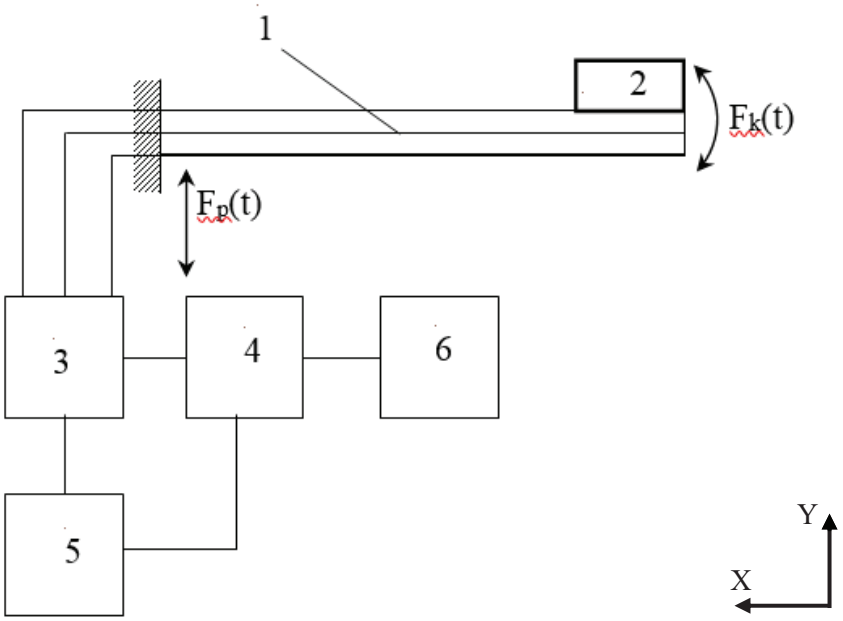

Fig. 1.20. The architecture of wireless vibration energy generator: (1) cantilever piezo bimorph, (2) concentrated inertial mass for the tuning of resonant frequency, (3) connection unit, (4) controller, electrical energy accumulator, (5) and (6) wireless transmitter [45]

Taking a turning tool as an example of a non-rotating tool, which only gets a feed relative to the rotating workpiece, it was identified that the turning tool vibrates on the main mode, depending on the clamping, i.e., the length of the tool hanging from the clamp in a range from 2.5 kHz to 5.6 kHz [46]. It means that commercial piezo-electric cantilevers are not available for the energy harvesting because of the low resonant frequency. For this purpose, the circular bimorph type piezo transducer, assuring the resonant frequency in the required diapason (2.5–5.6 kHz), was chosen (Fig. 1.21.).

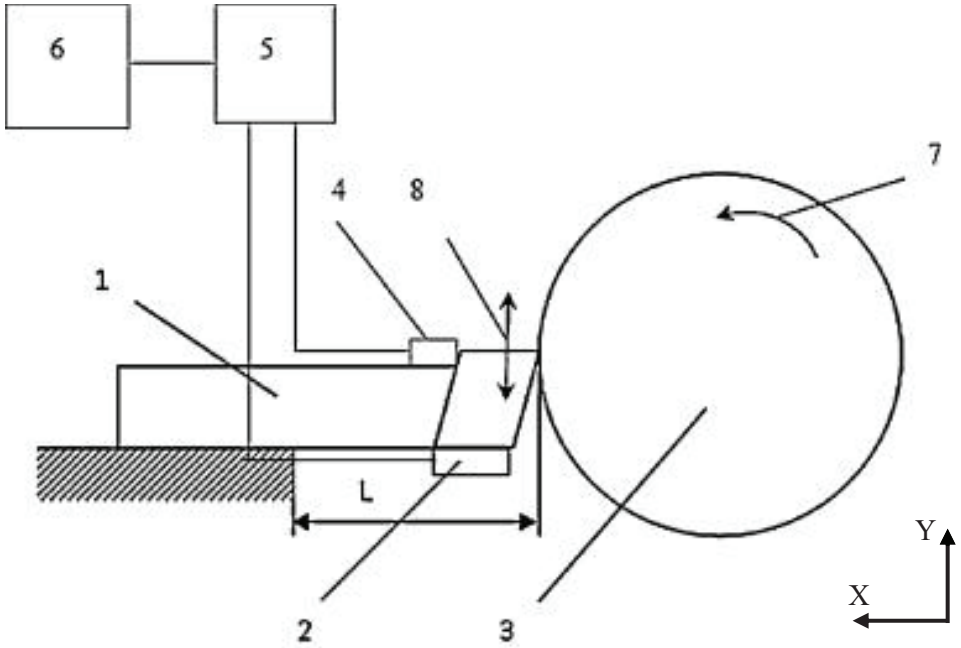

Fig. 1.21. Turning experiment set-up: 1 – turning tool, 2 – circular piezo transducer bimorph, 3 – workpiece, 4 – KD91accelerometer, 5 – Pico Scope 3424, 6-PC, 7 – cutting speed direction, 8 – excited turning tool vibration [46]

An attachable electromagnetic-energy-harvester system, as an alternative energy harvester, has been designed and verified in use during the milling operation [47].

The electromagnetic harvester is assembled out of four permanent NdFeB magnets, while the inductor is fixed stationary on the over arm that is placed near the spindle. Due to the electromagnetic induction during the spindle rotation, the alternative voltages are induced in the inductor by the cycled magnetic flux; therefore, the mechanical energy of the cutter rotation during the milling operation is collected and converted into the electrical energy. The performed experimental investigation shows that when the spindle is operating at a rotation speed of 1650 RPM and 3150 RPM, the power generated by the energy harvester is 230 mW and 313 mW, respectively. It shows that the power generation increases with the increase in the spindle rotational speed. Such energy harvester is enough to power a sensor node that is consisting of a power management circuit, three accelerometers for three axis measurements and incorporating wireless data transmission capability.

The milling operation, in general, can be described as an interrupted cutting process, where the tool interacts with the workpiece multiple times per second, during which the vibrations are excited in the tool. The dynamics of the metal machining process are transient in nature, and the vibrations generated in the milling tool during the metal cutting are free, forced, periodic and random, which as well change if there

is any chatter during machining. The highest amplitudes of these vibrations are achieved during the tool impact on the workpiece and that are sufficient to be used for the energy harvesting. At tool rotation of 3200 rpm, 100 g eccentric forces are generated; these eccentric forces can be harvested by attaching a cantilever piezoelectric transducer on one side of the tool and an equivalent counterbalance on the other side, thus eliminating any misbalance that might have been introduced [48].

The piezoelectric cantilever is attached to the milling tool so that its vibration amplitudes' direction and cutting direction are the same. In such configuration, the changes in accelerations during the milling process result in forces being excreted on the piezoelectric transducer, deforming it, and thus, generating voltage. The generated voltage is charging a capacitor and acting as a battery. When reaching a set charge level, the capacitor is discharged, and this voltage is used to power a wireless sensor node (Fig. 1.22.).

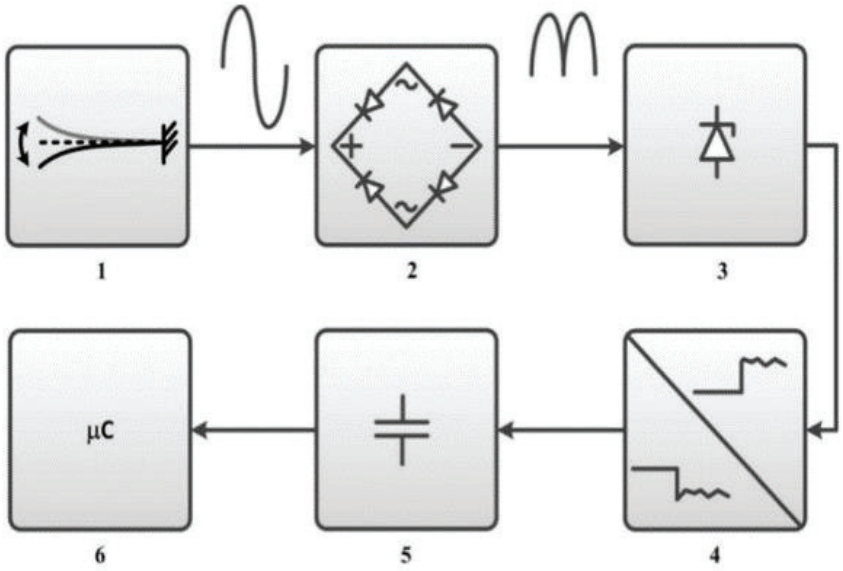

Fig. 1.22. Components of the energy recovery and storage device: (1) – power inverter, (2) – diode bridge, (3) – guard element, (4) – voltage conversion and stabilization electronics, (5) – energy storage, (6) – powered electronics [48]

Such energy harvesting from the milling tool vibration is dependent on the cutter condition, cutting regimes and the material of the workpiece. Milling tool condition degradation leads to the increase in cutting forces that are excreted on the tool during the machining process, thus leading to higher acceleration amplitudes. It has been observed that a worn out tool can lead up to 2–3 times more energy harvested by the piezoelectric transducer, when it is attached to the side of the tool. Increasing the spindle speed and feed rate as well leads to higher voltage that is generated by the piezoelectric transducer. Harder materials such as steel allow harvesting more energy than aluminium and other softer materials.

1.9. Modeling and simulation of end milling forces

In general, the end milling operation is a metal cutting process, which is performed by using a rotating cutter with several teeth, where the interactions between cutter and workpiece are intermittent. Finite element simulation of the milling process can be used as a supplement to the actual process, allowing to predict its critical variables that might be affecting the machining, thus enabling to select optimum conditions, especially in such applications as high-speed milling. Fig. 1.23. shows a model coordinate system for the end-milling operation from x–y and x–z planes.

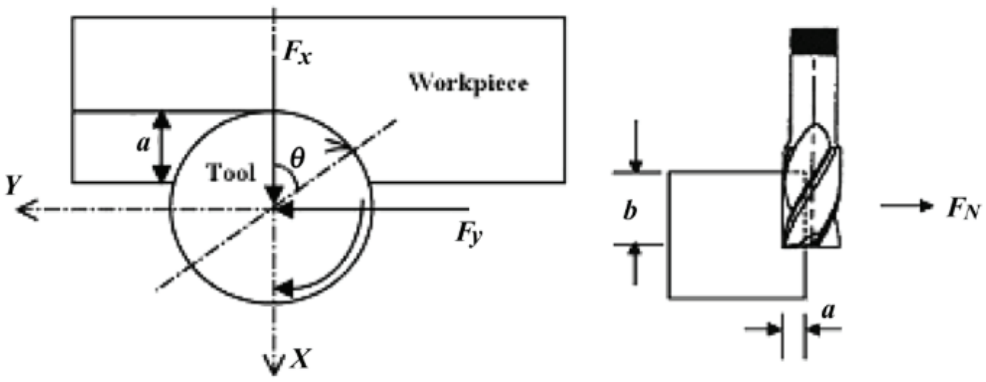

(a) (b)

Fig. 1.23. (a) Model coordinate system of end-milling operation, (b) axial and radial depth of cut [49]

The application of finite element method for the simulation of the cutting processes, such as end milling operation, can be used to predict various cutting process parameters, like cutting forces, temperature, strain, stress and tool wear. Compared to the analytical methods, this has the following advantages [49]:

- Material properties can be handled as functions of strain, strain rate and temperature.
- The interaction between the chip and the tool can be modelled as sticking and sliding.
- Non-linear geometric boundaries can be represented and used.
- Variables, such as cutting force, feed force and chip geometry, the local stress, temperature distribution etc., can be obtained as well.

In the end milling operation process, the variables, such as tool wear, have a significant impact on the cutting force, cutting temperature, tool wear rate, chip flow and burr formation [50] and can significantly affect the process efficiency and quality of the parts that are being manufactured.

One of the key machining process parameters are the forces that are acting on the cutter. The estimated accuracy of the cutting forces is especially important for

reducing errors and controlling stability when milling low-rigidity parts, such as thin-walled structural parts and thin-shell parts [51].

During the modelling of the end mill process, both the end mill tool and the workpiece can be discretized into a finite number of nodes in the longitudinal direction (cutting depth) of the model [52], when in the end mill tool, each of the nodes is in the form of a disk with thickness of Δz as presented in Fig. 1.24.

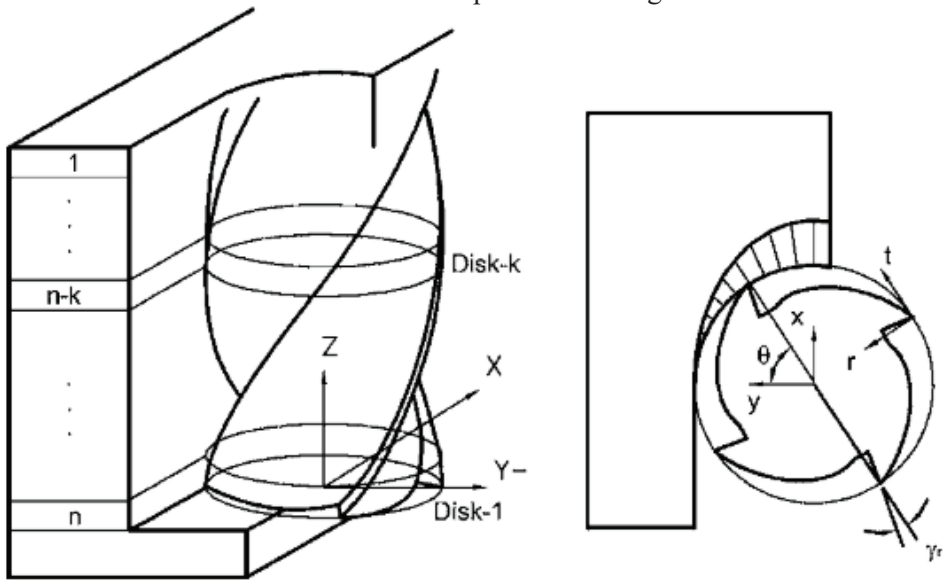

Fig. 1.24. End mill geometry and force model [52]

A simplified approach to calculate tangential, radial and axial end milling cutter forces according to the empirical formulas has been proposed in [53]:

$$F_c = 9.81(96.6)a_e^{0.88} f_z^{0.75} a_p z d_0^{-0.87}, \quad (1.1)$$

$$F_r \approx (0.80\sim0.90)F_c, \quad (1.2)$$

$$F_a \approx (0.35\sim0.4)F_c, \quad (1.3)$$

where F_c is the tangential milling force (N), F_r – radial milling force (N), F_r – axial milling force (N), a_p – milling depth (mm), d_0– cutter diameter (mm), z – number of cutter tooth, f_z – feed per tooth (mm/z).

The simulation of machining, either cutting or milling, is based on the numerical theory and technique approaches, primary mathematical formulations of continuum based Finite Element Method [54]:

- **Eulerian approach:** the mesh is fixed spatially, and the material flows through the mesh. This approach is suitable for the analysis of the cutting process steady state.
- **Lagrangian approach:** the mesh follows the material, allowing to simulate from the initial to the steady state of the cutting process

because the deformation of the free surface of the chip can be automatically treated by the elastic-plastic material deformation.

- **Arbitrary Lagrangian Eulerian approach:** it combines the features of pure Lagrangian and Eulerian approach, where the mesh is allowed to move independently of the material. This approach is effective for improving the mesh quality in the analysis of large deformation problems.

For the 3D modeling of the milling process, the Arbitrary Eulerian Lagrangian approach, combining both features of the Lagrangian and the Eulerian approaches, is used. There, the cutting tool can be modelled as a Lagrangian part, and the workpiece is represented as the assigned material in an Eulerian domain [55]. This allows the Eulerian grid to be fixed in the space, while the workpiece deforms, and any extreme deformation of the workpiece material does not distort the elements.

1.10. Theory of design and modeling longitudinal-torsional composite vibration horn-type waveguides

Many of the industrial applications and production technologies are based on the ultrasound technology. Often, the ultrasonic vibration cutting process (ultrasonic assisted machining) is employed as an effective method used for processing difficult to machine materials. This is performed by transmitting the ultrasonic vibrations directly on the cutting tool, transforming the interaction with the workpiece into a micro-vibro-impact process.

This application of ultrasonic vibrations provides cutting process improvements, such as reduction of cutting forces and tool wear, resulting in surface finish improvements up to 25–40%. In order to transfer the ultrasonic vibrations from the transducer to the tool, a wave-guide, known as the ultrasonic horn, is implemented between the transducer and the tool [56]. According to the application requirements, each ultrasonic horn has to be designed uniquely, though the most commonly chosen shapes are stepped, conical and exponential as shown in Fig. 1.25.

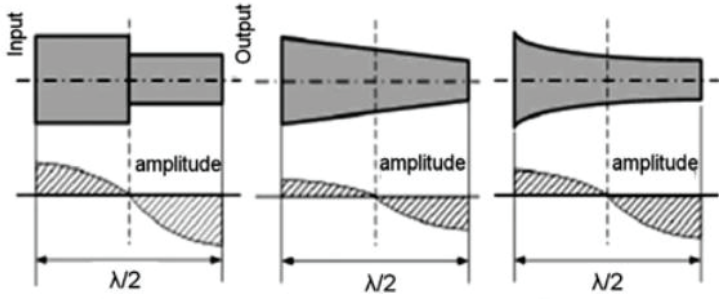

Fig. 1.25. Diagram of different shape ultrasonic horns and their respective amplitudes [56]

The principle function of the ultrasonic horn is to amplify the amplitude of the ultrasonic vibrations of the tool to the level that is required by the application in order

to be in a resonance state with the transducer. The governing equation of longitudinally vibrating ultrasonic horn type with variable cross-section S(x), which is valid for one-dimensional continuum in thin elastic bar, is expressed in the following form [57]:

$$\frac{\partial^2 u(x,t)}{\partial t^2} = c_p^2 \left[\frac{1}{S(x)} \frac{\partial S(x)}{\partial x} \frac{\partial u(x,t)}{\partial x} + \frac{\partial^2 u(x,t)}{\partial x^2} \right], \tag{1.4}$$

where x is the coordinate in the longitudinal direction, $u(x,t)$ is the longitudinal displacement of cross section, and $S(x) = \pi\big(r(x)\big)^2$ is the cross-section area. There, r(x) is the radius of the cross section. $c_p = \sqrt{E/p}$ is the velocity of the longitudinal waves in one-dimensional continuum, where E is the Young's modulus of the horn material, and ρ is the density of the horn material.

The inlet and outlet surfaces of the ultrasonic horn may move in the longitudinal direction, where the input surface of the horn is attached to a transducer, which is generating the excitation vibrations, and the output surface is attached either to a tool, or the tool is embedded together with the horn.

In order to achieve the required effect and the performance of the ultrasonic horn as required by the intended application, usually, only the first two resonance modes are used. Ultrasonic horn type waveguide has the full shape of the wave, as provided in Fig. 1.26.

NAME OF SHAPE	PARAMETERS	MODE SHAPE OF SONOTRODE VIBRATION
$\lambda/2$ – *"half wave"* shape	$k = 1$ $\lambda_1 = 2$ $f_{01} = \frac{1}{2l_0}\sqrt{\frac{E}{\rho}}$ $\vartheta_1 = 1$	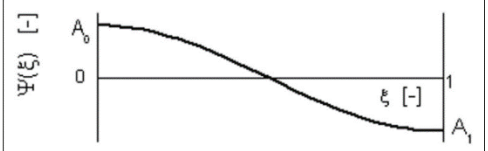
λ – *"wave"* shape	$k = 2$ $\lambda_2 = 1$ $f_{02} = \frac{1}{l_0}\sqrt{\frac{E}{\rho}}$ $\vartheta_2 = 1$	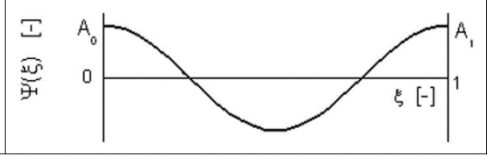

Fig. 1.26. Mode shapes of a cylindrical horn-type waveguide [57]

The implementation of the longitudinal-torsional (L&T) composite vibrational motion in rotary machining can further improve the process efficiency by reducing the cutting forces and improving the product quality. This is especially important when processing brittle composite materials that have high hardness and low fracture toughness properties. One of the main methods to achieve L&T ultrasonic vibration mode conversion is the introduction of cuts on the planar surface of the horn. During this conversion, a part of the excitation longitudinal waves are converted to the transverse waves, and thus, mode generation is realized, i.e., normal stress is converted to shear stress, resulting in torsional vibration. There, the reflected transverse wave, reflected longitudinal wave and refracted longitudinal wave are generated when a plane wave is incident with angle θ onto the interface between two different media [58].

The realization of longitudinal-torsional vibration mainly depends on the spiral slots within the ultrasonic horn, where single-excited longitudinal vibration is converted to the longitudinal-torsional vibration through these helical grooves [59]. Ultrasonic wave propagation in ultrasonic horn waveguide with spiral slots (L&T horn) is presented in Fig. 1.27.

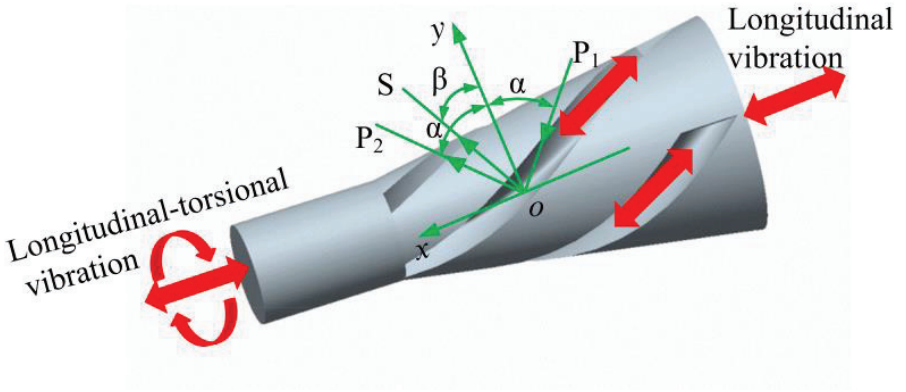

Fig. 1.27. Schematics of ultrasonic wave propagation in the L&T ultrasonic horn [59]

There, P_1 denotes the incident longitudinal wave with the incident angle of α, and P_2 and S represent the reflected longitudinal wave and transverse wave [59, 60].

The analytical calculation of cylindrical and symmetric horn type waveguide mode shapes is relatively simple. However, in applications, requiring the implementation of ultrasonic horn that is asymmetrical, has non-cylindrical shape or geometrical features on its planar faces, such analytical determination of these parameters becomes very complicated. Therefore, the implementation of the finite element method (FEM) is preferred instead of the analytical model in order to determine the modal properties of such more complex ultrasonic horn waveguide shapes [61].

Usually, the Finite Element Modelling (FEM) and the calculations of modal properties of horn type waveguides are performed by using commercial software packages like ANSYS [62], COMSOL [63], SAMCEF [64] and other.

1.11. Theory of design and modelling piezoelectric energy harvester

Piezoelectric materials produce electric charges when subjected to the mechanical strains that are causing deformations. The energy conversion of piezoelectric materials from mechanical to electrical and in reverse enables it to be used as both a sensor and an actuator in different applications. However, in recent years, there has been a great deal of focus on harvesting energy from the environmental sources, using piezoelectric transducers.

The analytical investigation process of piezoelectric material highly depends on its shape. A simple model of the beam, as an energy harvester, can be defined in Single

Degree of Freedom system, consisting of spring, mass and a damper, giving a close view of the problem, but limited to only first mode.

In case of a d_{31} unimorph piezoelectric beam, which is the most common piezoelectric energy harvester configuration, as provided in Fig. 1.28., the general equation of motion can be expressed as in [65]. Euler-Bernoulli beam equation method can be used in solving the following mathematical model [66]:

$$\frac{\partial^2 M}{\partial x^2}(x,t) + \rho A(x)\frac{\partial^2 w}{\partial t^2}(w,t) = f_0(x,t), \tag{1.5}$$

where $M(x,t)$ is beams bending moment, $\rho A(x)\frac{\partial^2 w}{\partial t^2}(w,t)$ is the inertia forces that are applied to the beam (ρ – mass density of the beam), $A(x)$ is the cross section area, and $\rho A(x)$ is mass per unit length of the beam. $f_0(x,t)$ are the forces per unit length that are acting on the beam. The beam's absolute displacement $w(x,t)$ can be expressed in terms of base displacement and its transverse displacement.

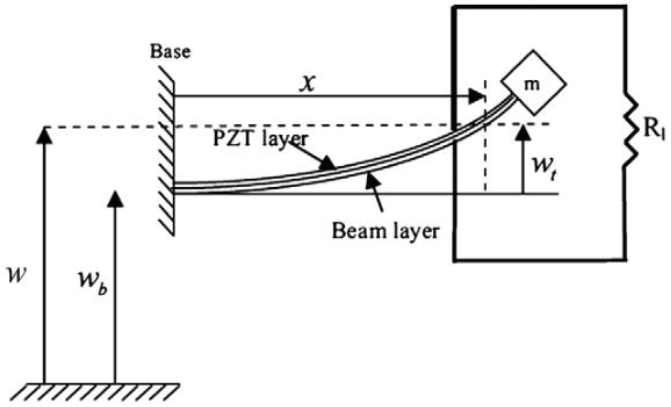

Fig. 1.28. Unimorph piezoelectric harvester with a tip mass excited under transverse base motion [65]

In less frequent configuration, a piezoelectric ring-type d_{33} single or stack configuration transducer is used for the energy harvesting applications, where it is subjected to compressive force load, and its tensional load is very small, as provided in Fig. 1.29. [67].

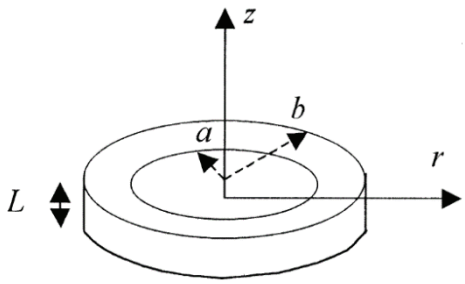

Fig. 1.29. Axially polarized ring-type piezo-generator [67]

A practical approach for accurate modeling of the piezoelectric energy harvester, involving complicated mechanical conditions and energy harvesting, can be achieved by applying the equivalent circuit method, which enables structural modeling and electrical simulation to be performed in a system. This model requires the mechanical parts of the system to be converted into an electric circuit by implying electro-mechanical analogies, allowing the electro-mechanical system to be investigated based on the circuit theory methods. The analogy between electrical and mechanical domains of piezoelectric generator, based on the equivalent circuit, is provided in Table 1.1. [68].

Table 1.1. Analogy between electrical and mechanical domains

Equivalent circuit parameters	Mechanical counterparts
Charge: $q(t)$	Modal coordinate: $\eta(t)$
Current: $i(t)$	Modal velocity: $\frac{d\eta(t)}{dt}$
Inductance: L	1
Resistance: R	$2\zeta\omega$
Capacitance: C	$1/\omega^2$
Voltage: $V(t)$	$-f\ddot{U}_g(t)$
Ideal transformer ratio: N	Electromechanical coupling: χ

The investigation of piezoelectric transducers can be significantly simplified by utilizing specialized software packages, allowing the simulation of piezoelectric phenomena in the electromechanical system. COMSOL Multiphysics is such a software package that allows the mechanical and electrical properties of a piezoelectric transducer to be modelled. COMSOL Multiphysics provides a user-friendly simulation package with predefined physics interfaces, employing the governing equations from a vast variety of physical boundary value problem and initial value problem for many homogeneous and in-homogeneous differential equations, building into a single Multiphysics simulation model [69].

Conclusions of chapter 1

The review of the literature leads to the following conclusions:

1. New era of manufacturing called “Industry 4.0” is the 4th industrial revolution that is promising high flexibility in production volumes, product customization and high levels of customer integration. At the core of “Industry 4.0” there is the high interconnectivity and M2M communication of machines, irrespective of geographical boundaries, utilizing Big Data applications.
2. Machining process monitoring is performed by directly or indirectly measuring physical signals such as: cutting forces, torque, vibration, acoustic emission, current, power, sound and temperature.

3. For the wireless sensors, it is important to have low maintenance requirements and a long life, which can be achieved by implementing ambient energy harvesting capability in the sensor.
4. Piezoelectric materials are a frequent choice for mechanical vibrational energy harvesting due to their simple structure, high efficiency, comparably good durability and high energy density.
5. The coupling of L&T modes is achieved by introducing diagonal slits on the planar surface of the waveguide. Such waveguide design could be used in reverse mode, where the torsional vibrations acting on the tool are transformed into the longitudinal vibrations in the waveguide, deforming the piezoelectric transducer that is generating energy.
6. In scientific literature that has been reviewed, several self-powered sensors are used for machining process monitoring, which are attached to the cutter, exposing them to environmental effect, thus reducing its service life.

2. THEORETICAL INVESTIGATION OF A PIEZOELECTRIC ENERGY HARVESTING FROM ROTATING SHANK-TYPE TOOL VIBRATIONS

Introduction

In this chapter, the theoretical investigation of using tool holder with uniformly distributed helical slots over its planar surface in order to achieve L&T vibrational mode coupling and evaluate its influence on the piezoelectric energy harvesting from the end mill tool vibrations is performed, and the results are presented and discussed. The evaluation tasks of proposed tool holder design optimization for the purpose of increasing the power output from the piezoelectric transducer are performed.

In order to achieve these tasks, in this chapter, 3D models of the horn-type tool holder, the end mill cutter and the piezoelectric transducer with back-mass, representing the actual device design, are created. FEM simulation is performed for the evaluation of the following:

- Vibrational modal response of the end mill tool for the evaluation, whether a simplified tool model in a form of cylinder can be used in simulation assemblies;
- Vibrational modal response of the horn-type tool holder with uniformly distributed helical slots on its planar surface; generation of L&T mode coupling phenomena;
- Vibrational L&T mode coupling frequency dependence on geometrical parameters of the helical slots, introduced on the planar surface of the tool holder and the tool holder's material properties.
- Surface displacement of the tool holder under the excitation of the end mill tool by forces, simulating the machining operation;
- Tool holder's surface displacement dependence from the amplitude of milling force components exciting the end mill tool;
- Voltage and power output from piezoelectric transducer, embedded together with the tool holder, which is deformed by generated surface displacements;
- Voltage and power output from a piezoelectric transducer dependence on the value of load resistance;
- Voltage and power output from a piezoelectric transducer dependence on the amplitude of milling force components, exciting the end mill tool.
- Voltage and power output from piezoelectric transducer dependence on the geometrical parameters of the uniformly distributed helical slots, introduced on the planar surface of the tool holder.

The shape of the 3D models that are used in the theoretical investigation are built by using Solidworks computer aided design software package, which is imported into COMSOL Multiphysics. From here on, it is referred to as COMSOL, computer aided engineering software package to perform simulations, employing finite element method to solve complex physical problems, governed by partial differential equations (PDEs).

The evaluation of the vibrational modes and conditions for the longitudinal-torsional mode coupling effect to take place for the tool holder model and L&T mode frequency dependence on geometrical and material parameters was performed in Solid Mechanics (solid) module of COMSOL software package. The surface displacement analysis of the tool holder's contact surface with piezoelectric transducer was carried out in the module called Solid Mechanics (solid), performed in the frequency domain. For a complete tool holder with piezoelectric transducer simulation, where the voltage and power output from the piezoelectric transducer were evaluated, when the end mill of the tool holder was excited, was performed integrating Electrical Circuit (cir), Electrostatics (es) and Solid Mechanics (solid) modules. A block diagram coupling of the modules that are used in FEM model calculations are provided below in Figure 2.1.

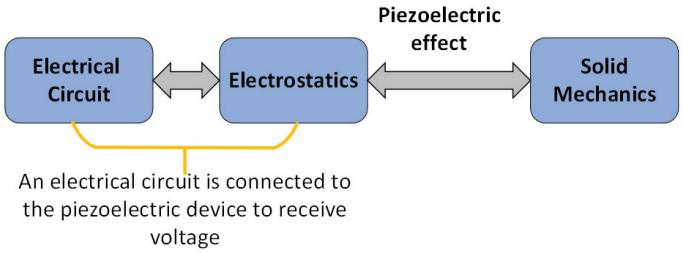

Fig. 2.1. Used physics coupling of piezoelectric transducers in COMSOL software environment for the FEM calculations

Figure 2.2. presents a block diagram in more detail explaining the complete implemented model that is used for theoretical investigation, consisting of geometrical components, physical coupling and inputs/outputs for/from the performed simulations.

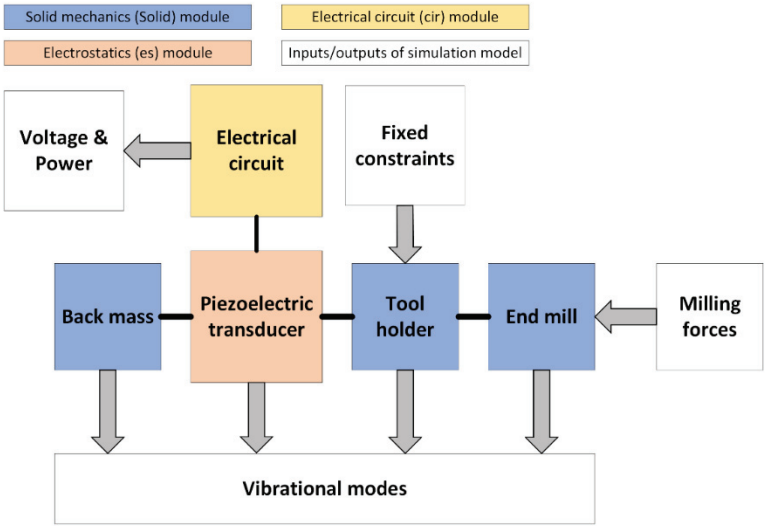

Fig. 2.2. Principal block diagram of FEM simulation model

Figure 2.3. shows the assembly of geometrical models for the research, where piezoelectric transducer voltage and power output were evaluated. It is the top most assembly of the proposed device that is used in simulations, consisting of the end mill tool, the tool holder (either with or without uniformly distributed helical slots on its planar surface) and the ring type piezoelectric transducer pre-stressed by a back-mass.

The material used in the simulation for the end mill tool is molybdenum (common application in high-speed cutting tools), for tool holder, carbon steel, and for back-mass, aluminium 3003. Table 2.1. shows the key properties of these materials.

Table 2.1. Properties of linear elastic materials used in simulations

Materials	Density (kg/m^3)	Young's Modulus (GPa)	Poisson's ratio	Loss factor
Molybdenum	10000	320	0.38	0.001
Carbon steel	8000	210	0.28	0.01
Aluminium 3003	2700	690	0.33	0.02

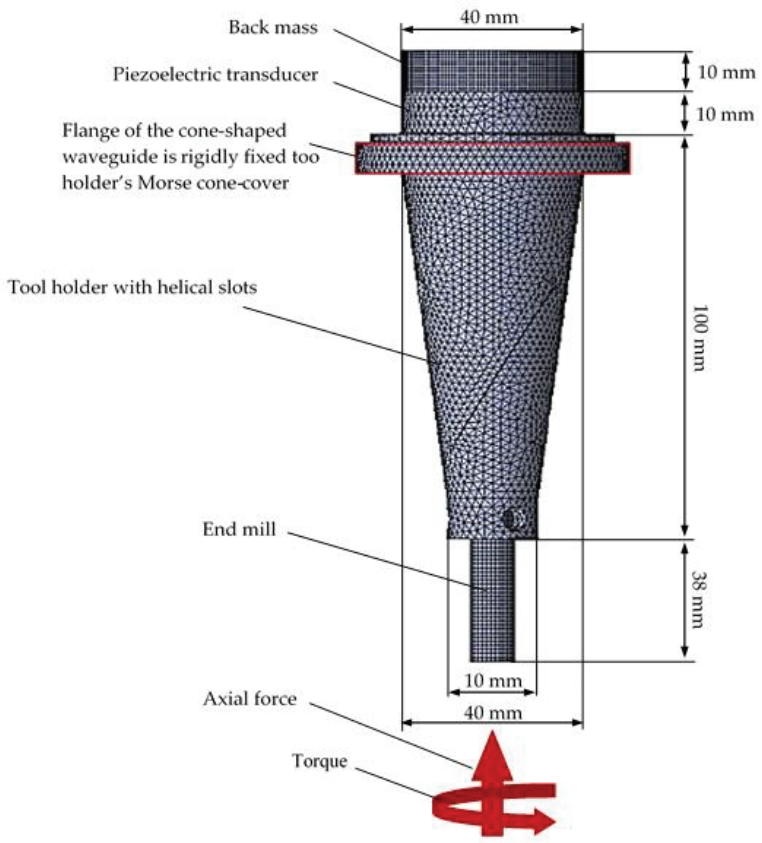

Fig. 2.3. Schematic representation of the tool holder assembly node used during the simulation

PZT-5H (Lead Zirconate Tritanate) has been selected for piezoelectric ceramic material, because it has the best piezoelectric material properties (exhibiting the highest piezoelectric properties at room temperature, i.e., k_{eff}, k_p, d_{31}, d_{33}) when compared to the widely available and used PZT-5 and PZT-4 groups. Table 2.2. shows the key properties of this piezoelectric material.

Table 2.2. Key properties of piezoelectric ceramic PZT-5H

Material	Density (kg/m^3)	Young's Modulus (GPa)	Poisson's Ratio	d_{31}	d_{33}	k_{33}	T_c
PZT-5H	7500	200	0.3	320	650	0.75	250

The PZT-5H piezoceramic that is used in simulations is composed of four stacked rings, where each piece is 2.5 mm tall, 4 mm thick with inner radius of 32 mm and outer radius of 40 mm, as provided in Figure 2.4.

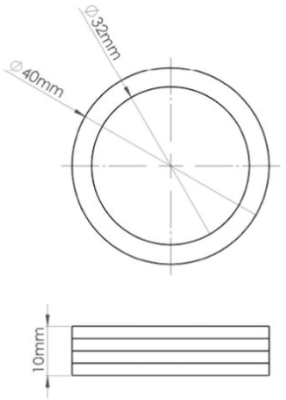

Fig. 2.4. Geometrical properties of PZT-5H piezoelectric ceramic stacked rings used during FEM modeling

Eigenfrequency and frequency response studies are performed on the proposed FEM model to evaluate the system response to the excitation in the form of surface displacement and voltage output from the piezoelectric transducer.

There, the eigenfrequency study is performed for the first ten eigen-modes of the assemblies or the parts where the geometrical components are in the following configurations:

- End mill rigidly fixed over its cylindrical surface;
- Tool holder rigidly fixed over the exterior flange surface, as provided in Figure 2.3.;
- The assembly of the tool holder with the end mill, where the tool holder is rigidly fixed over its exterior flange surface;
- The assembly of the end mill tool, the tool holder, the piezoelectric transducer and the back mass, where rigid constraints are implemented on relevant tool holder domains, as described in the previous step.

The performed eigenfrequency study allows to observe and evaluate the longitudinal, torsional vibrational modes and their coupling phenomena. During the FEM evaluation, the domains for fixed constraint conditions are selected for each configuration in a way to represent the actual device assembly or its positioning inside a CNC spindle as close as possible.

The L&T mode coupling frequency dependence on the introduction of helical uniformly distributed slots on the planar surface of the tool holder is as well evaluated. The L&T mode coupling changes, when the geometrical parameters, such as length, width, depth and tilt angle of the helical uniformly distributed slots, vary.

The frequency response study over 10–20 kHz range is performed on the tool holder with the end mill assembly and complete assembly as provided in Figure 2.3. In each case, the models are excited by applying axial, torsional and radial milling force components on the end mill, as it would be expected during the milling operation; depending on the model assembly, either displacement of piezoelectric transducer contact surface or its voltage and power output are measured.

As discussed previously, during frequency response analysis of the tool holder with or without uniformly distributed helical slots, the displacement in axial direction of the surface intended for the contact with piezoelectric transducer is evaluated at torsional and axial modes of vibration.

During the frequency response analysis of piezoelectric transducer voltage and power output evaluation, its ground and voltage boundaries are applied to the bottom and top surfaces. The polling is in the axial direction; thus, the piezoelectric transducer has d_{33} main operating mode. The piezoelectric transducer voltage output V_{out} and power output P_{out}, are evaluated accordingly in the FEM model:

$$V_{out} = abs(cir.R1\_v), \tag{2.1}$$

$$P_{out} = realdot(cir.R1\_i, cir.R1\_v), \tag{2.2}$$

where $cir.R1\_v$ and $cir.R1\_i$ are the parameters of voltage and current amplitudes, as measured over the applied electrical load.

The performed eigenfrequency and frequency response studies show whether the L&T mode coupling effect can be achieved by manipulating the tool holder planar geometry and how it can be utilized to achieve the charge generation properties of a piezoelectric transducer. The obtained voltage and power output measurements from the simulations allow evaluating whether sufficient amount of power can be generated during the milling operation with the proposed design energy harvester. This energy can be used to power ultra-low power electronics, enabling data processing and wireless transmission and how the power output can be optimized by varying tool holders' geometrical parameters.

2.1. Simulation of rotating shank-type tool vibrational characteristics

Finite element modeling of the milling tool was performed in order to evaluate its vibrational characteristics and evaluate the possibility to simplify the 3D model of the tool to a simple cylindrical shape, thus reducing requirements for computational

resources and removing unnecessary complexity of the simulation model at the same time avoiding any relevant negative effect on the results.

For this purpose, two geometrical models, i.e., a two-flute end mill tool and its simplified cylindrical shape representation, have been created with Solidworks software. Both geometrical models are provided in Figure 2.5. For both models, the main geometrical parameters have been kept identical.

Molybdenum has been selected as a material for both end mill models, as it is a common material used for HSS (high speed steel) cutting tools. The material properties are presented in Table 2.1.

The fixed boundary conditions that have been used during the simulation represent the actual expected clamping conditions of the end mill tool, when assembled together with a cone shaped tool holder. The fixed boundary conditions, eliminating displacement in x and y directions, have been used for both end mill tool models and are displayed in Figure 2.6. (a). Both end mill models have been meshed by using free tetrahedral elements (Fig. 2.6. (a) and (b)).

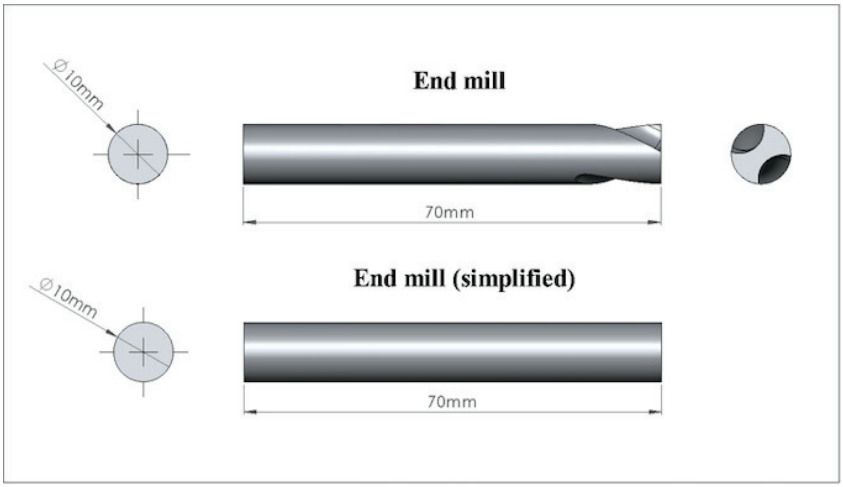

Fig. 2.5. Geometrical models of the end mill tool and a proposed simplified version of it

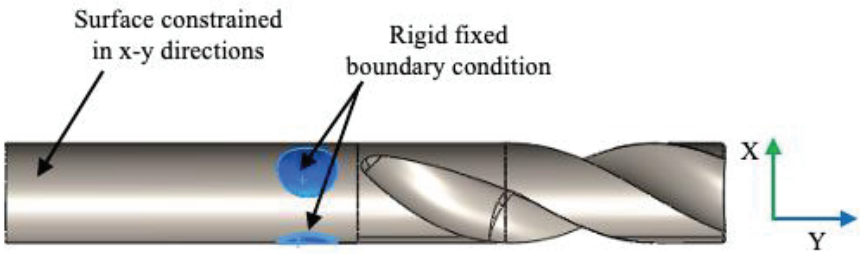

(a)

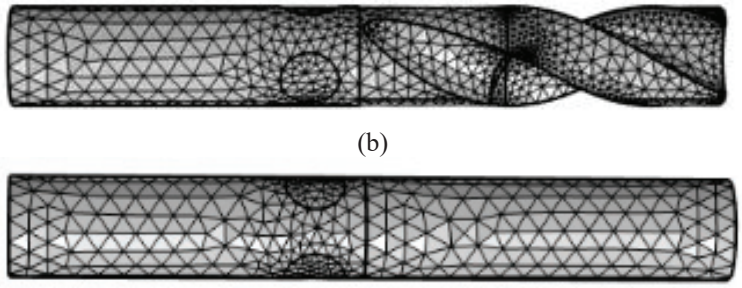

(b)

(c)

Fig. 2.6. (a) Boundary conditions set for both end mill models, (b) meshed two flute end mill models and (c) meshed simplified end mill models using free tetrahedral elements

The eigenfrequency study has been performed for both end mill models to investigate the torsional and the axial mode of vibration, as the focus of this study is to achieve the L&T mode coupling. The results of the performed eigenfrequency simulation showed that torsional and axial modes of vibration were at 16.76 kHz and 33.794 kHz for the actual end mill geometrical model, and for the simplified cutter model, at 20.775 kHz and 33.313 kHz. The results of the study are presented in Figure 2.7.

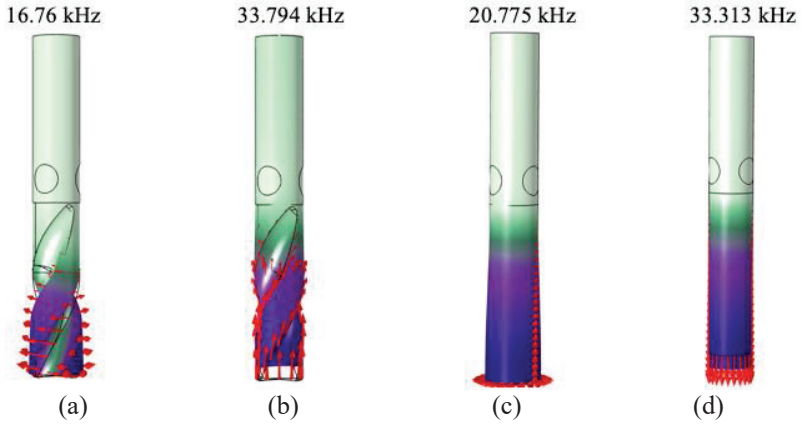

Fig. 2.7. Vibrational modes: (a, c) – torsional mode, (b, d) – axial mode for two flute and simplified end mill models

As presented in Table 2.3., the obtained eigenfrequency study results show that the difference between axial vibrational mode frequencies for the actual and simplified end mill model is 1.4%, though the torsional mode frequency between the

two end mill models is 19%. This can be expected, as the replacement of the actual two-flute geometry by a cylinder increased the model's torsional stiffness.

Table 2.3. Frequency difference between torsional and axial modes for actual and simplified end mill tool models

Vibrational mode	Actual end mill	Simplified end mill	Difference %
Torsional	16.76 kHz	20.775 kHz	19.3%
Axial	33.794 kHz	33.313 kHz	-1.4%

Taking into account that the end mill tool is a relatively small part of a larger assembly, a further investigation was performed in order to evaluate the axial and torsional vibrational mode frequency for the actual and simplified cutter geometrical models when they are assembled together with the cone shaped tool holder. The assembly CAD model of a simplified end mill tool fixed inside with the tool holder is provided in Figure 2.9.

The material for the end mill tool model was left molybdenum, and for the tool holder, plain carbon steel was selected. Respective properties of both materials used in simulation can be found in Table 2.3.

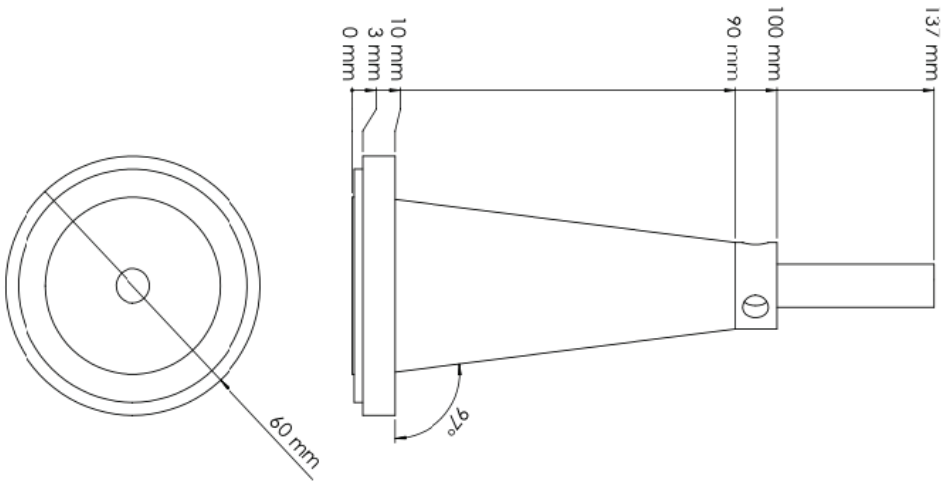

Fig. 2.8. Geometrical assembly model of simplified end mill tool with tool holder

During FEM eigenfrequency analysis, the tool holder was rigidly fixed over its flange surface domains, as provided in Figure 2.10. Such fixation of the tool holder is intended to replicate its actual expected assembly together with the Morse cone.

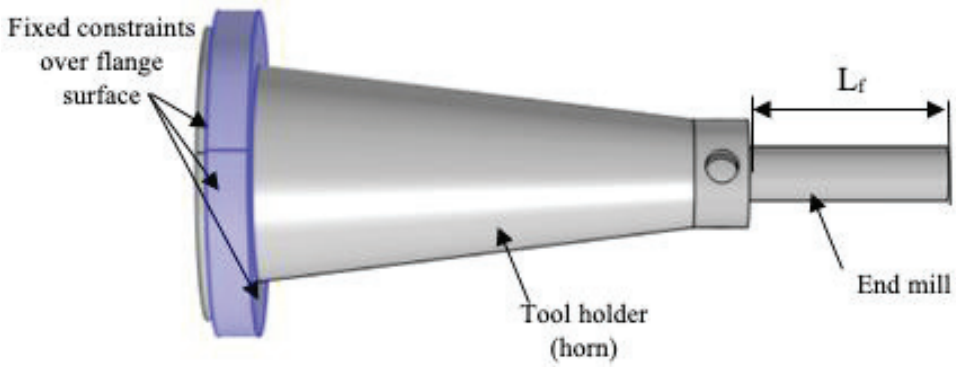

Fig. 2.9. Tool holder with end mill tool geometrical model; rigid fix constraint boundary conditions; L_f = 37 mm

As in the previous simulation step, the assembly models with actual and simplified end mills have been subjected to eigenfrequency study in order to evaluate their torsional and axial vibrational mode frequencies. There, the first ten eigenfrequency modes have been evaluated.

The results from this study are presented in Fig. 2.10., where axial and torsional vibrational mode frequencies can be seen. For assembly model with actual two-flute end mill geometrical model, the torsional vibrational mode is achieved at 14.226 kHz and the axial mode at 15.286 kHz, while for the assembly, implementing simplified end mill model, the torsional mode of vibration was observed at 14.491 kHz and axial mode at 14.823 kHz. In this case, the difference between torsional mode frequencies is 1.5%, and between axial mode frequencies it is 3.9%. These results are provided in Table 2.4. as well.

Table 2.4. Frequency difference between torsional and axial modes for tool holder assembly models with two-flute and simplified end mills

Vibrational mode	Actual end mill	Simplified end mill	Difference %
Torsional	14.226 kHz	14.491 kHz	1.8%
Axial	14.823 kHz	15.286 kHz	-3%

From the obtained results, it is evident that the use of a simplified end mill model in assembly for FEM studies with horn type tool holder does not result in significant impact on the system's vibrational response. Although such tool model simplification enables to reduce the complexity of the final FEM model, thus reducing the computational time and the required resources for the simulation. For this reason, in further simulation steps, only simplified end mill model shall be used.

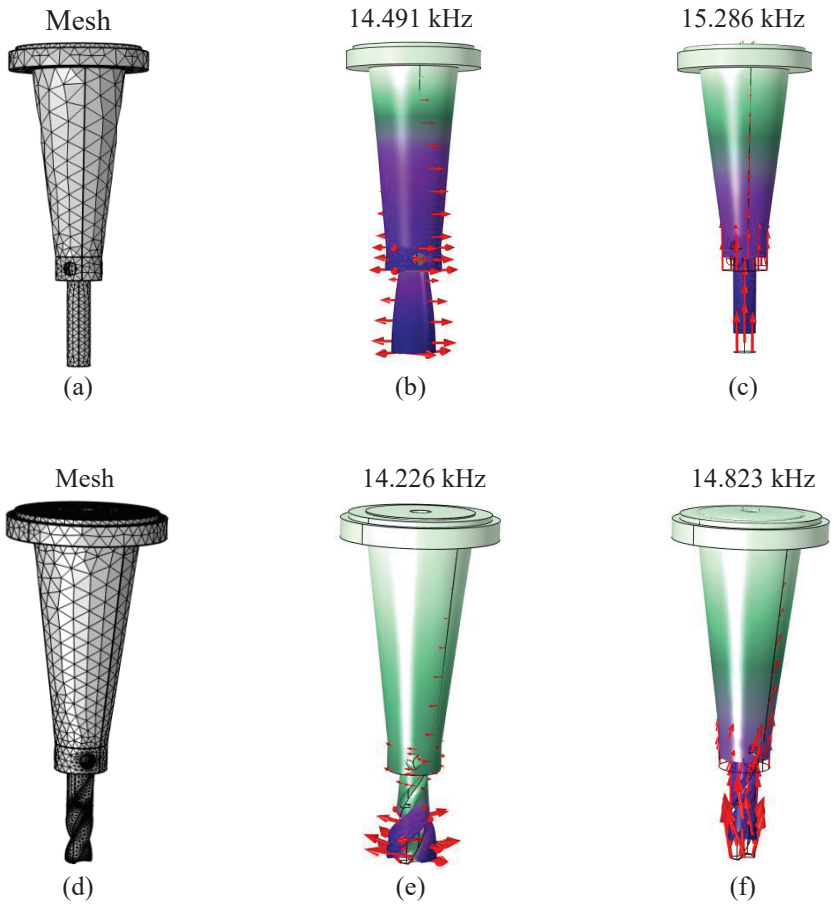

Fig. 2.10. (a) Mesh of assembly with simplified end mill model and (b) torsional (c) axial vibrational mode study results, (d) mesh of assembly together with detailed tool model and (e) torsional (f) axial vibrational mode study results

2.2. Simulation of horn-type waveguide with helical slots L&T mode coupling

Cone-shaped tool holder, sometimes, in scientific literature as well referred to as “horn”, is usually used in machining processes, where it is applied to concentrate specific mode vibrations, exciting the tool, which helps to reduce the cutting forces and improve the surface quality of the machined workpiece. In such applications, the motion generated at the tool-workpiece interface is usually of longitudinal, torsional or longitudinal and torsional composite form, which can be achieved either by utilizing a transducer that is able to synchronically generate both vibrational modes at once or by means of introduction of geometrical features on the surface of the tool holder that enable the transformation of the longitudinal motion by the transducer into the L&T form at the tool.

This part of simulation work is performed in order to investigate whether the approach where the introduction of geometrical features in the form of slots on the planar surface of the horn can be used in reverse action. In such way, when the end mill tool is excited by torsional vibrations, once these vibrations are transferred to the tool holder, they shall be partially transformed into longitudinal vibrations. In order to perform such investigation, a horn type tool holder design has been created by using Solidworks computer aided design (CAD) software package with helical slots formed on its planar surface (Fig. 2.11.). This tool holder model was imported into COMSOL for FEM studies to perform eigenfrequency and frequency response analysis.

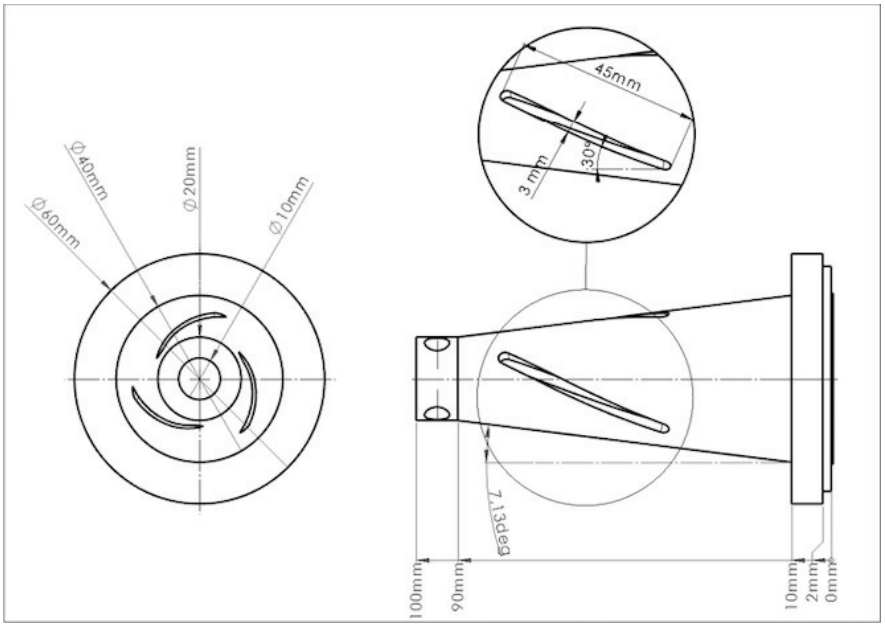

Fig. 2.11. Horn type tool holder model design with helical slots formed on its planar surface

The tool holder, presented in Figure 2.11., has three uniformly distributed helical slots, formed on its planar surface, which are 45 mm in length, 3 mm in width and 3 mm in depth, with a 30° angle, formed with the tool holder's longitudinal axis. The tool holder, as in the previous studies, is assembled together with a simplified end mill tool's model. The selected material for the tool holder is plain carbon steel, and for the end mill tool, molybdenum.

As a first step of the simulation, the eigenfrequency study was performed. During the eigenfrequency analysis, the tool holder's fixed boundary condition was set over its whole flange surface, as defined in the previous simulations (Fig. 2.9.).

The results from the performed modal analysis are presented in Fig. 2.12. There, the obtained results show a frequency of 13.9 kHz for the torsional vibrational mode and 15.4 kHz for the longitudinal/axial vibrational mode.

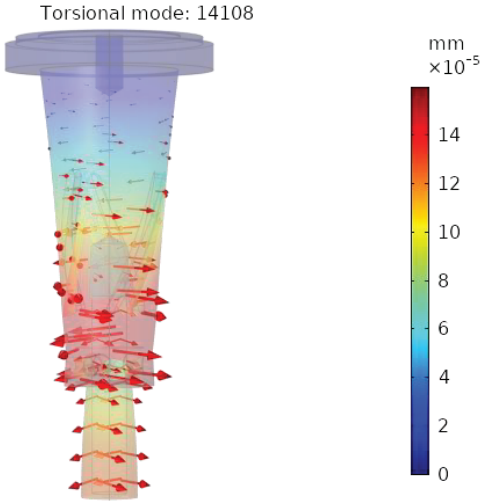

(a)

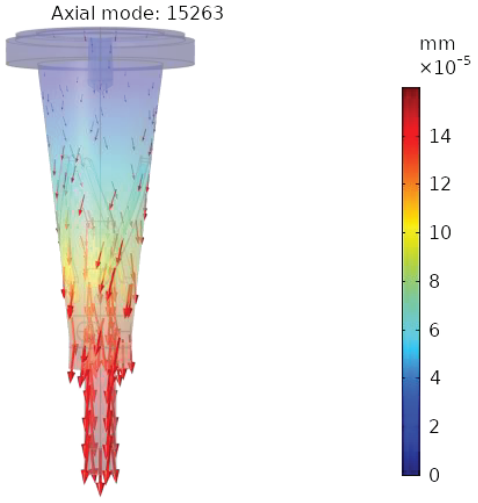

(b)

Fig. 2.12. Tool holder with helical slots (a) torsional and (b) axial modes of vibration

The close frequency of the torsional and the longitudinal mode shows the introduction of the mode coupling effect where the horn can be excited to resonate in both modes simultaneously.

Further, the eigenfrequency study has included a parametric study evaluating how the use of different materials for the tool holder influences the formation of the torsional and axial modes of vibration. For this study, three different materials, namely, steel, aluminium and brass, have been selected. Their mechanical properties are presented in Table 2.5.

Table 2.5. Mechanical properties of steel, aluminium and brass materials

Materials	Density (kg/m^3)	Young's Modulus (GPa)	Poisson's ratio
Steel	8000	210	0.28
Aluminium	2700	69	0.33
Brass	8730	113	0.34

The performed parametric study results are presented in Figure 2.13. These results indicate that the softer material is selected for the tool holder, the higher decrease of an L&T mode frequency is observed. This is important in cases where the application required lower L&T mode coupling frequency, but the reduction of the structure stiffness is acceptable.

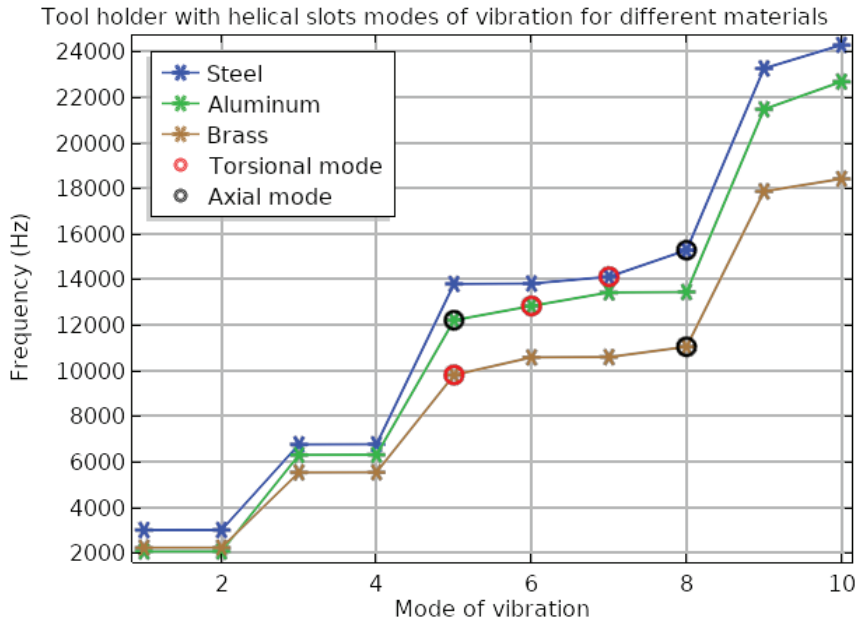

Fig. 2.13. Frequency dependence of torsional and axial vibrational modes of tool holder with helical slots on the material type

The efficiency of conversion from longitudinal to torsional vibrations and vice versa is dependent on the geometrical parameters of the slots, such as tilt angle, length, width and depth. Changing these geometrical parameters affect the increase or the decrease in difference (bandwidth) between torsional and longitudinal mode frequencies. Eigenfrequency study has been extended to evaluate how changes in these geometrical parameters of the slots, formed on the planar surface of horn type tool holder, affect the longitudinal and the torsional modes and their coupling. The material, which has been selected for the horn type tool holder, is plain carbon steel.

The parametric sweep for the denoted geometrical parameters of the slots has been performed, evaluating how their variations effect the formation of the torsional

and the axial mode frequency. The variations of these parameters during eigenfrequency study are presented in Table 2.6. The study results are presented in Figure 2.14. as well as Table 2.7. and Table 2.8., separating the parameters individually.

Table 2.6. Geometrical parameters of the slots used during the parametric study

Parameter	Start value	Step value	End value
Tilt angle	0°	10°	70°
Length	0 mm	10 mm	70 mm
Width	1 mm	1 mm	10 mm
Depth	1 mm	1 mm	6 mm

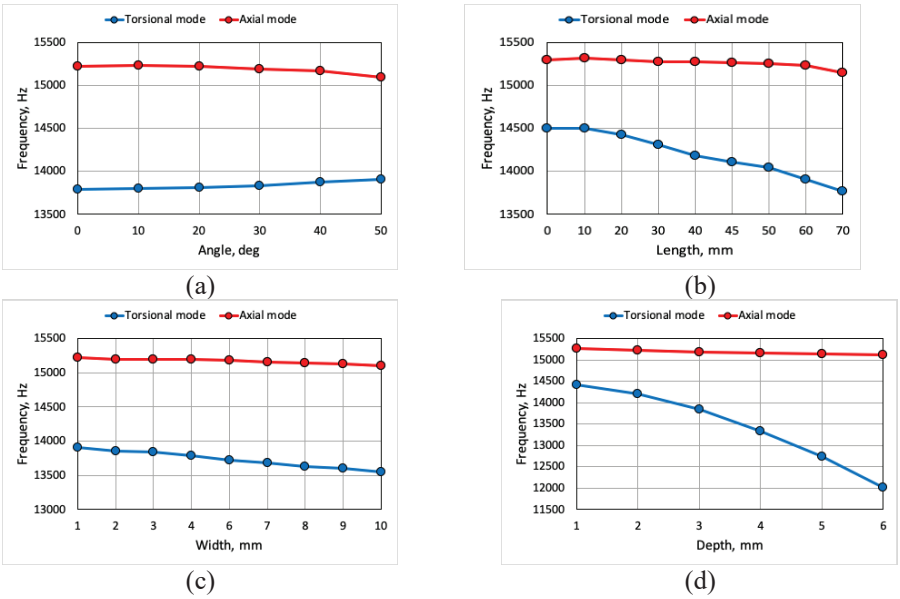

Fig. 2.14. The frequency dependence of torsional and axial vibrational mode of tool holder on (a) tilt angle, (b) length, (c) width and (d) depth geometrical parameters of the slots

Table 2.7. The frequency change of torsional mode of tool holder with varying slot parameters

Parameter	Torsional mode frequency at the start value	Torsional mode frequency at the end value	Difference, %
Tilt angle	13790 Hz	13905 Hz	+0.9%
Length	14499 Hz	13771 Hz	-5%
Width	13914 Hz	13556 Hz	-2.5%
Depth	14422 Hz	12030 Hz	-16.5%

Table 2.8. The frequency change of axial mode of tool holder with varying slot parameters

Parameter	Axial mode frequency at the start value	Torsional mode frequency at the end value	Difference, %
Tilt angle	15228 Hz	15094 Hz	-0.9%
Length	15301 Hz	15148 Hz	-1%
Width	15222 Hz	15107 Hz	-0.8%
Depth	15268 Hz	15109 Hz	-1%

From the results, it is clear that the increase in the geometrical parameters of the slots have negligible effect on the axial mode frequency, though for torsional mode, specifically, the increase of depth leads to a significant decrease in mode frequency and widening of the frequency gap between the torsional and the axial mode, thus resulting in L&T mode degeneration. This is due to the increased depth of the slots, when the stiffness in the torsional direction of the tool holder is decreased, it leads to higher torsionality. For the application of the tool holder use during the milling operation, the depth parameter was selected 3 mm, ensuring relatively high torsionality and close L&T mode coupling frequency, while retaining sufficient structure stiffness. Other parameters of the helical slots for the tool holder have been set to 45 mm in length, 3 mm in width and 30° tilt angle.

In the next part of the study, the impact that the tilted slots have on the generation of the longitudinal vibrations during L&T mode coupling was evaluated. This has been done by performing a frequency response study over 10–20 kHz frequency range, when the end mill tool is subjected to the end milling excitation forces.

For this purpose, two tool holder models (Fig. 2.8. and Fig. 2.11.), assembled together with the simplified end mill design, were imported into the simulation model. In this study, the denoted two tool holder models were subjected to the axial, tangential and radial milling component forces, applied on the surface boundaries of the end mill, as provided in Fig. 2.8. The applied axial, tangential and radial forces were calculated according to the equations (1.1–1.3). Milling process parameters (milling depth, feed per tooth and radial depth of cut), used in the calculation of these machining forces, exerted on the end mill tool, have been selected as applicable to rough milling operation of the steel workpiece and are provided in Table 2.9.

Table 2.9. The selected milling process parameters for the calculation of force components acting on the milling tool

Description and symbol	Value	Unit
Milling depth, a_p	1	mm
Cutter diameter, d_0	10	mm
Feed per tooth, f_z	0.05	mm/tooth
Radial depth of the cut, a_e	0.4	mm

During the frequency response study, the average displacement value of the tool holder surface in longitudinal (Y) direction was measured. The view of this tool holder surface is provided in Figure 2.15. It is the intended contact surface with piezoelectric transducer.

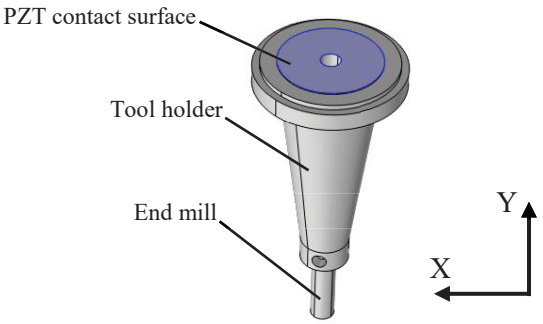

Fig. 2.15. Tool holder surface (blue colour) used to measure the longitudinal displacement

Study results, presented in Figure 2.16., indicate that the introduction of the slots not only causes the displacement in the longitudinal direction at the torsional mode, but leads to the L&T mode coupling effect as well.

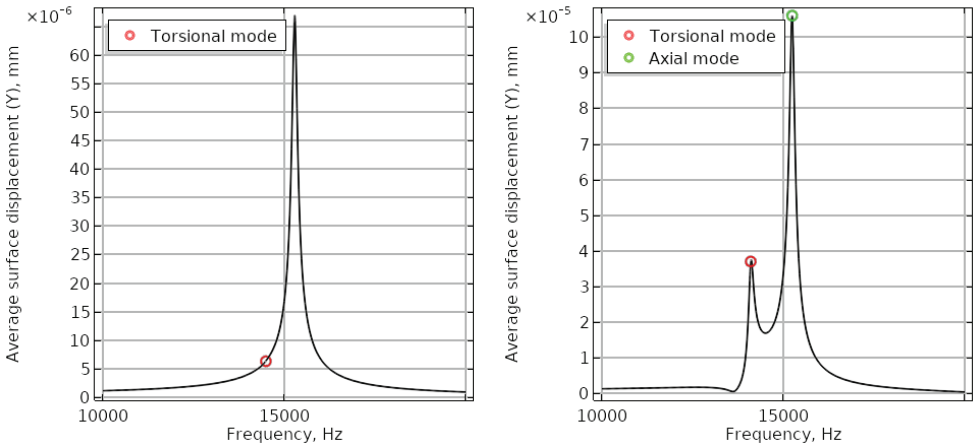

Fig. 2.16. Average surface displacement measurement results for (a) tool holder without slots and (b) tool holder with slots

Furthermore, when comparing the obtained results (Fig. 2.17.), it can be seen that the introduction of helical slots leads not only to the formation of the L&T mode coupling, but also to the increase in the longitudinal surface displacement at the axial mode of vibration of the tool holder assembly, which is almost two times higher. This can be understood as the effect of the helical slots, which increases the torsionality of

the tool holder, partially allowing to transform the radial and the torsional force components, acting on it, into the contraction and the extension of the horn, expressed as additional longitudinal motion.

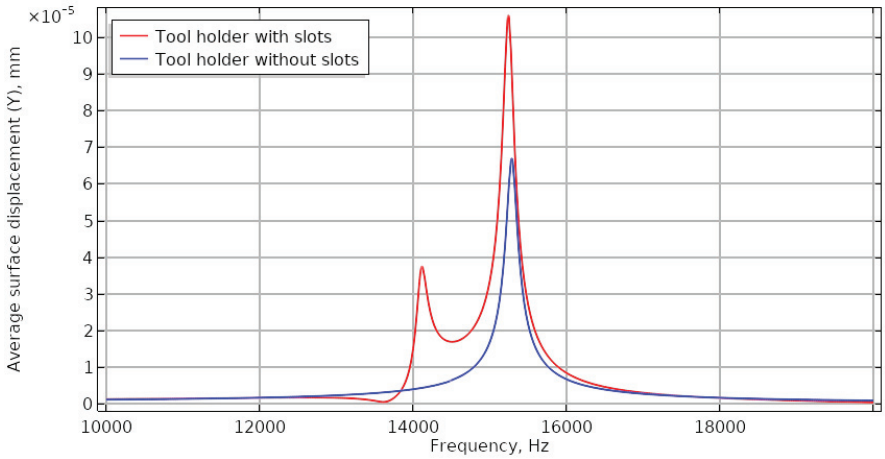

Fig. 2.17. The comparison of the average surface displacement measurement results for the tool holder with and without helical slots

This is clearly visible in contour displacement visualizations that are presented in Figure 2.18., where both tool holders are excited at the torsional mode; the tool holder with helical slots experiences more than five times higher surface deformations in the longitudinal direction, which is transferred to the PZT contact surface.

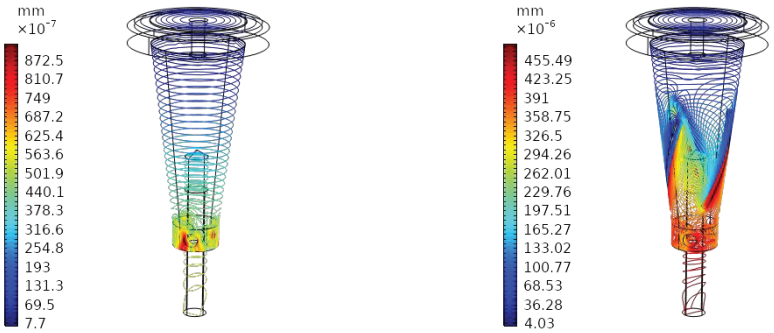

(a) (b)

Fig. 2.18. Surface longitudinal displacement at the torsional mode for (a) the tool holder without helical slots and (b) the tool holder with helical slots

Further on, during the frequency response study, the surface displacement in the longitudinal direction for the tool holder with helical slots was evaluated when milling forces varied. The variations of the milling force component values are presented in Table 2.10.

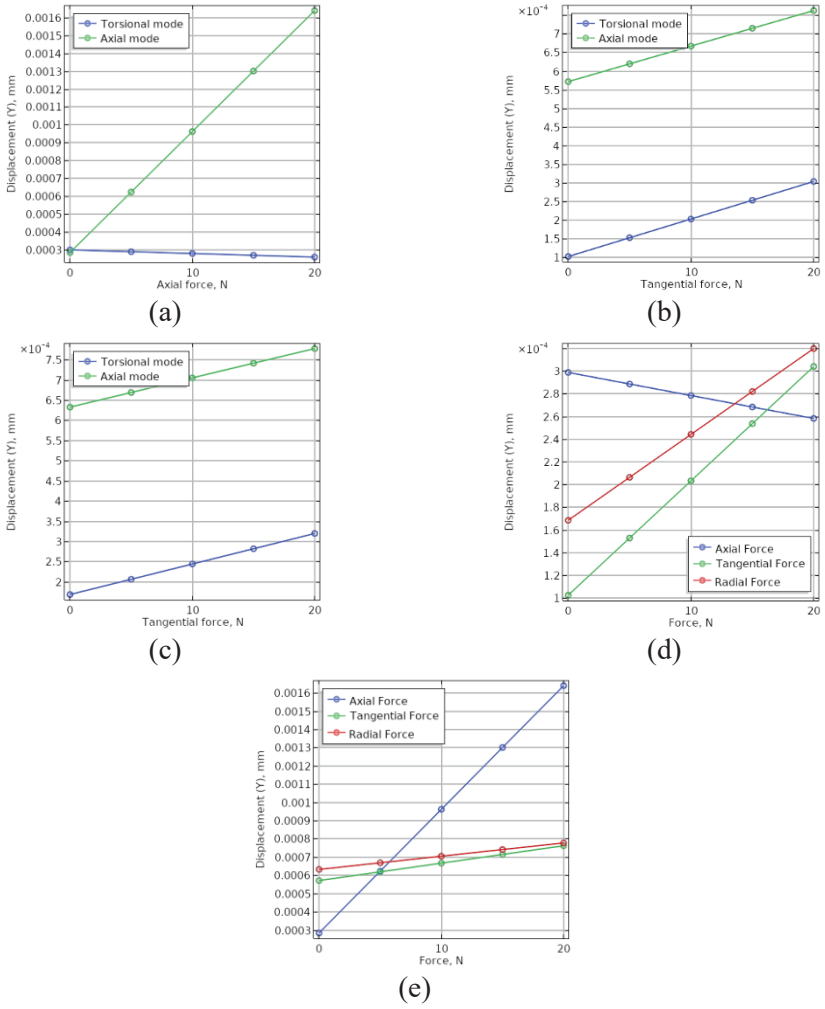

Fig. 2.19. Tool holder surface longitudinal displacement at torsional and axial modes of vibration depending on change in (a) axial force component, (b) tangential force component, (c) radial force component; surface displacement dependence on milling force components when the tool holder is excited at (d) torsional mode and (e) axial mode

Table 2.10. Milling force exerted on the end mill component values of the slots used for the frequency response parametric study

Force	Start value	Step value	End value
Axial	0 N	5 N	20 N
Tangential	0 N	5 N	20 N
Radial	0 N	5 N	20 N

The obtained results indicate that in case of the tool holder, excited at the axial mode of vibration, the increased amplitude of the axial milling force component has the highest impact on the formation of the longitudinal vibrations, while at the torsional mode of vibration, the increase in the radial and torsional milling force component leads to higher change in the longitudinal displacement.

2.3. Simulation of energy harvesting from rotating shank-type tool vibrations

Up to this point, the research findings show that the tool holder with uniformly distributed helical slots on its planar surface enables to transform dominant broadband torsional vibrations partially, which are present during the milling operation, into longitudinal motion, which is complimenting the already existing axial vibrations. These longitudinal vibrations in the design of the proposed device are to be used for deforming an axially polarized d_{33} piezoelectric transducer that is embedded together with the tool holder, thus producing electrical charge.

In order to evaluate the piezoelectric transducer, which is embedded together with the tool holder energy generation properties, a frequency response analysis over 10–20 kHz frequency range, which covers both torsional and axial vibrational mode frequencies, has been created and performed.

This study has been performed on two different geometrical models of the tool holder, i.e., with and without helical slots. During the simulation, the tool holder has been assembled together with the piezoelectric transducer and pre-stressed by a back mass. The view of the assembly model with relevant milling force components applied on the end mill is provided in Fig. 2.3.

As in the previous chapter, during the FEM study, the simplified end mill tool model is subjected to the axial, radial and torsional milling force components, calculated according to formulas (1.1–1.3), allowing to simulate the milling operation. The fixed boundary conditions are set over the whole surface area of the tool holder's flange. The voltage response from the piezoelectric transducer is measured and normalized over the defined frequency range for both tool holder models, enabling to compare the energy generation differences that have been obtained from the piezoelectric transducer.

During this study, the 40 x 32 x 10 mm size PZT-5H ceramic piezoelectric d_{33} type transducer, comprising of 4 ring-shaped elements, was selected (Fig. 2.4.) and fixed together with the tool holder on the surfaces, opposite to the end mill tool position. The PZT-5H material properties are provided in Table 2.2. The piezoelectric transducer was pre-stressed by the ODxIDxH = 40 x 10 x 10 size aluminium back-mass. Back-mass design is provided in Figure 2.20.

The size and design of the piezoelectric transducer were selected according to the maximum surface axial displacement results, which were obtained during tool holder torsional resonant mode, to optimize its deformations and voltage output.

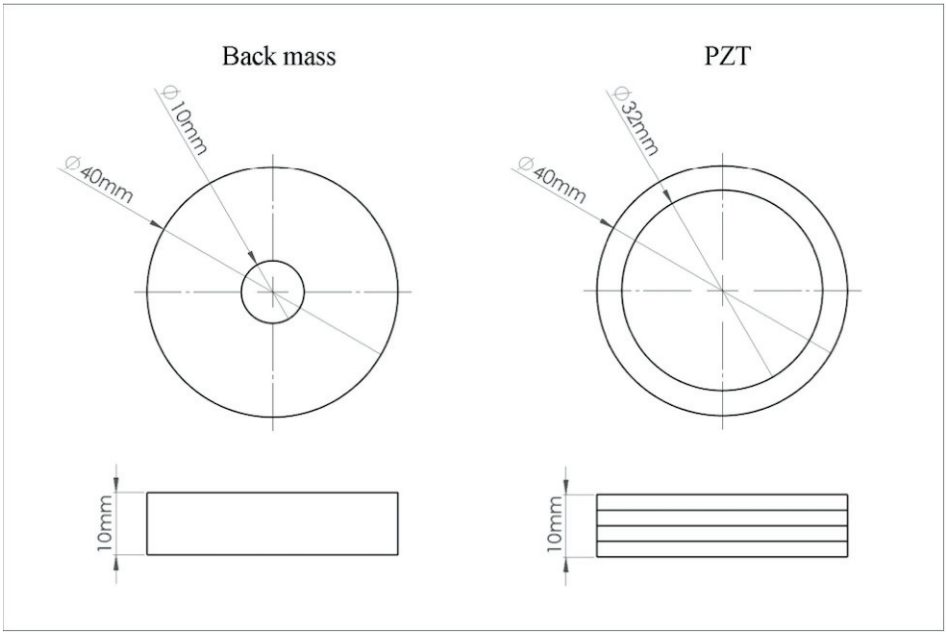

Fig. 2.20. Drawing of back-mass and piezoceramic transducer design embedded together with tool holder

The first and the second subscripts "33", used in piezoelectric "d" constants of the selected piezoelectric transducer, define the direction of the field and the direction of the resulting strain for charge constant. For piezoelectric voltage constant, the first subscript defines the direction of the generated voltage, and the second one indicates the direction of the applied force. Thus, the selected piezoelectric transducer, when deformed in its axial direction, will produce a charge.

Besides, the updated geometry with a PZT and back mass rings, in order to simulate the voltage output from the piezoelectric transducer, two additional COMSOL Multiphysics software packages were introduced into the existing simulation model, i.e., electrostatics and electrical circuits.

For the study of the frequency response simulations, the piezoelectric transducer has been connected to a resistor load, which varied from 10 Ω to 100 kΩ, where the voltage and the power, which was generated across this load, has been measured at torsional and axial vibrational mode frequencies of the tool holder. This evaluation study enables to assess and select an optimum matching load resistor, ensuring optimal power generation properties from the piezoelectric transducer. The results that have been obtained from this study (Fig. 2.21.) show that the maximum power output from the piezoelectric transducer at the torsional and axial vibrational modes is obtained when a resistor load of 31.6 kΩ is connected to the piezolelectric transducer. This load resistor value shall be used in all other studies when evaluating the output from the piezoelectric transducer.

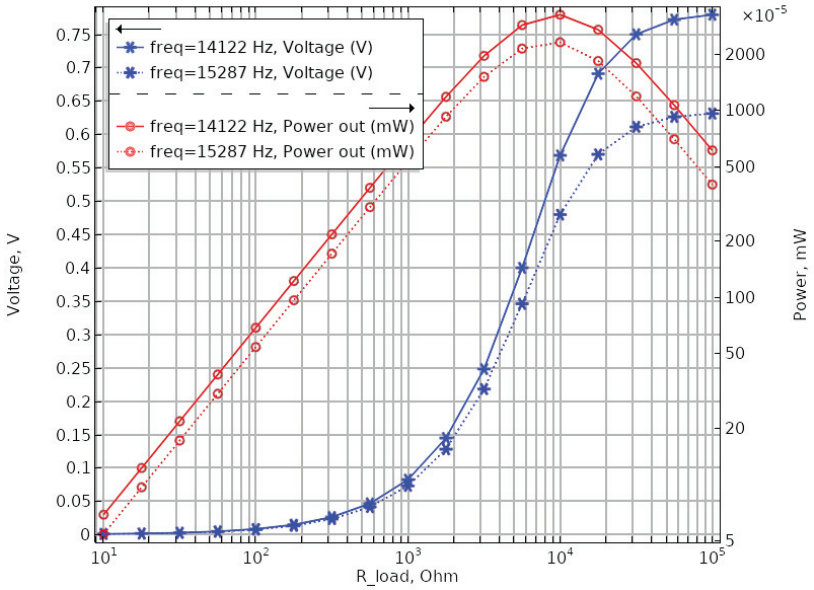

Fig. 2.21. Piezoelectric transducer generated voltage and power output dependence on the load resistor value

In the next step of the study, the load resistor value that was used in the model has been selected according to the results from Fig. 2.21. with voltage and power output from the piezoelectric transducer that was measured over the frequency range of 10–20 kHz.

From the study results, presented in Fig. 2.22., it can be observed that the tool holder with uniformly distributed slots, embedded with axially polarized piezoelectric transducer, will generate the highest voltage and power output, when the tool holder is excited to resonate at its torsional mode of vibration. These result values are presented in Table 2.10. From the obtained results, it is clear that the tool holder with helical slots will experience the L&T mode coupling when excited; the L&T mode coupling results in frequency bandwidth between the torsional and axial vibrational modes, where a significant power output from the piezoelectric transducer can be expected under the excitation conditions.

Table 2.11. Voltage and power output from the piezoelectric transducer when the tool holder is excited at torsional and axial vibrational modes

Measured output	Torsional mode, 14125 Hz	Axial mode, 15297 Hz	Difference, %
Voltage, (V)	0.75 V	0.62 V	17%
Power, (mW)	0.017 mW	0.012 mW	29.4%

During the simulation, the obtained power output measurement results from the piezoelectric transducer, when the tool holder is excited at the longitudinal and

torsional mode coupling frequency, is enough to power ultra-low power application microcontrollers that are available in the market.

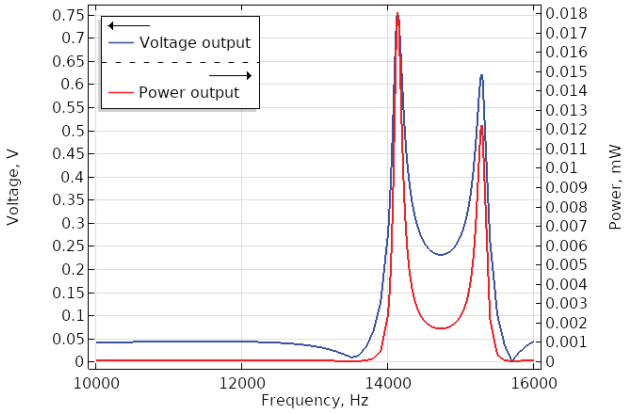

Fig. 2.22. Piezoelectric transducer generated voltage and power output over 10–20 kHz frequency range

A frequency response study has been updated by importing the tool holder's geometrical model without helical slots and performing measurement of voltage and power output from the piezoelectric transducer over 10–20 kHz frequency range. The obtained voltage and power results were compared to a tool holder with helical slots. The graphical study results for voltage output comparison are presented in Figure 2.23. and power output between the tool holder with and without helical slots in Figure 2.24. The summary of the results can be found in Table 2.12.

Table 2.12. Comparison of the measured voltage and power output from the piezoelectric transducer for the tool holder with and without helical slots

Tool holder	Torsional mode		Axial mode	
	Voltage (V)	Power (mW)	Voltage (V)	Power (mW)
Without helical slots	0.09	0.00095	0.36	0.004
With helical slots	0.75	0.017	0.62	0.012

It is clear from the results that the transducer that is embedded together with the tool holder with helical slots on its surface generates significantly higher power output as compared to the assembly, where instead a tool holder without helical slots is used; this supports the previously obtained results presented in Fig. 2.17. where the highest surface displacement in the longitudinal direction is achieved when the tool holder with helical slots is excited to resonate at its torsional mode. This shows that these geometrical features, i.e., helical slots, introduce the longitudinal and torsional mode coupling effect, enabling to transform torsional vibrations partially at the end mill/tool interface into longitudinal vibrations that are transferred through the tool holder, deforming piezoelectric transducer and producing higher voltage output, when

compared to a traditional design tool holder. The L&T mode coupling as well enables to increase the frequency range of the transducer, at which, when excited, a significant amount of power can be generated.

As for the tool holder without helical slots, the excitation at the torsional mode of vibration does not lead to a significant transformation of this motion into longitudinal deformations; the voltage output from PZT is more than eight times lower, and basically, an insignificant amount of power is generated in this mode.

In case where the tool holder with helical slots is excited at its axial mode of vibration, the piezoelectric transducer is generating 40% more voltage and three times more power as compared to the output from the piezoelectric transducer, embedded with a traditional design tool holder, because in this case, the torsional vibrations are still partially transformed into longitudinal vibrations, supplementary deforming the piezoelectric transducer.

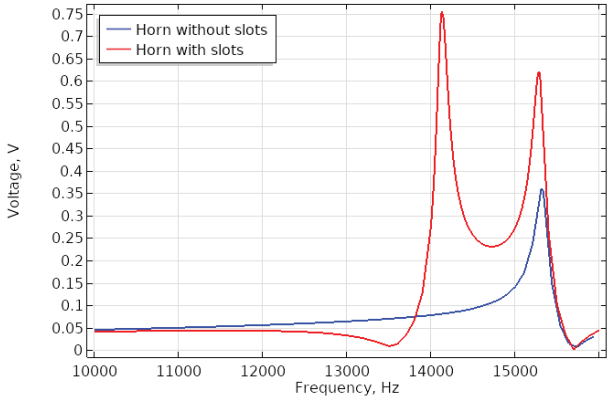

Fig. 2.23. Piezoelectric transducer generated voltage output for the tool holder with and without helical slots

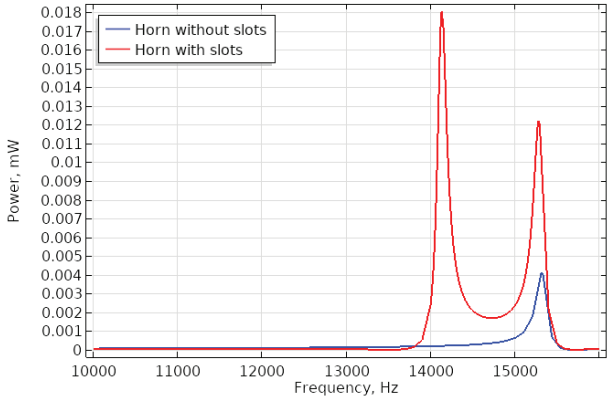

Fig. 2.24. Piezoelectric transducer generated power output for the tool holder with and without helical slots

The frequency response study, where the voltage output from the piezoelectric transducer embedded in the tool holder with helical slots is measured, has been further developed to evaluate the change of the voltage output from the piezoelectric transducer when the component values of the milling forces that are acting on the end mill tool vary. For this study, the milling force component values have been changed, as provided in Table 2.13.

Table 2.13. Range of milling forces used for parametric study

Force	Start value	Step value	End value
Axial	0 N	5 N	20 N
Tangential	0 N	5 N	20 N
Radial	0 N	5 N	20 N

Parametric study results are presented in Figure 2.25. It can be seen from the obtained results that in case of the tool holder, excited at the axial mode of vibration, the increased amplitude of an axial milling force component has the highest impact on the formation of voltage output from the piezoelectric transducer. While at torsional mode of vibration, the increase in the radial and torsional milling force component leads to a higher rate of change in voltage output from the PZT. The voltage rate of change dependence on the milling force component is provided in Table 2.14. At the torsional mode of vibration, the tangential force component has the highest effect on the increase in voltage that has been generated from the piezoelectric transducer; while at the axial mode of vibration, the force that is acting in longitudinal direction of the end mill tool influences the voltage output the most.

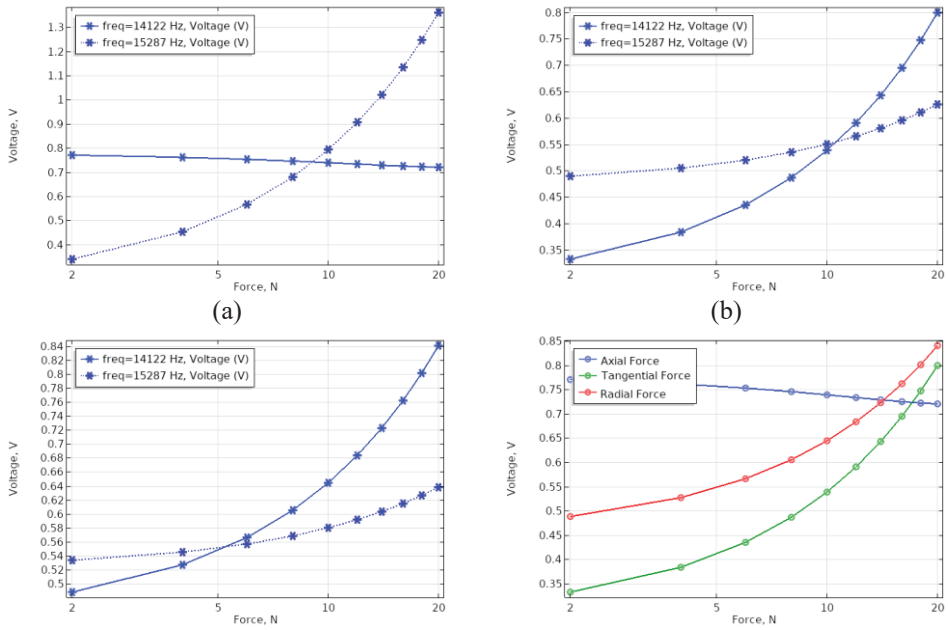

(c) (d)

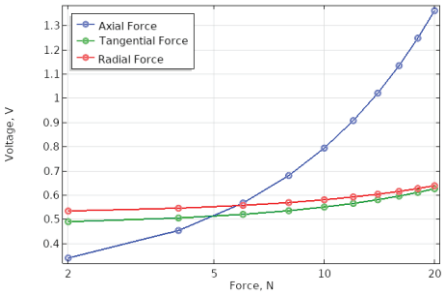

(e)

Fig. 2.25. Piezoelectric transducer voltage output when the tool holder is excited at torsional and axial modes of vibration dependence on (a) axial force component, (b) tangential force component, (c) radial force component; voltage output dependence on milling force components when the tool holder is excited at (d) torsional mode and (e) axial mode

Table 2.14. Voltage output from piezoelectric transducer rate of change dependence on milling force components at torsional and axial modes of vibrations

Milling force component	Voltage rate of change (V/N)	
	Torsional mode	Axial mode
Axial force	-0.002 V/N	0.05 V/N
Tangential force	0.025 V/N	0.007 V/N
Radial force	0.02 V/N	0.0057 V/N

Conclusions of chapter 2

In this chapter, the theoretical research of the horn type tool holder with helical slots has been performed. The vibrational response of the tool holder and vibration energy harvesting from torsional vibrations, using axially polarized piezoelectric stack type transducer, were carried out during this study. In the FEM study, the end mill tool was excited by axial, radial and tangential forces, representing force components that were expected during the milling operation. As the horn type tool holder with helical slots has complicated geometry, its modal and energy harvesting properties were investigated by using FEM.

Based on the performed studies, the following conclusions were formulated:

- The milling tool model can be simplified to a cylindrical shape without significantly affecting its frequency response characteristics when it is assembled together with a horn type tool holder.
- A frequency response study has shown that the introduction of helical slots on the planar surface of a horn type tool holder can achieve the effect of an L&T mode coupling.
- The evaluation of the parameters of the helical slots showed that the depth of the slots has the highest impact on the frequency of the longitudinal and

torsional modes, while the other parameters have basically a negligible effect: increasing the depth parameter from 1 to 5 mm increases the difference in the frequency of the L&T mode by 16.5%, decreases the torsional frequency and increases the torsional frequency of the tool holder.

- The frequency response study showed that the tool holder with helical slots on its planar surface experiences a longitudinal surface displacement at its torsional vibrational mode (which is absent in the tool holder without helical slots), and the average displacement at the axial mode is 39% higher when it is excited by the milling forces.
- The frequency response of the tool holder with helical slots on its flat surface and equipped with a piezoelectric transducer results in an 8.3 times higher output voltage in torsional mode and a 1.7 times higher output voltage in axial mode, compared to the frequency response of the tool holder without helical slots.
- During the frequency response study, the output power of the piezoelectric transducer was 17 μW and 12 μW, when the tool holder was excited at its torsional and axial vibrational modes. Such amount of generated power would be sufficient to power low power electronics, like microcontrollers.
- L&T mode coupling effect, which is present in the tool holder with helical slots on its surface, enables increasing the frequency range (between torsional and longitudinal modes), where a significant amount of voltage and power by piezoelectric transducer can be generated.

3. DESIGN OF A ROTATING SHANK-TYPE TOOL CONDITION MONITORING DEVICE

Introduction

In this chapter, the design of a device for rotating shank-type tool condition monitoring is presented. The device was constructed from a horn type tool holder, implementing uniformly distributed helical slots, which enable L&T mode coupling, a piezoelectric transducer for energy harvesting from the end mill tool vibrations and electronics, ensuring data processing and wireless communication functionality.

The key feature of the proposed device is the ability to detect tool condition changes and communicate them to the other devices with a special interest devoted to the architecture of the sensor, its electronics and working principle.

3.1. Mechanical design of rotating shank-type tool condition monitoring device

For the experimental research, the design of a device for monitoring condition of rotating shank-type tools was proposed. The proposed device, according to the obtained FEM study results from the previous chapter, was comprised of a cone-shaped tool holder with three uniformly distributed helical slots on its planar surface, a piezoelectric transducer and a PCBA (printed circuit board assembly). A CAD 3D model of the device that was designed with SolidWorks software is presented in Fig. 3.1., providing the cross-section and exploded views with the elements of the assembly that are defined in Table 3.1.

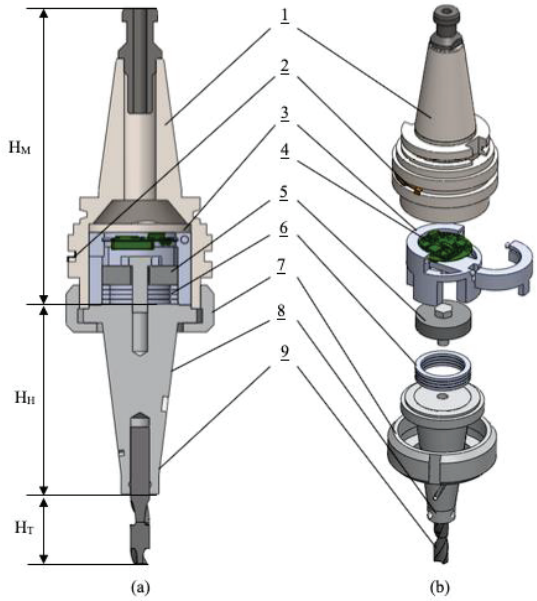

Fig. 3.1. (a) Energy harvester device assembly section view, (b) energy harvester device assembly exploded view

The general geometrical parameters of the proposed vibrational energy harvester are provided in Fig. 3.1., where HM = 156 mm, which is the height of the Morse cone, HH = 100 mm is the height of the cone shaped tool holder, and HT = 36 mm is the free length of the end mill. A more detailed drawing of the energy harvester assembly model is provided in Fig. 3.2.

Table 3.1. Elements constituting rotating shank-type tool condition monitoring device

Number	Component description
1	Holder's Morse cone for the assembly inside CNC centre
2	Antenna for wireless data transmission
3	PCBA holder inside the tool holder
4	PCBA with data processing and transmission components
5	Back-mass
6	Stack type piezoelectric transducer
7	A flange for assembling tool holder with a Morse cone cover
8	A cone shaped tool holder with helical slots
9	The end mill tool

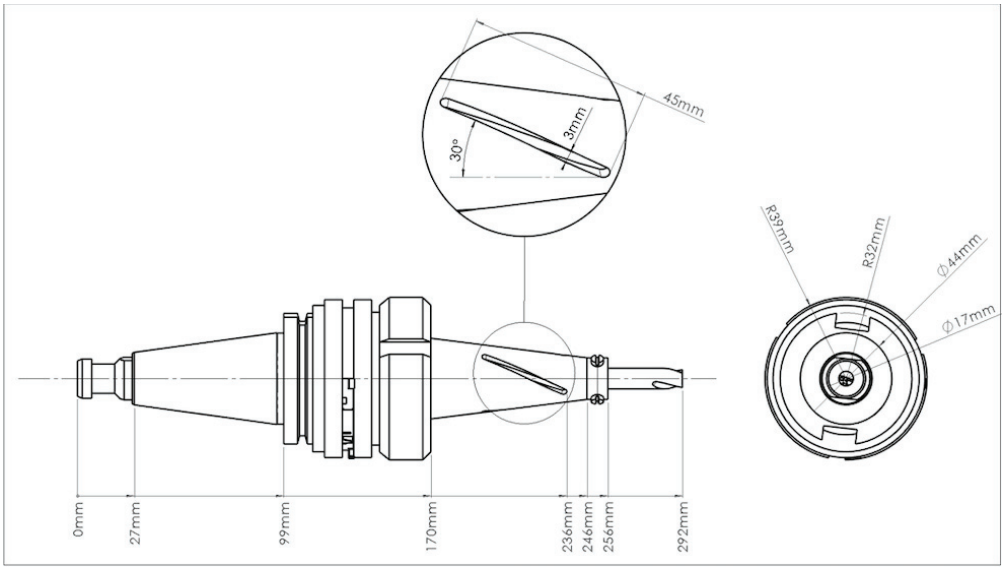

Fig. 3.2. Detailed assembly drawing of designed energy harvesting devices

The 3D model of a horn type tool holder made from steel C45 1.0503 with three uniformly distributed helical slots cut on its planar surface is presented in Fig. 3.2. The size and the shape of the tool holder are identical, as used during FEM modeling (Fig. 2.12.). In this case, three uniformly distributed helical slots of 45 mm in length, 3 mm in width, 3 mm in depth and having a 30º angle with the longitudinal axis of the tool holder are introduced on its cone-shaped surface.

3.2. PCBA design and the schematics of the wireless sensor

Inside the Morse cone, together with the piezoelectric transducer and a back-mass, the PCBA (printed circuit board assembly) is included. PCBA was designed to enable power management, data processing and wireless communication of a sensor. The 3D model of the designed PCBA is presented in Fig. 3.3.

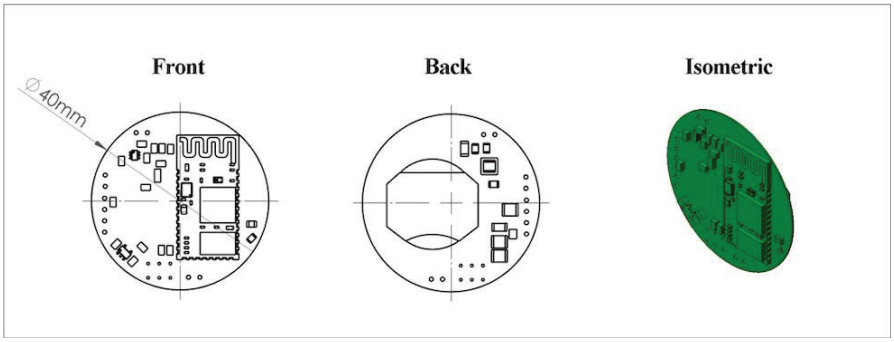

Fig. 3.3. Front, back and isometric views of PCBA with MCU and Bluetooth module; back view of the designed PCBA show introduced placement of the coin type battery

As the proposed device is designed to operate on a tough power budget, it is important that all of the electronics are selected taking low power budget requirements into account. For this reason, an MCU ULP (ultra-low power) microcontroller MSP-430G2553 from Texas Instruments has been selected, which has great performance characteristics for the use in energy harvesting applications. The MCU-MSP430 operates at the range of 1.8–3.6 V, has a standby current of less than 0.5 μA and active current of 230 μA/MHz, its wakeup time is less than 1 μs. Other options that are available on the market for microcontrollers that are designed for low power application are Atmel ATMega 8-bit MCU series, NXP ARM Cortex-M0 based LPC111x series, ST STM32 ARM family MCUs and Nordic Semiconductor Bluetooth system-on-chip modules with ARM Cortex-M4 microcontrollers. Power performance characteristics for some of the mentioned microcontrollers are provided in Table 3.2. The MSP430 series from TI has been selected due to its comparable performance characteristics, as compared to the available alternatives, as well as because of the existing knowledge of the microcontroller architecture.

For wireless communication, a MLT BT-05 BLE 4.0 (Bluetooth low energy) serial communication module is included. This Bluetooth module comes with the operating voltage between 3.6–6 V, standby power consumption of around 90–400 μA, has fast response speed of 400 ms, as well ensuring effective communication distance of 7–10 meters from the transceiver with a maximum transmitter power of 6 dBm. Though the distance of more than 10 meters (up to 60 meters) is possible, the connection quality substantially decreases when the range increases, exceeding 10 meters. On the opposite side of the PCBA, an optional external power supply in the

form of a 3V coin type battery is implemented for the use during the experimental investigation of uninterrupted data transmission.

Table 3.2. Power performance characteristics for some low power microcontrollers that are available on the market

MCU Manufacturer	MCU Type	Operating voltage	Current consumption		
			Active	Stand by	Off mode
Texas Instruments	MSP-430G2553	1.8–3.6 V	230 µA / MHz	< 0.5 µA	< 0.1 µA
Microchip (Atmel)	ATmega128L	2.7–5.5 V	5.5 mA at 4 MHz, 5V	N/A	0.15 µA
NXP	LPC111x	1.8–3.6 V	150 µA / MHz	6 µA	220 nA
ST	STM32L4	1.71–3.6V	120 µA / MHz	35 µA / MHz	330 nA

The electrical schematics of the designed device PCBA are presented in Fig. 3.4. The schematics include a voltage multiplier, which is composed of Schottky diodes (D1A and D1B) and capacitors (C2, C3, C5, C6), to which the generated voltage from the piezoelectric transducer is being fed during the machining operation. The Voltage from the voltage multiplier is fed to charge the capacitor C4. The charge level is measured by the MCU U2 10bit ADC input and compared to a set threshold of the charge level value, which is set in the MCU. In case the measured C4 capacitor voltage level increases above this set voltage threshold level, a load, consisting of resistors R1 and R2, is switched by a Q1 N-channel field transistor, discharging the C4 capacitor. Once the C4 capacitor is discharged, another measuring cycle is initiated.

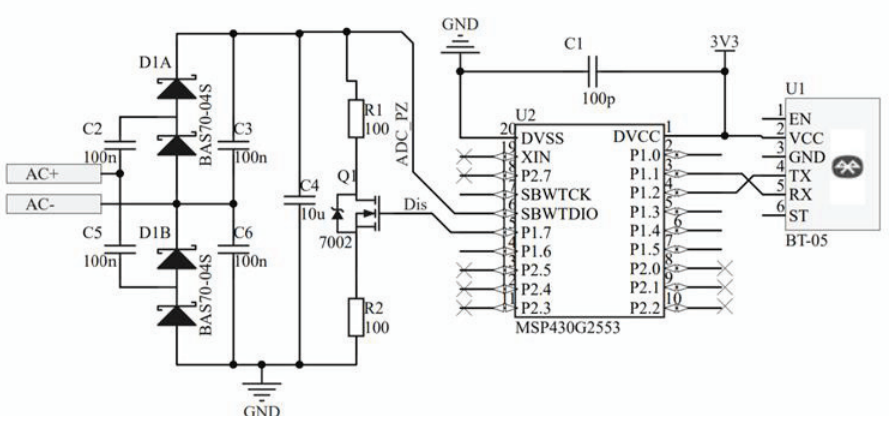

Fig. 3.4. Electrical schematics of the prototype PCBA used with the designed sensor

The voltage discharged from the C4 capacitor is fed to a power accumulation unit, which in the proposed design is a super capacitor, where it is stored and can be

used to power up the electronics of the sensor, providing the self-powering capability. The event of the capacitor discharge is registered by the MCU, and the instance of the event information is sent wirelessly via Bluetooth to another Bluetooth enabled device, such as a smartphone, where time intervals between them are being logged and evaluated.

3.3. The architecture of the device and its working principle

The architecture of the designed device is provided in Fig. 3.5. together with its flow diagram that is depicting its operation during milling, presented in Fig. 3.6.

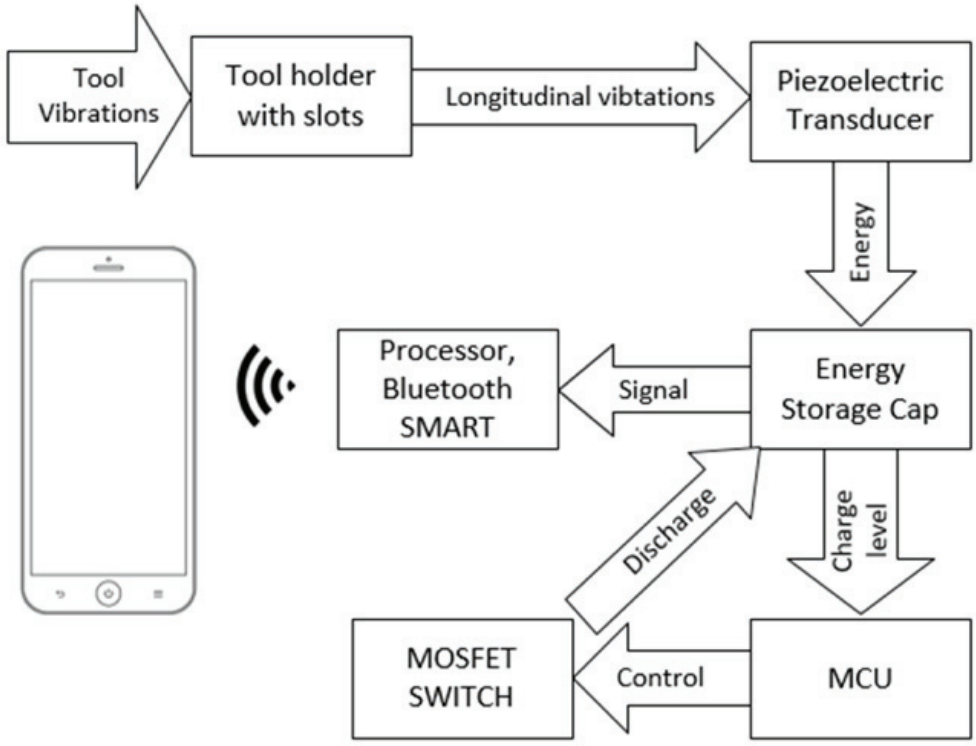

Fig. 3.5. Architecture of the designed wireless sensor system level

The working principle of the proposed device is based on the energy harvesting during the machining operation, implementing rotating shank-type tools. During the operation, as the tool wear condition appears and increases, the torsional forces that are exciting the tool increase as well [70]. These vibrations that are excited in the tool are transferred to the tool holder, where, due to the introduced helical slots, they are partially transformed into longitudinal vibrations, which are transferred to the interface with a piezoelectric transducer, deforming it and producing voltage that is fed to the C4 capacitor.

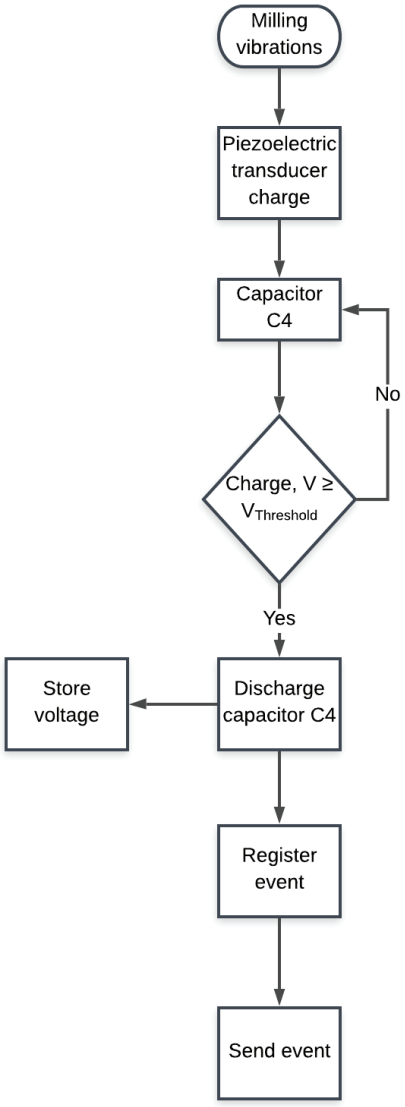

Fig. 3.6. Operational process flow of the designed sensor

In this scenario, an increase in the end mill tool wear condition leads to the increased deformation of the piezoelectric transducer, thus increasing the amount of the generated voltage and reducing the C4 capacitor charging time, this way relating the increase in the end mill tool wear to the decrease in the C4 capacitor charging time. In the sensor, the capacitor charge level is measured by the MCU and is compared to the set voltage threshold level. In case this threshold is reached, the capacitor C4 is discharged into a power storage unit, i.e., a super capacitor or other power cell, and the capacitor discharge event is registered. Then, the information

about the capacitor discharge event is sent wirelessly to a defined auxiliary smart device, such as smartphone.

An important functionality of the sensor is to differentiate between the RUNNING (actual operation) and the IDLE milling condition states. The sensor's process flow for differentiating between these two states is presented in Fig. 3.7.

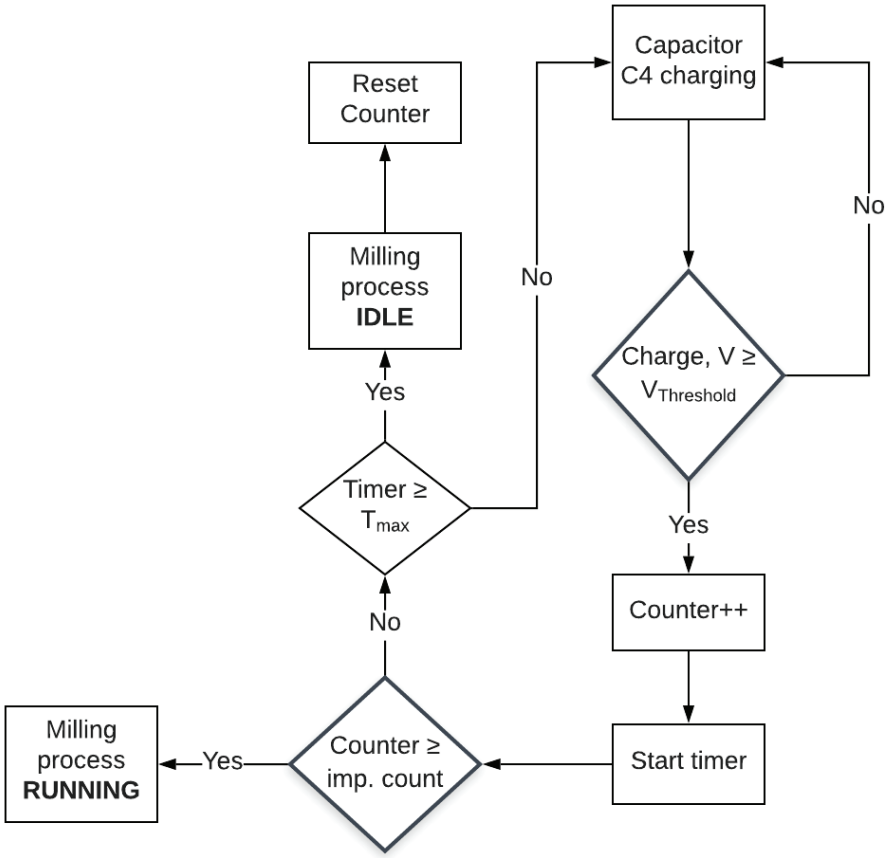

Fig. 3.7. Wireless sensor decision on the flow of operation status process

If the capacitor is charged and its charge level exceeds the specified voltage limit, it will be discharged. In the case of capacitor discharge event, the "counter" value is increased by +1, and the timer is initiated; the "counter" value is used to compare to the "imp. count" value, which is set and represents the number of consecutive capacitor discharge events that are required for the status to be evaluated as actual milling operation, i.e., RUNNING. However, if the "counter" value is lower than the set threshold, the sensor checks if the Timer value has reached or exceeded Tmax. If Tmax is exceeded, it evaluates the milling operation as not running and goes

to the IDLE state. Otherwise, the sensor waits for consecutive capacitor discharge events.

In this case, the Tmax value is set and represents the maximum time interval, during which, if no capacitor discharge event is present, the sensor has to go to IDLE/sleep state.

The primary communication device, to which the information about the capacitor discharge event during the milling operation is sent from the proposed wireless sensor over LAN or PAN network, is defined as an edge device. There, the communication with the edge device is performed over RF using WI-FI, Bluetooth, Bluetooth Smart, ZigBee other communication protocol, depending on the constraints that are set by the required data throughput, the distance from the transceiver, the environment as well as the available device power budget.

In general, the edge devices provide local on-site data pre-processing, data feedback and display, at the same time acting as a gateway to the internet (Fig. 3.8.).

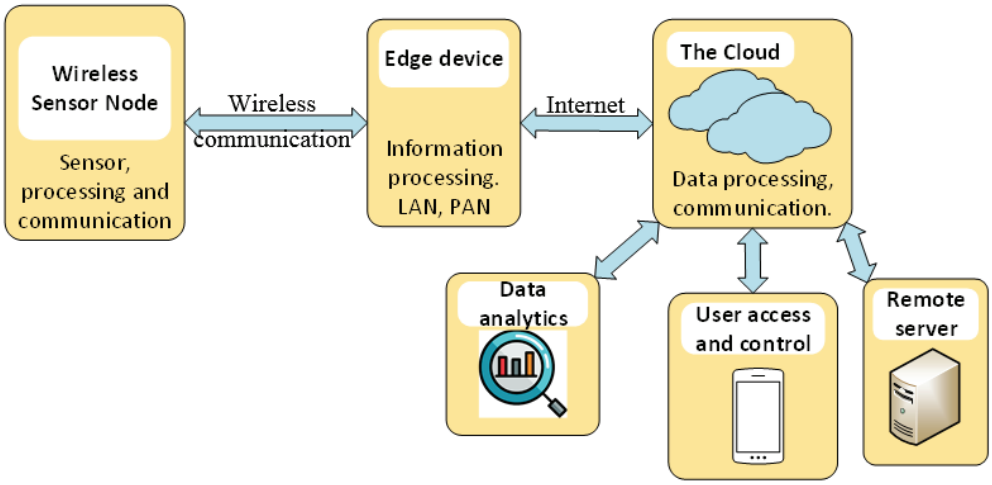

Fig. 3.8. Wireless sensor's network architecture

Through the edge device, the pre-processed data from the wireless sensor node can be sent to the Cloud services for the higher-level data analytics and archiving in remote servers. Such Cloud services enable the user to access and view the collected information in the form of the generated clear data reports over dedicated application. The cloud service interface can as well be used to interact with the device itself, allowing to change its settings or perform other tasks, such as OTA (over the air) firmware updates.

In this research, the role of the edge device has been assigned to a Bluetooth enabled iOS or Android smartphone that is capable of establishing and maintaining a wireless Bluetooth connection with the designed sensor, where the data received from the sensor is displayed in the real-time on the smartphone's screen and at the same time written as a text file on the device's hard drive. This text file is saved and can be

exported for further data processing to other devices, such as PC. Thus, in the following experimental research, the sensor data is not sent via internet to any kind of Cloud service, but it stored on a smartphone. The proposed architecture of the device supports such extensions for the future applications. The operation flow chart for the edge device is presented in Fig. 3.9.

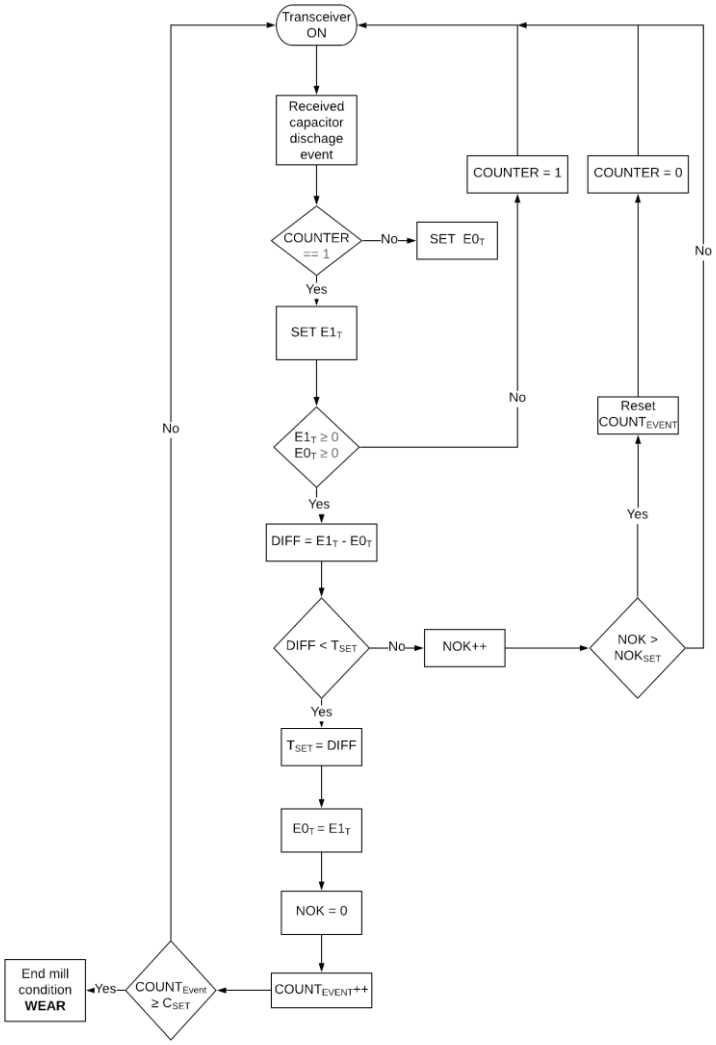

Fig. 3.9. The flow of edge device operation process

There, the condition of the edge device is ON, meaning its transceiver is turned on, and it is ready to communicate information with the sensor. If the information about the capacitor discharge event from the sensor is received, it is stored in the reference value denoted as $E0_T$.

There, $E0_T$ stores the first received time value, representing the capacitor discharge event instance information, which is represented by the time value after

IDLE condition. Subsequently received capacitor discharge event information, which is as well represented by time, is stored in value $E1_T$ container. These time values represent the time instance of the capacitor discharge event.

This process continues until both $E0_T$ and $E1_T$ values are registered, and once this is achieved, the time difference between $E1_T$ and $E0_T$ values is calculated by subtracting them and set to DIFF holder, which has to be checked in comparison to $T_{SET.}$ T_{SET} is a set threshold reference value, which is representing the minimum time interval between the two consecutive capacitor discharge events that can be regarded as a possible tool wear condition occurrence. If this condition is not fulfilled, the process is restarted.

If T_{SET} is higher than the calculated DIFF value, T_{SET} value is updated with DIFF value, and $E0_T$ is updated with $E1_T$ value. This is done so that the consecutive capacitor discharge event occurrences would be compared to the previous event instance, because if the tool condition is starting to wear out, the time interval between two capacitor discharge events will start to reduce after each consecutive capacitor discharge event.

In case all previous conditions are fulfilled, the $COUNT_{EVENT}$ value will be incremented in a continuous loop, until it exceeds set C_{SET} value. If this condition is true, the tool will be evaluated as worn out, and the edge device will send information back to the operator or the machine, informing it about the tool condition in order to prepare for a tool change. There, the C_{SET} value is a set value, representing a threshold of the consecutive decreases in the capacitor discharge events, after which the tool condition can be indicated as worn out.

Conclusions of chapter 3

In this chapter, the design of the end milling tool vibration energy harvester with a wireless sensor, which is used for the detection of the wear condition for the end mill tool, has been presented. The proposed rotating shank-type tool condition monitoring device assembly and operation is described as follows:

- The designed cone shaped tool holder with three uniformly distributed helical slots, assembled together with a stack type d_{33} piezoelectric transducer and an embedded system.
- The designed sensor architecture, consisting of the PCBA, manufactured according to the electrical schematics.
- The architecture for sensor data management by the edge device is provided together with the process flow diagrams, describing how the device operated and how the tool wear condition is detected.

4. EXPERIMENTAL RESEARCH AND PREDICTION OF A ROTATING SHANK-TYPE TOOL CONDITION MONITORING DEVICE

Introduction

This chapter describes the results that have been obtained during the experimental research, performed with a device, designed for detection of rotating shank-type tool wear condition.

The performed experiments evaluated the developed device for the following:

- The vibrational response, when it is assembled in the CNC machining centre;
- The energy harvesting properties from milling tool vibrations during the actual machining operation;
- The effect of the use of the device on the surface roughness of the workpiece;
- The detection of the tool wear condition, expressed as an increase in the capacitor charging rate during the milling operation.

4.1. Vibrational response investigation of a cone shaped tool holder

In order to investigate how the introduction of helical slots affects the vibrational response of the tool holder, two prototypes have been manufactured, according to the prepared 3D CAD model (Fig. 2.12.). Both tool holders were manufactured from the C45 1.0503 steel, as defined during the FEM simulations in the research.

The difference between the prepared prototypes was that one had uniformly distributed helical slots (Fig. 3.2.), machined on its cone shaped surface, while the other was kept without any geometrical alterations. These two manufactured tool holders have been used during the vibrational response study to evaluate whether the introduction of helical slots on the surface of the tool holder results in the increase in longitudinal displacement of the surface, which is intended to be in contact with the piezoelectric transducer. The experimental setup block diagram used for this study is presented in Fig. 4.1., while the actual view from the performed experiment is presented in Fig. 4.2. The experimental setup that was used for both tool holders was identical.

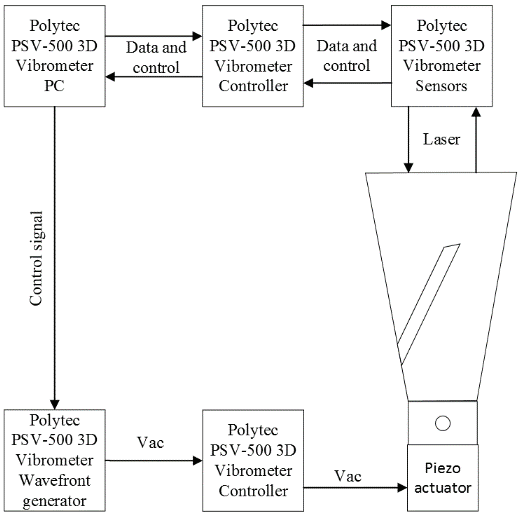

Fig. 4.1. Vibrational response test setup used for the tool holder with and without helical slots

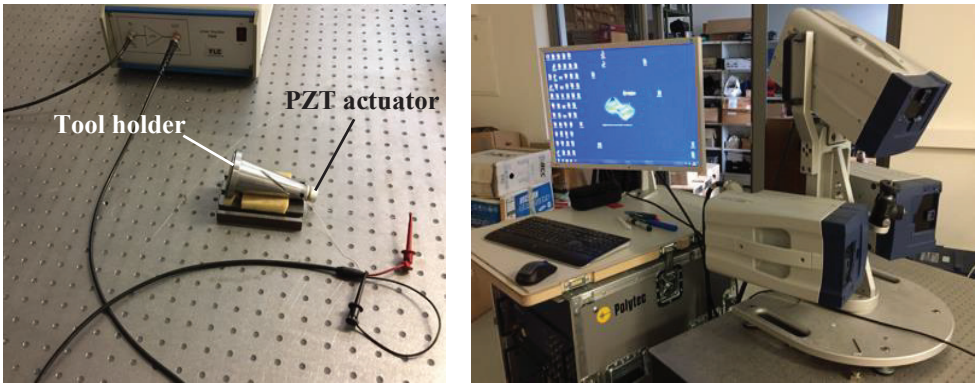

(a) (b)

Fig. 4.2. Tool holder with and without helical slots vibrational response, actual experimental setup: (a) the view of the tool holder with fixed piezoelectric actuator, (b) the view of the Polytec PSV-500 3D laser doppler vibrometer

As presented in the block diagram of the experimental setup, the end of the tool holder, where the end mill tool was going to be fixed, was used as a contact surface with the piezoelectric actuator, exciting the tool holder. The piezoelectric generator was connected to a waveform generator, exciting it by a chirp type signal in the 0–50 kHz frequency range.

A Polytec PSV-500 3D laser doppler vibrometer was used to perform non-contact surface displacement measurements. These measurements were made on the tool holders' surface, which is dedicated to contact with the piezoelectric transducer, see Fig. 4.1. The results from the performed vibrational response experiment are presented in Fig. 4.3.

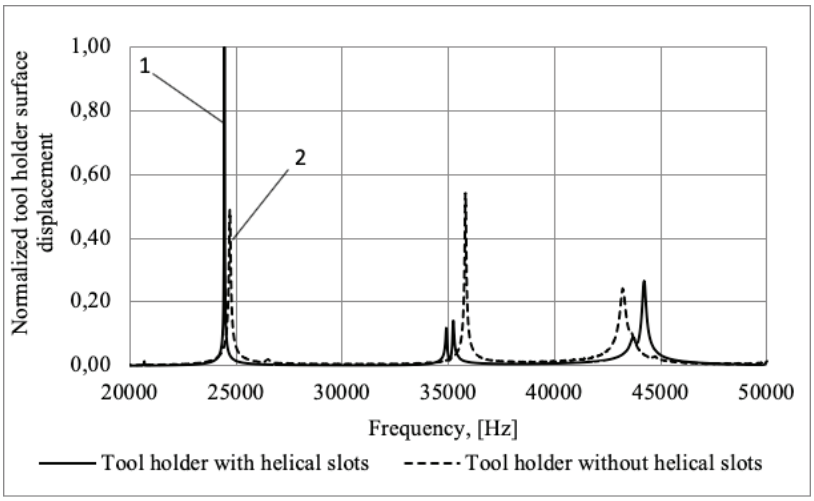

Fig. 4.3. The measured surface displacement amplitudes for the tool holder with and without helical slots excited at axial mode: 1 the tool holder with helical slots, 2 the tool holder without helical slots

It can be seen from the findings that in case of the tool holder with helical slots, if it is excited to resonate at its axial mode, the measured surface displacement amplitude is twice as high, when compared to the obtained results for the tool holder without helical slots, when it is as well excited to resonate at its axial mode. The vibrational response study results agree with the results that have been obtained during the FEM modelling of the tool holder (Fig. 2.18.), showing that under the same excitation condition, the tool holder with helical slots has significantly higher longitudinal surface displacement amplitudes, when compared with the tool holder without these helical slots. The frequency differences, when compared to the FEM model, are due to the different fixing positions that have been used. In FEM model, the tool holder is fixed over its outer flange surface, (Fig. 2.10.) whereas in the experimental study, it is placed on its own free weight; nonetheless, the study results show the trend observed during the FEM studies that the introduction of helical slots on the tool holder lead to the increase of longitudinal vibrations.

This is achieved because the introduction of helical slots enables partial transformation of torsional vibrations that have been generated at the input surface of the tool holder into the longitudinal motion, reinforcing the already existing longitudinal vibrations. These combined longitudinal vibrations are transferred through the tool holder, deforming a piezoelectric transducer.

4.2. An experimental research of vibrational energy harvester response to the impact excitation

The second stage of the experimental research was performed to investigate the vibrational response of the developed device during the impact test. For this, the cone shaped tool holder with three uniformly distributed helical slots on its cone shaped surface was assembled together with three flute end mill, axially poled PZT-5H

piezoelectric transducer, aluminium 6082 back mass and a wireless sensor with an embedded system, all of which were installed inside the Morse cone mounted on the spindle. The whole device was assembled inside the Leadwell V-20 CNC milling centre's spindle, as provided in the experimental setup block diagram in Fig. 4.4.

In order to determine the vibrational response and the resonant modes of the assembled device, an impact test has been performed, where the teeth edge of the end mill tool has been excited mechanically. The response of the excitation was recorded in the form of voltage output from the piezoelectric transducer. For this reason, the piezoelectric transducer output to the wireless sensor electronics was disconnected and instead connected directly to a PicoScope oscilloscope, which was used to capture the change in the voltage, generated by the piezoelectric transducer during the impact test. This piezoelectric transducer output signal is recorded by a dedicated PicoScope software package and can be analysed later.

The results of the voltage output over the time from the piezoelectric transducer during the impact test, which were recorded by a dedicated PicoScope software package, are presented in Fig. 4.5.

From the presented results, a very interesting phenomenon has been observed, i.e., the amplitude modulation of the exponentially decreasing transient vibrations, as well known as the beating phenomenon. The beating phenomenon is an amplitude modulated response, i.e., a combination of two vibration signals with slightly offset frequencies from one another. From these results (Fig. 4.5.), it is visible that two close longitudinal and torsional vibrational modes interfere constructively and destructively, causing signal amplitude modulation in a regular pattern.

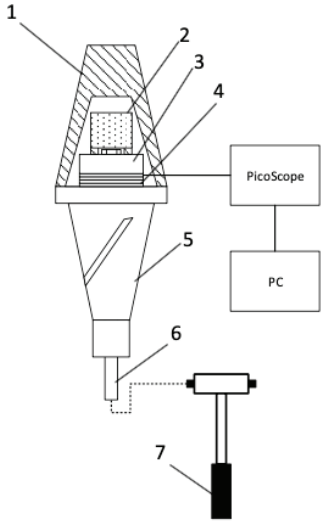

Fig. 4.4. Vibration energy harvester impact test setup: 1 – Morse cone, 2 – embedded system, wireless sensor, 3 – aluminium back mass, 4 – axially poled piezoelectric transducer, 5 – horn type tool holder with helical slots, 6 – three flute end mill tools, 7 – device excitation tool

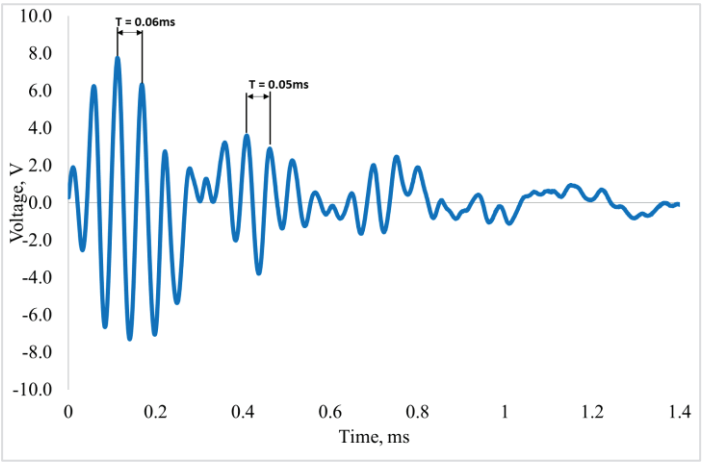

Fig. 4.5. Voltage output from a piezoelectric transducer during the performed impact test

This observed beating frequency can be expressed by the following formula:

$$f_b = |f_T - f_L|, \tag{4.1}$$

where f_T and f_L are torsional and longitudinal vibrational mode frequencies of the tool holder [71].

Such high-frequency spontaneous excitation of the milling tool's axial vibration is similar to the vibrational milling, where the tool is excited by additional high-frequency vibrations. In such case, a versatile method of transforming the milling vibrations into voltage is proposed, where the energy of the cutting tool's torsional vibrations is captured by a piezoelectric transducer, while at the same time being a low-frequency oscillating milling method, which does not require the need for an additional piezoelectric actuator.

This widely applicable cutting technology, which is able to handle a broad range of machining shapes and materials, is ideal for cutting difficult-to-cut materials. It is as well the state-of-the-art technology, which reduces risks associated with the machining these materials, such as the nesting of chips and built-up edges.

In the proposed prototype, the torsional vibration generated during the milling operation lead to the simultaneous axial deflection and elongation of the slotted cone shaped tool holder, i.e., the elongation and contraction of the structure, which is consistent with Bayly's model [71]. Then, the excited longitudinal vibrations are transferred through the body of the tool holder, deforming the embedded piezoelectric transducer and generating charge.

4.3. An experimental research of piezoelectric energy harvesting during the milling operation

The third part of the experimental research was focused on evaluating the energy harvesting properties of the developed device under actual milling conditions and its dependence on the milling process parameters.

The milling process is described as an interrupted cutting process, because during this process, the rotating teeth of the end mill tool are subjected to an impact force cycle, when they enter and exit the workpiece, exciting the tool and machine tool vibrations. The intensity of these vibrations induced in the end mill tool depends on the manufacturing regimes and the condition of the tool itself, such as its tooth cutting edge wear. This means that it is not possible to avoid the milling tool vibrations, though such vibrations could be harvested and converted to electrical voltage for other uses.

Exploiting machine vibrations is one of the most effective forms for harvesting the environmental ambient energy, which can further be used to power small sensor, eliminating the need for wired connections and frequent maintenance, when compared to the use of other types of power supply.

The experimental test setup block diagram, which was used to evaluate the energy harvesting properties of the developed device during the milling operation, is presented in Fig. 4.6. with an actual view inside CNC milling centre, as presented in Fig. 4.7.

There, the full energy harvester assembly has been prepared with a spindle of the Leadwell V-20 CNC milling centre. The device configuration matched, as provided in Fig. 3.1., consisting of three flute HSS end mill fixed inside the tool holder, and on the other side, the axially polled piezoelectric transducer, the back mass and an embedded system with a wireless communication capability, embedded inside the Morse cone.

During the actual milling operation, the two tool holders, one with helical slots and one without, were used. Two different configurations of the device allowed to assess how strongly the helical slots on the planar surface of the tool holder affect the amount of energy collected by the piezoelectric transducer during the milling process.

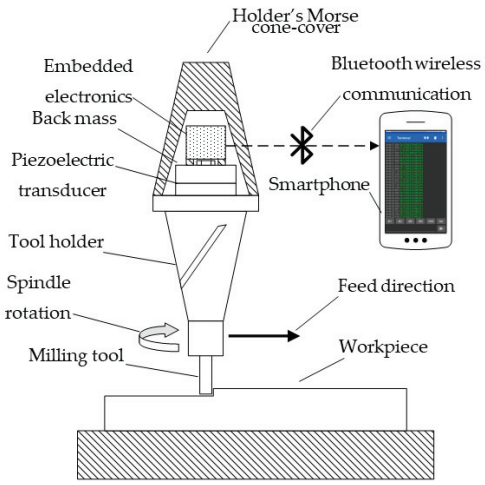

Fig. 4.6. Vibration energy harvester device for energy harvesting during the milling operation test setup

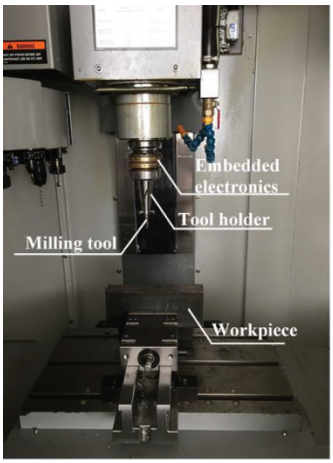

Fig. 4.7. Vibrational energy harvester device, assembled inside the CNC milling centre

During the milling operation, a block LxHxB 250mm x 50mm x 50mm of 1.0037 steel has been machined as a workpiece, for which the milling process parameters were selected according to the used end mill tool and workpiece material, as provided in Table 4.1.

During the milling operation, the wireless sensor was configured to send the information representing the actual C4 capacitor (Fig. 3.3.) charge voltage level via Bluetooth every 500 milliseconds to a Bluetooth enabled smartphone. The received information was then stored inside the hard drive of the smartphone in a form of a text file. The text file included the received message with a timestamp and C4 capacitor charge level at the instance, when it was sent from the sensor. This information, stored inside the smartphone, was extracted for further data processing and evaluation.

Table 4.1. The selected milling process parameters used during the experiment

Parameter	Spindle speed	Feed speed	Feed per tooth	Depth of cut
Value	1210 RPM	148 mm/min	0.041 mm/tooth	1 mm

A wireless sensor was configured to discharge the capacitor C4 if its voltage level reached or exceeded a set threshold of 0.7 V and reset and repeat the capacitor charging process.

The results recorded on the smartphone from the experiment during the milling operation for capacitor charging levels over the time are presented in Fig. 4.8.

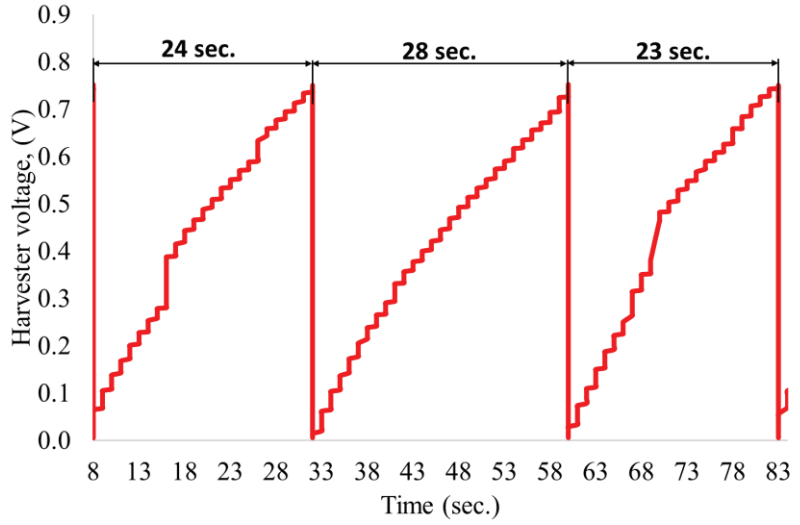

(a)

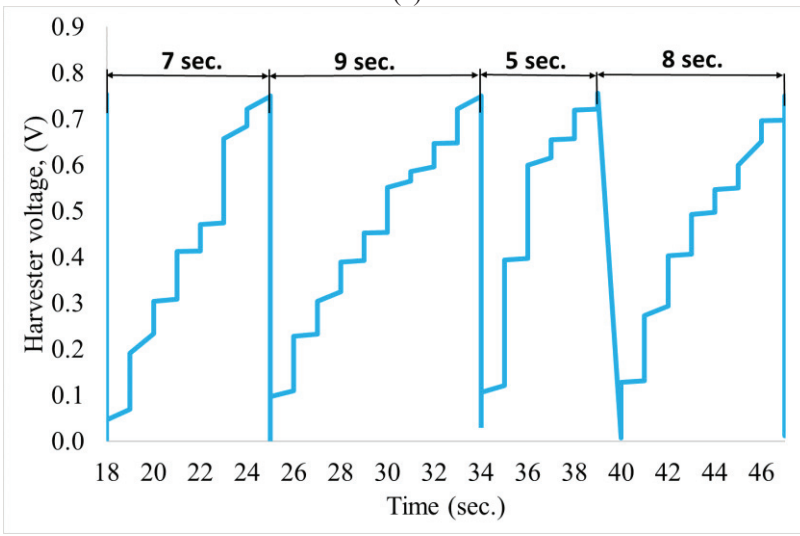

(b)

Fig. 4.8. Experimental results of capacitor C4 charging times when tool holder without (a) and with (b) slots is used during the milling operation

Fig. 4.8. (a) represents a part of these results, showing the capacitor charging period during the milling operation, when the tool holder without helical slots is implemented, and Fig. 4.8. (b) shows the capacitor charging rate, where the tool holder with three uniformly distributed slots is assembled with the analysed device.

It can be seen from the obtained results that the average capacitor charging period to reach the set threshold of 0.7 volt. is 7.25 seconds for the tool holder with helical slots, and in case the tool holder without slots is used, the average capacitor charging time is 25 seconds. The results show that the charging of the capacitor is

faster by more than 3.4 times for the tool holder with helical slots; this means that up to 3.4 times more vibrational energy is harvested during the milling operation over the same time interval if a device is implementing a tool holder with helical slots. The results of the experimental study are summarized in Table 4.2.

Table 4.2. Capacitor charging time results for the tool holder with and without helical slots

Tool holder	Depth of cut	Average capacitor charge time	Difference
With slots	1 mm	7.25 sec.	3.44 times
Without slots	1 mm	25 sec.	

In the next step, the experiment was repeated, but this time, the milling process parameter, i.e., the milling depth, has been increased. The milling depth was increased from 1 mm (used in the previous experimental step) to 1.5 mm, leaving all other process parameters and test setup the same, as defined in Fig. 4.3. and Table 4.1. The experiment was repeated for both assemblies with a tool holder that has helical slots and a tool holder without helical slots. The results for this experiment iteration with an increased milling depth are presented in Fig. 4.9. The results of the experimental study are provided in Table 4.3.

The obtained results show that when the milling depth is increased to 1.5 mm, the average capacitor C4 charging time to the set threshold of 0.7 volt. is 4.7 seconds for the tool holder with helical slots and 18.7 seconds for the tool holder without helical slots.

The results show that for the device implementing helical slots, the capacitor charging time is 4 times faster, compared to a device, using the tool holder without helical slots, meaning that four times more vibrational energy is harvested during the milling operation over the same time period.

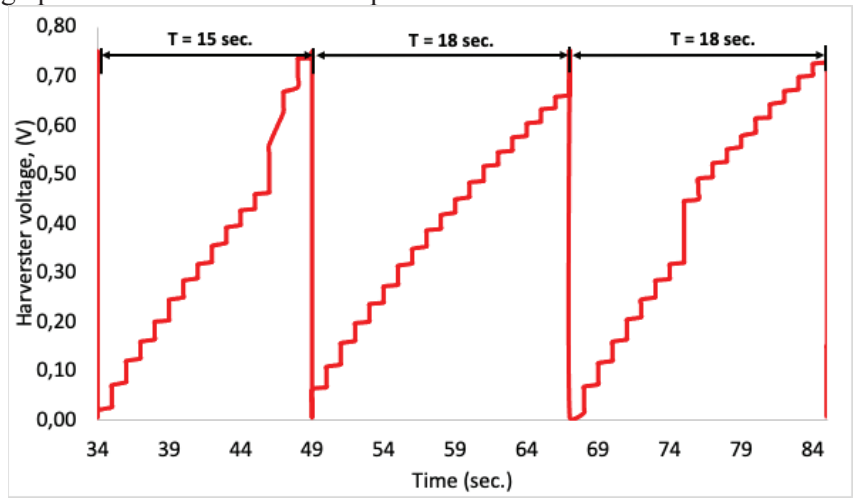

(a)

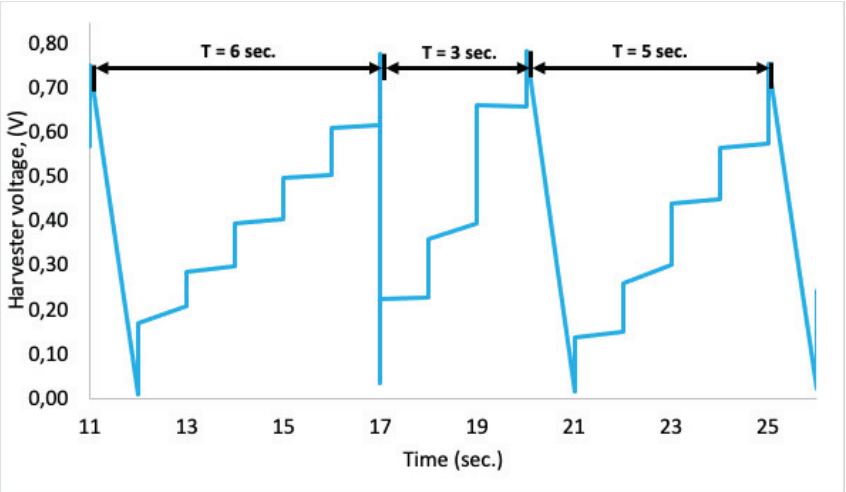

(b)

Fig. 4.9 Experimental results of capacitor C4 charging period when the tool holder without (a) and with (b) helical slots is used during the milling operation where the milling depth is 1.5 mm

Table 4.3. Capacitor charging time results for the tool holder with and without helical slots

Tool holder	Depth of cut	Average capacitor charge time	Difference
With slots	1.5 mm	4.7 sec.	3.97 times
Without slots	1.5 mm	18.7 sec.	

In both cases of the performed experiments, the capacitor charging time decreases, as compared to the results from Fig. 4.8., which means that more vibrational energy is harvested when the milling depth parameter is increased from 1 mm to 1.5 mm. For the tool holder without helical slots, it increased by 30%, and for the tool holder with helical slots, by 35%. This means that the increase in the milling depth results in higher torsional vibrations, excited in the end mill tool during the operation.

The last iteration of the experiment was performed with another milling process parameter, i.e., the spindle speed, which increased from 1210 RPM to 1500 RPM, while other process parameters were maintained with the milling depth at 1.5 mm. The experiment was performed to evaluate the vibration energy harvesting properties for both tool holders with and without helical slots, and the results are presented in Fig. 4.10.

The results show that the increase in spindle speed from 1210 RPM to 1500 RPM leads to a significant decrease in the capacitor charging time until the set threshold is reached for both tool holders with and without helical slots.

The recorded average C4 capacitor charging period for a device assembled with the tool holder without helical slots was 1.8 seconds, and for the tool holder with

helical slots, it was 0.44 seconds. The results show that, as in the latter step of the experiment, the difference between implementing the tool holder with helical slots results in 4 times faster capacitor charging, compared to when the device is implemented with a tool holder without helical slots. The results are summarized in Table 4.4.

An important observation is that the capacitor C4 charging time decreased significantly for the tool holder with or without helical slots with an increase in milling depth and spindle speed, which means that the process parameters have a significant effect on the amplitude of vibrations excited in the end mill tool during the operation.

The increase in the amount of the harvested energy can be anticipated with an increase in the spindle speed, because it leads to the increased frequency of tool teeth interaction instances with the workpiece, thus leading to the increased frequency of the milling tool excitation events. The increase in milling depth leads to higher forces

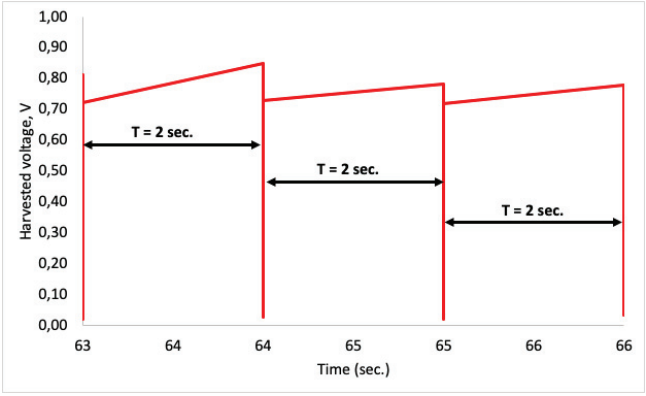

(a)

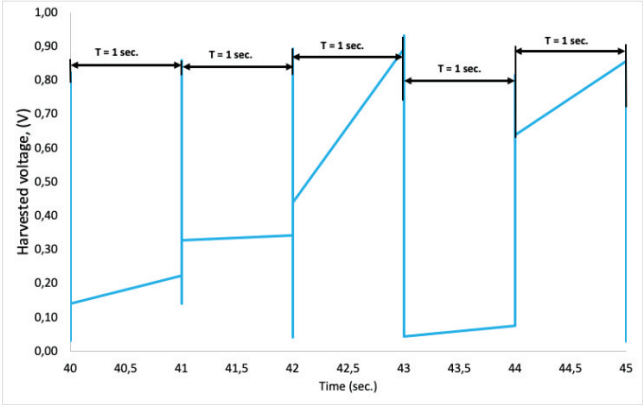

(b)

exerted on the milling tool cutting edge during its impact cycle as well.

Fig. 4.10. Experimental results of capacitor C4 charging times when the tool holder without (a) and with (b) helical slots is used during the milling operation when the spindle speed is increased from 1210 RPM to 1500 RPM

Table 4.4. Capacitor charging time results for the tool holder with and without helical slots

Tool holder	Spindle speed	Depth of cut	Average capacitor charge time	Difference
With slots	1500 RPM	1.5 mm	0.44 sec.	4.09 times
Without slots	1500 RPM	1,5 mm	1,8 sec/	

In general, the increase in the harvested energy, where the tool holder with uniformly distributed helical slots is used during the milling operation, can be attributed to the appearance of an L&T mode, as observed during the frequency response evaluation of the developed device (Fig. 4.5.). When the device is excited at the frequency of L&T mode coupling, the radial and tangential milling force components that are acting on the end mill tool are transferred to the tool holder, where they are transformed into longitudinal deformations exciting piezoelectric transducer, where this effect is not present for the tool holder without helical slots.

4.4. An experimental research for detecting milling tool wear from piezoelectric energy harvester during the milling operation

The last part of the experimental study was focused on evaluating whether the proposed device can be used to detect the end mill tool wear condition during the actual milling operation. The tool wear condition is to be expressed as a change, i.e., an increase in the C4 capacitor charging rate. The ability to use the designed device as a tool wear condition monitoring sensor is based on the operation where:

- As the milling tool cutting edge wear increases, the torsional forces increase as well, which excite the tool during its tooth impact with the workpiece cycles;
- The torsional vibrations are transferred through the tool to the cone shaped tool holder with uniformly distributed helical slots, where they undergo partial transformation into longitudinal vibrations;
- The longitudinal vibrations are then transferred through the tool holder to the axially polled piezoelectric transducer, deforming it and producing the charge;
- The voltage generated by the piezoelectric transducer is used to charge the capacitor C4 until the set voltage threshold level;
- When the capacitor charge level is reached or exceeded, it is discharged, and the information about the capacitor discharge event is sent wirelessly to the auxiliary smart device;
- The auxiliary smart device evaluates the received data, i.e., time periods between the capacitor discharge events, and can inform about the tool wear

condition if the time required for the capacitor to charge until the set threshold level continuously decreases, reaching a certain set value.

The working principle of the proposed wireless sensor is that with an increased wear of the tool's cutting edges, the capacitor C4 charging time decreases, thus forming a relationship between the capacitor charging rate and the end mill tool condition. As provided in Fig. 3.8., the auxiliary smart device, i.e., the "edge device", which is receiving capacitor discharge event information from the sensor, can evaluate whether the capacitor charging time is gradually decreasing, reaching a value, which can be regarded as a tool wear condition, requiring for the operator or the machine to plan a tool change event before the tool condition negatively affects the quality of the parts being machined or reaches a critical tool failure.

The setup for this step of the experimental study has been left the same, as defined in Fig. 4.6., where the sensor has been assembled together with a cone shaped tool holder, implementing three uniformly distributed helical slots, the Morse cone and an end mill tool (Fig. 3.2.), all assembled inside Leadwell V-20 CNC centre. The capacitor C4 discharge threshold level has been left the same as well, equal to 0.7 volts. If the capacitor charge exceeds this threshold, it is discharged, and the information about this event is sent wirelessly over Bluetooth. As in the previous steps, a Bluetooth enabled smartphone was used as the receiving device.

The workpiece was changed to aluminium 6082 block L x H x B 300 mm x 25 mm x 150 mm to be machined with two flute carbide end mill tools, having a 25□ helix corned radius. The selected end mill tool is designed for specifically machining the aluminium alloys. According to the selected workpiece material, the end mill tool milling process parameters were set as provided in Table 4.5.

Table 4.5. Milling process parameters used during the experiment set up to evaluate the end mill tool wear condition

Parameter	Spindle speed	Feed speed	Feed per tooth	Depth of cut
Value	4000 RPM	300 mm/min	0.037 mm/tooth	1 mm

Two end mill tools of identical design were used for the experiment. The difference between the used end mills is that one of the end mills was in a new condition, while the other had an artificial and gradual deterioration, which was achieved by increasing the damage to the cutting edges of the tool teeth.

For the one end mill, the damage to its cutting edges was formed at three locations, where the crater wear was formed ≤ 0.05 mm, the flank wear ≤ 0.5 mm, and the corner wear ≤ 0.05 mm. A magnified view of these end mill tool tooth wear conditions is presented in Fig. 4.11.

The results of the experiment evaluating the capacitor charging time during the milling operation for new and worn out end mill tool conditions are presented in Fig. 4.12.

It can be seen that when completely new end mill tool is used during the milling operation, the average capacitor charging time until the set threshold of 0.7 V is 40 seconds (Fig. 4.12. (a)), while for the milling tool with worn out cutting edges as

provided in Fig. 4.11., the average capacitor charging time decreases to around 7 seconds (Fig. 4.12. (b)); these results show that for the worn out end mill tool during the milling operation, the capacitor charging time is around 6 times faster when compared with the use of a new end mill tool. The experimental study results are presented in Table 4.6.

Table 4.6. Capacitor charging time comparison for the worn out and new end mill tools

End mill tool condition	Average capacitor charge time	Difference
New	7 sec.	5.7 times
Worn out	40 sec.	

As already discussed, this is achieved because the increase in the milling tool teeth cutting edge wear leads to higher torsional forces exerted on the tool during its impact force cycles with the workpiece during the milling operation. These torsional forces increase with the increase of the tool wear condition as well leading to the increase in longitudinal vibrations converted from the torsional vibrations by the cone shaped tool holder that deform and excite the piezoelectric transducer charging C4 capacitor.

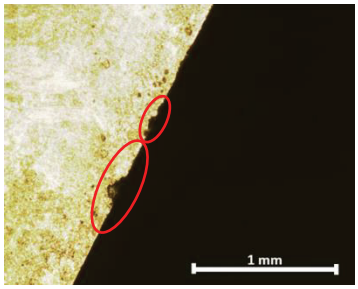

(a)

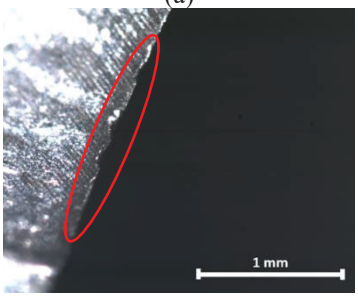

(b)

Fig. 4.11. (a) and (b) views of the edge wear, artificially formed on the end mill, used during experiment, evaluating worn out tool condition

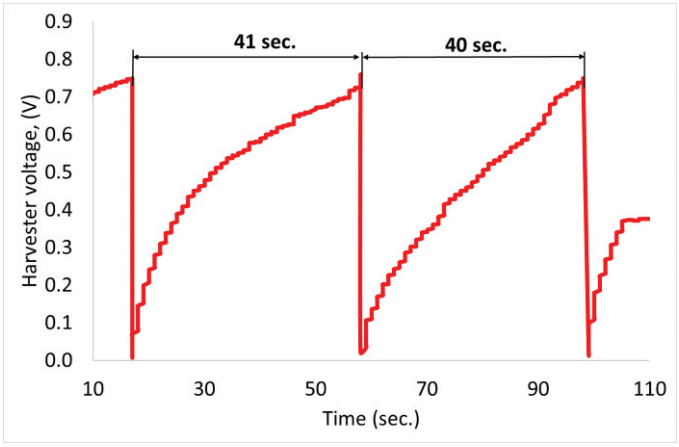

(a)

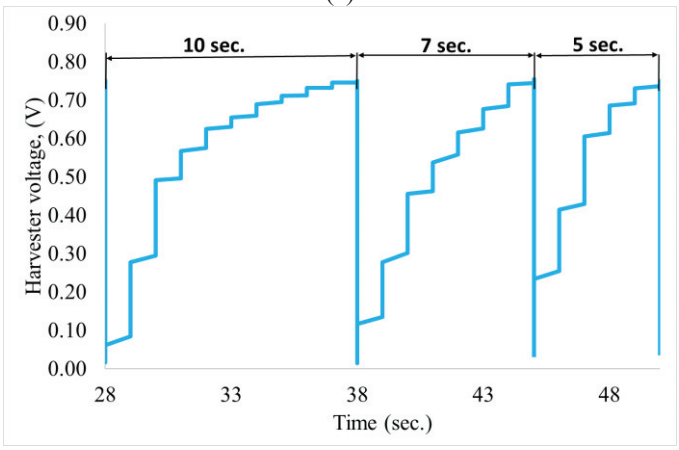

(b)

Fig. 4.12. Average capacitor charging times where (a) is a new, (b) is a worn out end mill tool, used during the milling operation

From the obtained results, it is possible to conclude that the proposed wireless sensor design with a cone shaped tool holder that is implementing uniformly distributed helical slots can be used in the milling operation to detect the degradation in the milling tool condition, i.e., wear, which can be expressed as a property of the increase in the capacitor charging rate. During the milling operation, with an increase in wear of the milling tool, a significant increase in charge, generated by the piezoelectric transducer, has been observed as well. This harvested ambient energy can be used not only as a milling tool condition indicator, but it can be stored and utilized later to power the wireless sensor, enabling self-powering functionality of the device.

After the milling operation with worn out and new end mill tools was performed (worn out condition for milling tool is defined in Fig. 4.11.), the workpiece surface roughness has been evaluated in order to understand the impact that the introduction of helical slots on the tool holder had on the dynamic characteristics and dynamic

stability of the machining process. The surface roughness measurement of the workpieces was performed with Mitutoyo SJ-210 portable surface roughness tester, performing R_a test point measurements. Table 4.7. and Figure 4.13. present workpiece surface roughness measurement results from the machining with a new end mill, using the tool holder with and without helical slots.

Table 4.7. Workpiece surface roughness parameters for the tool holder with and without slots, employing new end mill tool during the machining operation

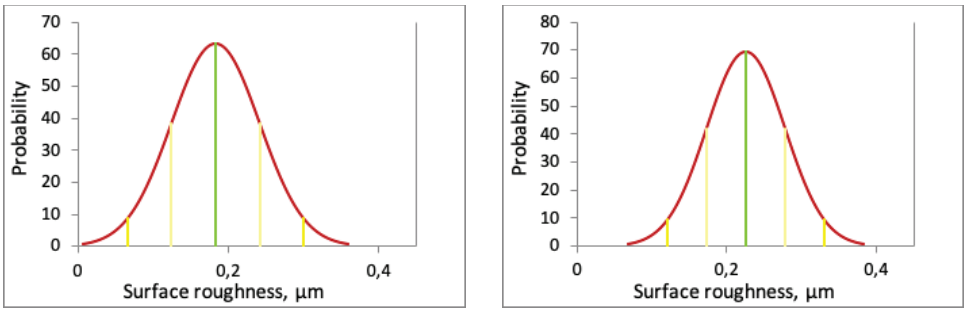

(a) (b)

Tool holder type	Min, Ra	Max, Ra	Mean, Ra	Range, Ra
Without slots	0.114 µm	0.486 µm	0.183 µm	0.372 µm
With slots	0.15 µm	0.391 µm	0.225 µm	0.241 µm

Fig. 4.13. Normal distribution of workpiece surface roughness measurement results after milling with a new end mill for the tool holder (a) without slots and (b) with slots

The surface roughness results, presented for a workpiece machined with a new end mill tool, show that the surface roughness mean value, where the tool holder with helical slots is used, is 18.6% lower than for the tool holder without helical slots, but the range of the measured surface roughness values (spread) is 35% lower. Thus, it seems that due to the introduced torsionality, the stiffness reduction of the tool holder, when machining with a new end mill tool, lower surface quality for the workpieces can be expected, but the surface quality variance shall be lower.

Table 4.8. and Figure 4.14. present the results of the measurement of the surface roughness of the workpiece after it has been machined with a worn-out tool, using the tool holder with and without helical slots.

Table 4.8. Workpiece surface roughness parameters for the tool holder with and without slots, employing worn out end mill tool during the machining operation

Tool holder type	Min, Ra	Max, Ra	Mean, Ra	Range, Ra
Without slots	0.16 µm	0.485 µm	0.275 µm	0.325 µm
With slots	0.188 µm	0.365 µm	0.265 µm	0.177 µm

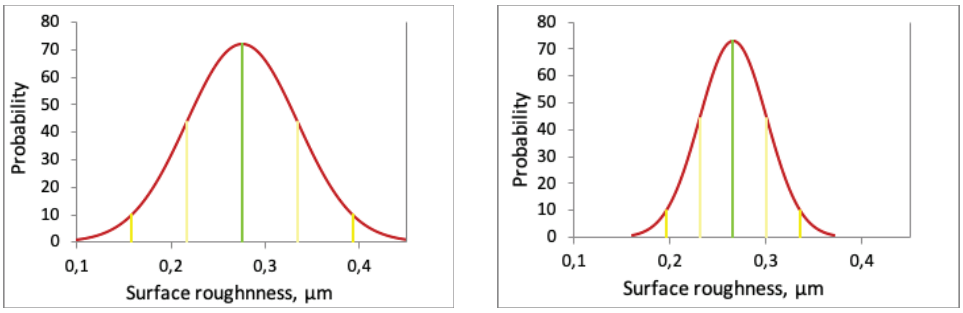

(a) (b)

Fig. 4.14. Normal distribution of the workpiece surface roughness measurement results after milling with a worn out end mill, using the tool holder (a) without slots and (b) with slots

As the worn out end mill tool is used for machining aluminium workpiece, the surface roughness results for the tool holder with helical slots show that the mean measured values are almost the same, when compared to the results obtained for the tool holder without helical slots, and the spread of the measured values (variance) is reduced even more by 45.6%, when the tool holder with helical slots is used. Now, these results show that as the wear of the end mill tool increases, the beating phenomenon, as seen in Fig. 4.5., during the impact test, becomes more dominant in the tool holder with helical slots, creating a combination of longitudinal and torsional mode frequency response in the tool, somewhat replicating effects used in ultrasonic machining, leading to workpiece surface quality improvement, prolonging useful lifetime of the tool. A further investigation is necessary to evaluate the influence of helical slot geometrical parameters on the tool holder stiffness during the machining operation and the dynamic response of the tool holder.

4.5. Experimental research measuring cutter wear with wireless sensor node by applying machine learning models

In the next step of the experimental study, the ability of the proposed sensor node to detect gradual tool wear during the milling operation was investigated. For this purpose, the device (Figure 3.1.) was assembled with sharp (new) four flute D10 mm HSS end mill tool to machine a L x H x B 250 mm x 50 mm x 50 mm 1.0037 type steel workpiece top surface under process parameters as defined in Table 4.9.

Table 4.9. Milling process parameters used during the experiment set up

Parameter	Spindle speed	Feed speed	Feed per tooth	Depth of cut
Value	1210 RPM	148 mm/min	0.031 mm/tooth	1 mm

The experimental study was performed by machining the workpiece top face 61 times continuously starting with a sharp (new) end mill tool to gradually (over milling operation) achieve its wear. During the milling operation of the workpiece top surface, once the machining was started, the data from the sensor node with capacitor charge level was sent every 250 ms. For receiver, a smartphone with Bluetooth connectivity

was used to visually present the data on the screen in real time and store the data for later processing. Each time the milling operation of the workpiece top face was completed, its surface roughness has been measured and logged at 15 different points using Mitutoyo SJ-210 surface roughness tester. The flowchart of the experiment process steps for each milling iteration during the experimental execution is presented in Figure 4.15. Two parameters were recorded during the experiment, i.e., the capacitor charge level continuously during the actual milling and the workpiece surface roughness measurements after each milling iteration. The two recorded parameters from the sensor node were subjected to SVM (support vector machine) based prediction model in order to evaluate if they can be used to detect gradual tool wear in the real time during the milling operation, expressed as relationships between the change of capacitor charge level and an increase in the workpiece surface roughness.

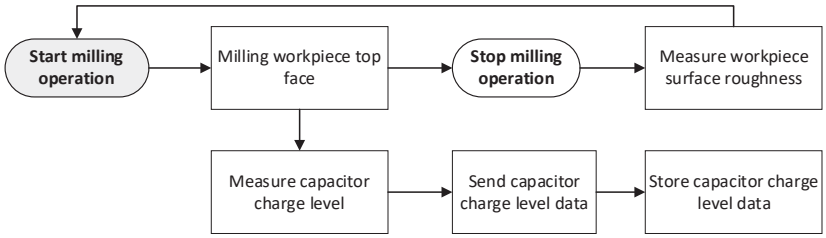

Fig. 4.15. Process steps flow chart used during the experiment execution

Each milling iteration of the workpiece top surface took on average 10 minutes, during which 2400 data points have been recorded for the capacitor charge level, and 15 different surface points were taken to measure the average surface roughness after the milling operation. The average values of the surface roughness are considered the output of SVR model. However, the raw data, representing capacitor charge level measured every 250 ms, are not very suitable as input for the model. Therefore, seven common statistical measures [72] have been calculated from the distribution of capacitor charge level as provided in Table 4.10.

Table 4.10. Calculated statistical features used as SVR model input data

Feature name	Explanation
Avg	The average value of capacitor charge level values
Var	The variability value of capacitor charge level values
Sd	The standard deviation of capacitor charge level values
ACorr	The autocorrelation value of charge level values
$\boldsymbol{M_4Avg}$	4 data point simple moving averages of charge level values
InterQ	The interquartile value of charge level values
Energy	The absolute energy od charge level values

The feature Avg is a simple average value of all 2400 data points, denoting capacitor charge level. The variation Var and standard deviation Sd are calculated accordingly.

The autocorrelation function (ACF) is a useful characteristic for finding repeating patterns. This characteristic shows the degree of similarity between the values of the same variables over two time intervals. This concept was used for defining the attribute ACorr, which provides the average value of autocorrelations, calculated between two measures of capacitor charge level at times x_t and x_{t-k}:

$$ACorr = \frac{1}{n-1}\sum_{i=1}^{n} ACF(x_i, x_{i-k}), k = 1,2,3 \ldots, \quad (4.2)$$

where value k is the time interval (the lag), which represents the autocorrelation between values that are one time interval apart.

The feature M_4Avg calculates the moving averages. In the analysed case, four data points are taken and their average is calculated:

$$MAF = \frac{(x_i + x_{i+1} + \cdots + x_{i+(M-1)})}{M}, \quad (4.3)$$

$$M_4Avg = \frac{1}{n-(M-1)}\sum_{i=0}^{n-(M-1)} MAF_i, \quad (4.4)$$

where n – data points, M – the size of the sliding window and in the analysed case $M = 4$.

Another quite informative characteristic is interquartile InterQ, which calculates the difference between the third quartile and the first quartile for data:

$$InterQ = Q_3 - Q_1, \quad (4.5)$$

where Q_1 is the first quartile and Q_3 – the third quartile.

Feature Energy is the sum over the squared data values:

$$Energy = \sum_{i=0}^{n-1} (x_i)^2. \quad (4.6)$$

Three specific measures have been derived using the expert knowledge:

- *BigV* provides the percentage amount of very high values of capacitor charge level, $x_i > 360, \ \ i = \overline{1,n}$. It has been noticed that the amount of such values has a positive relationship with the surface roughness, and the correlation coefficient is equal 0.811.
- $Signal_{jump}$ provides a sum of squared differences $(\Delta x_i)^2$, including the condition: value $(\Delta x_i)^2$ must be more than 0.9 quantile of data points differences, $Q_{\Delta x_i}(p), \ p = 0.9$:

$$Signal_{jump} = \sum_{i=0}^{n-1} (\Delta x_i)^2 > Q_{\Delta x_i}(0.9), \quad \text{where } \Delta x_i = (x_{i+1} - x_i), \quad (4.7)$$

where Q – quantile function, $p -$ probability value, $0 < p < 1$. This feature highly correlates with the output (see Table 4.10.).

- *Avg_cycle* is the average length of one capacitor charge cycle, until the set threshold level. The end of the cycle is determined if the difference between

data points is relatively large: $\Delta x_i > h$. The most appropriate threshold value $h = 150$ was determined experimentally. The average cycle length *Avg_cycle* is calculated considering all recorded lengths at the capacitor charge level. It has been observed that the higher values of workpiece surface roughness (Ra) have smaller values of the average capacitor charge cycle. For example, if roughness is 1.959, the average capacitor cycle length is 59 time intervals (1 time interval = 250 ms), which is $59 \times 250\text{ms} = 14750\text{ ms} = 14.759\text{ s}$; meanwhile, if roughness is more than 4, then cycle is very small, averaging about 1.750 s. The relation between the decrease in average capacitor charging cycle time and the increase in surface roughness is provided in Figure 4.16.

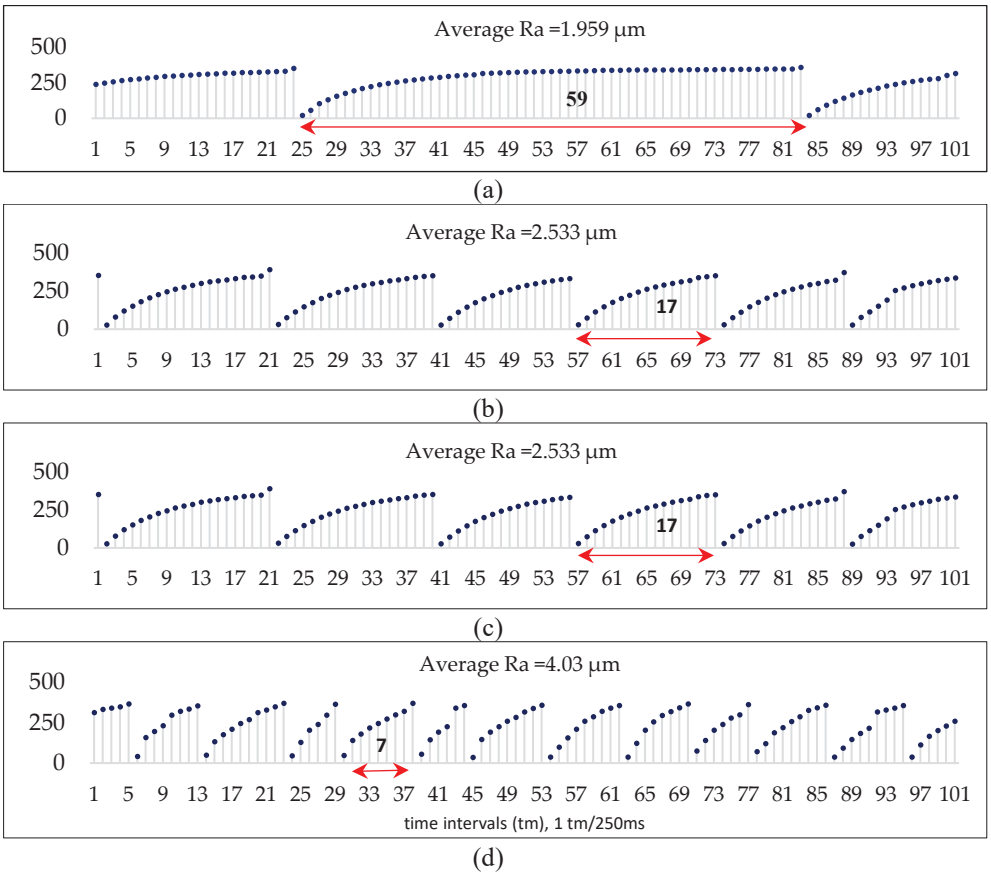

Fig. 4.16. Capacitor charge cycle duration dependence on the surface roughness of the workpiece: (a) 14.759 seconds vs. Ra = 1.959 μm; (b) 4.25 seconds vs. Ra = 2.533 μm; (c) 3.25 seconds vs. Ra = 3.138 μm; (d) 1.75 seconds vs. Ra = 4.03 μm

It can be seen from the obtained results that there is a negative correlation ($r = -0.743$) between capacitor charging cycle time and workpiece surface roughness, which is caused due to the milling tool cutting edge wear.

There, the capacitor charge level during the measurement instance was expressed in integers, where one unit is equal to 0.0015 volts, and the MCU was set to discharge the capacitor, when it reached 350 integer value, that is when its charge level is equal to 0.5 volts. During the milling operation, once the capacitor voltage charge from the piezoelectric transducer reaches or exceeds the set threshold value, the capacitor is discharged, and the cycle repeats itself.

For prediction task, ten features have been included, and just from the obtained correlation coefficients (see Table 4.11.), it can be seen the most informative features are *ACorr*, *InterQ*, Energy, *BigV* and $Signal_{jump}$. The most irrelevant feature ($r = 0.574$) is the standard deviation of the capacitor charge level.

Table 4.11. Pearson's correlation coefficient values

	Avg	**Var**	**Sd**	**ACorr**	**M_4Avg**	**InterQ**	**Energy**	**BigV**	**Signal$_{mp}$**	**Avg_cycle**
Roughness	-0.739	0.641	0.574	-0.817	-0.767	0.825	0.812	0.811	0.889	-0.743

All modeling experiments have been carried out using Python programming language in Jupyter notebook in Google Colab environment. The fit of the SVR model was evaluated by calculating the coefficient of determination and prediction error.

R^2 (coefficient of determination) is commonly used to evaluate the model performance. R^2 is a regression score, which is a statistical measure of how close the data are to the fitted regression line. In regression, it is the measure of how well the regression predictions approximate the real data. The R^2 of 1 indicates that the regression predictions perfectly fit the data.

$$R^2 = \frac{SSR}{SST} = \frac{\sum_{i=1}^{m}(y_i - \hat{y}_i)^2}{\sum_{i=1}^{m}(y_i - \bar{y})^2}, \tag{4.8}$$

where SSR is the sum of squares of residuals, SST – total sum of squares, y_i – actual value, $\hat{y}_i$ – predicted value and $\bar{y}$ mean value.

From the provided results (Fig. 4.17.), it can be seen that R^2 value for RBF-SVR model varies from 0.930 to 0.975, depending on the number of kernels varying from 1 to 4. These results indicate that the RBF-SVR model explains all the variability of the response data. More R^2 scoring variations can be observed in the Polynomial SVR model, i.e., from 0.838 to 0.911. The regression score for the Linear SVR model is more or less stable at around 0.77.

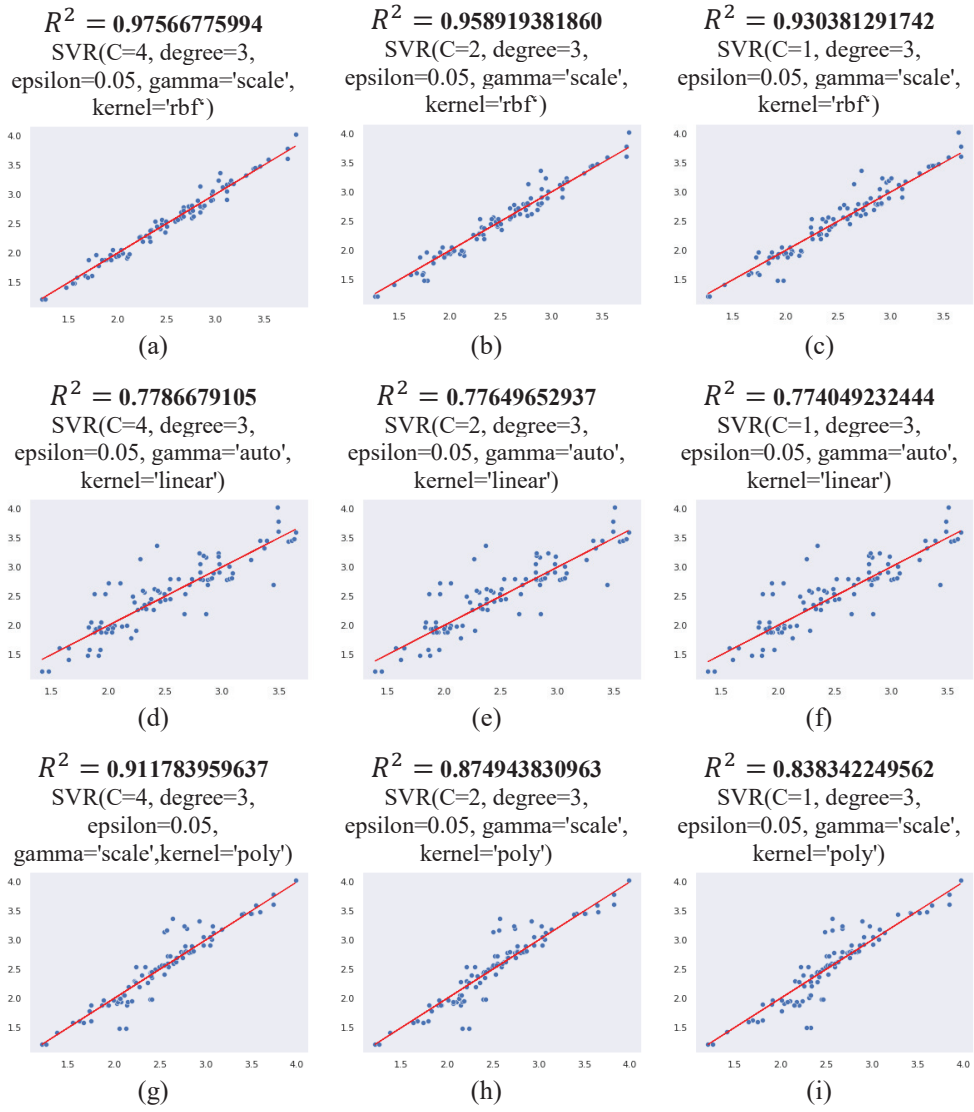

Fig. 4.17. Coefficient of determination R^2 value for RBF-SVM model, depending on the number and type of kernels: (a) – 4 rbf kernels, (b) – 2 rbf kernels, (c) – 1 rbf kernel, (d) – 4 linear kernels, (e) – 2 linear kernels, (f) – 1 linear kernel, (g) – 4 polynomial kernels, (h) – 2 polynomial kernels, (i) – 1 polynomial kernel

Three error measures for time-series prediction are calculated: Root mean squared error (RMSE); Mean absolute deviation (MAD) and Mean absolute percentage error (MAPE). In the conducted experiments, MAPE is calculated to evaluate the prediction accuracy of the SVR models.

MAPE is a relative error measure that uses relative errors in order to compare the predicted accuracy between time-series models. The formula for calculating the MAPE is provided below:

$$E_M = \frac{1}{n}\sum_{i=1}^{n}\left|\frac{y_i - \hat{y}_i}{y_i}\right| \cdot 100, \tag{4.9}$$

where n is number of time point, y_i – the actual value at a given time period i, $\hat{y}_i$ – the predicted value.

For the model testing, the author of the dissertation used the data (capacitor's charge level values in time) from different 31 milling operations. The average MAPE value for SVM model predictions with radial basis function kernel and C=4, is equal to 2.420%. Using SVM with polynomial kernel and C=4, the obtained average MAPE value is equal to 5.431%, and the highest error is observed using linear kernel 8.608%. The predicted and real (actual) values of surface roughness during the testing are presented in the Figure 4.18.

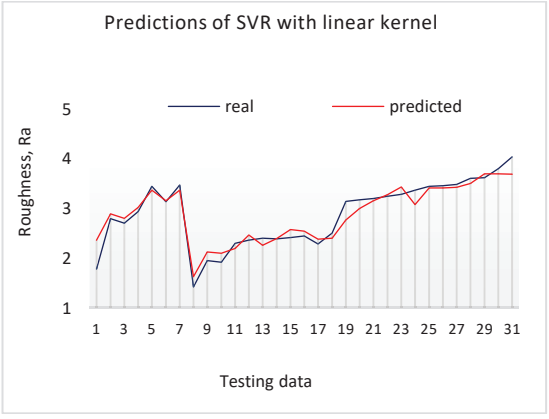

(a)

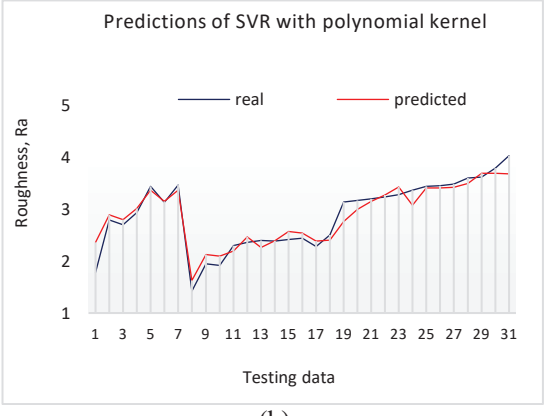

(b)

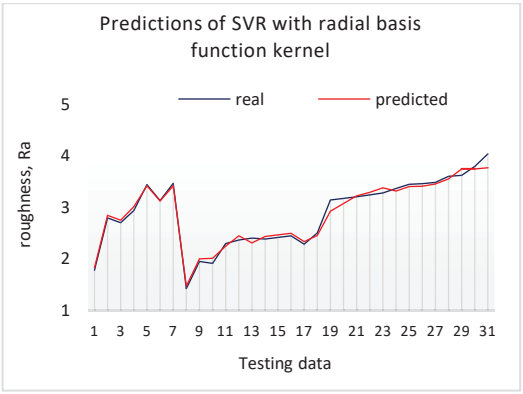

(c)

Fig. 4.18. Testing results of SVR model with different kernels: (a) – linear, (b) – polynomial, (c) – radial basis function

In this experimental study step, the SVM regression approach was employed to solve milling wear prediction problem by using surface roughness measurements as the key indicator of tool condition. The SVR with radial basis function kernel provides the smallest error of prediction (2.420% MAPE), when compared to polynomial (5.431% MAPE) and linear (8.608% MAPE) kernels. By exploring the computed empirical features, it has been observed that the time series features, such as autocorrelation, interquartile, absolute energy, entropy, are most relevant to the problem. However, according to the correlation coefficient, the most informative is the specially created feature $Signal_{jump}$ (r =0.889) for determining signal jumps due to 90% confidence level of the data points difference.

Conclusions of chapter 4

In this chapter, the vibrational response, energy harvesting properties and detection of the end mill tool wear conditions during the milling operation of the designed vibrational energy harvester device have been investigated experimentally by performing the following:

- A study of a cone shaped tool holder's vibrational response with Polytec PSV-500 3D laser doppler vibrometer showed that the introduction of helical slots on the tool holder's cone shaped surface lead to two times greater longitudinal vibrations generated at the contact surface with piezoelectric transducer.
- The performed impact test on a fully assembled device fixed inside the CNC milling centre resulted in the observed appearance of the beating phenomenon, where two close longitudinal and torsional vibrational modes interfere constructively and destructively, causing signal amplitude modulation in a regular pattern.
- The investigated energy harvesting properties of the proposed device during the milling operation showed that the use of the tool holder with uniformly formed helical slots on its cone shaped surface lead to up to four times higher charge,

generated by the piezoelectric transducer during the operation, as compared to the tool holder without helical slots.

- A study during the actual milling operation with artificially introduced cutting edge wear condition in the milling tool teeth showed that with an increased tool wear, the capacitor charge rate increases almost six times; thus, the proposed device can be used as a means to detect the degradation of the end mill tool during the real time machining operation.
- The measurement of the workpiece surface roughness after the milling operation with a tool holder with and without helical slots and new and worn out tool showed that when the new end mill tool with a tool holder implementing helical slots is used, the workpiece surface roughness is 18.6% higher (0.183 μm vs. 0.225 μm), but its distribution is 35% (0.325 μm vs. 0.241 μm) lower when compared to machining with a tool holder without helical slots. While using the worn out end mill tool together with a slotted tool holder, 3.5% (0.275 μm vs. 0.265 μm) improvement in workpiece surface roughness and 45.6% (0.325 μm vs. 0.177 μm) lower distribution are observed as compared to the machining with a tool holder without helical slots.
- The SVM regression machine learning approach was used for predicting the end mill tool wear based on the capacitor charge rate, measured by wireless sensor node. The surface roughness measurements were used as the key indicator of the tool condition showing good results with MAPE smallest error of 2.420%, employing radial basis function kernel.

After positive results were obtained during the experimental research, the patent "Wireless sensor to assess the quality of rotating tools" has been submitted for the developed device at The State Patent Bureau of the Republic of Lithuania [73].

CONCLUSIONS

1. The literature review revealed that, in relation to “Industry 4.0”, there exists a real need for wireless, self-powered smart sensors capable of performing real-time machining process monitoring tasks.
2. A universal piezoelectric energy harvester, employing rotating shank-type tools, has been designed. The results of the modelling using COMSOL Multiphysics CAE software package revealed the following:
   - The introduction of the L&T mode coupling effect enables the conversion of the torsional forces that are acting on the tool into longitudinal motion.
   - The most important influence on the frequency of the torsional mode is the parameter of the depth of the slots, which, when increased from 1 mm to 6 mm, reduces the resonant frequency by 16.5%, while the other parameters only have a slight/marginal effect.
   - A tool holder with helical slots experiences more than 2 times higher surface displacement in the longitudinal direction than a tool holder without slots.
   - The voltage and the power output from the piezoelectric transducer are respectively 2 and 4.5 times higher when embedded inside the tool holder with helical slots.
3. The piezoelectric energy harvester has been implemented to act as a sensor and as a power supply source, allowing to detect changes in the tool condition, such as its gradual wear. The performed experimental results have shown that:
   - During the impact test, the tool experiences a beating phenomenon, which is manifested by an amplitude-modulated response in the form of a combination of two vibration signals (L&T) with slightly different frequencies.
   - A tool holder with uniformly distributed helical slots is able to generate up to 4 times more voltage during the milling operation when compared to one without slots, expressed as a capacitor charging rate.
   - The capacitor charging rate increases with increasing process parameters of both tool holders equally.
4. The energy harvesting measurements during the milling operation have shown that the proposed sensor architecture enables the detection of the tool wear condition, which is expressed as a change in the capacitor charge rate, supplied by the piezoelectric transducer, as the tool deforms.
   - A milling operation with a new and a worn out end mill showed that the worn out tool leads to up to 4 times faster capacitor charging as compared to the new tool. Thus, the changes in the capacitor charge and discharge frequency can help to determine the lifetime of the rotating shank-type tool.
   - The changes in the frequency of the capacitor pulses that are sent wirelessly allow the condition of the rotating shank-type tool to be monitored.
   - The use of a tool holder with helical slots results in a lower impact on the surface roughness of the workpiece, as the tool becomes worn out (3.5%

difference) and provides a smaller spread of the measured surface roughness values for the workpiece (45.6%).

- The SVM radial basis function achieved a minimum prediction error of 2.420% for the end mill tool wear in terms of change in the workpiece surface roughness.

The developed universal sensor system has been patented at The State Patent Bureau of the Republic of Lithuania.

REFERENCES

1. Shrouf, F., Ordieres, J., & Miragliotta, G. (2014). Smart factories in industry 4.0: A review of the concept and of energy management approached in production based on the Internet of Things paradigm. In *2014 International Conference on Industrial Engineering and Engineering Management, 9-12 December, Selangor, Malaysia,* (pp. 667-701). IEEE.
2. Heiner, L., Fettke, P., Kemper, H.G., Feld, T., & Hoffmann M. (2014). Industry 4.0. Information Systems and Engineering. *Business & Information Systems Engineering*, 6 (4), 239-424. doi: 10.1007/s12599-014-0334-4
3. Zhong, R.Y., Xu, X., Klitz, E., & Newman S.T. (2017). Intelligent manufacturing in the context of Industry 4.0: A review. *Engineering*, 3 (5), 616-630. doi: 10.1016/J.ENG.2017.05.015
4. Anitha, V., & Deepaknath T. (2014). Wireless requirements and challenges in Industry 4.0. In *2014 International Conference on Contemporary Computing and Informatics (IC3I), 27-29 November, Mysore, India,* (pp. 634-368). IEEE.
5. Qin, J., Liu, Y., & Grosvenor, R. (2016). A categorical framework of manufacturing in industry 4.0 and beyond. *Procedia CIRP*, 52, 173-178. doi: 10.1016/j.procir.2016.08.005
6. Dominic, G., Schmitt, M., Loskyll, M., & Zuhkle, D. (2014). In *12th IEEE International Conference on Industrial Informatics (INDIN), 27-30 July, Proto Alegre, Brazil,* (pp. 289-294). IEEE.
7. Xun, X. (2012). From cloud computing to cloud manufacturing. Robotics and Computer Integrated Manufacturing. *Robotics and Computer Integrated Manufacturing,* 28 (1), 75-86. doi: 10.1016/j.rcim.2011.07.002
8. Park, H.S., & Tran, N.H. (2015). Development of a cloud based smart manufacturing system. Journal of Advanced Mechanical Design. *Systems and Manufacturing*, 9 (5). doi: 10.1299/jamdsm.2015jamdsm0030
9. Lee, J., Lapira, E., Bagheri, B., & Hung, K. (2013). Recent advances and trends in predictive manufacturing systems in big data environment. *Manufacturing Letters*, 1 (1), 38-41. doi: 10.1016/j.mfglet.2013.09.005
10. Lei, R., Lin, Z., Lihui, W., Fei, T., & Xudong, C. (2014). . Cloud manufacturing: key characteristics and applications. *International Joural of Computer Integrated Manufacturing*, 30 (6), 501-515. doi: 10.1080/0951192X.2014.902105
11. Kang, H.S., Lee J.Y., Choi, S., Kim, H., Park, J.H., Kim, B.H., & Noh, S.D. (2016). Smart manufacturing: Past research, present findings and future directions. . *International Journal of Precision Engineering and Manufacturing-Green Technology*, 3, 111-128. doi: 10.1007/2Fs40684-016-0015-5
12. Zhang, Y., Ren, S., Liu, Y., & Si, S. (2017). A big data analytics architecture for cleaner manufacturing and maintenance of complex products. *Journal of Cleaner Production,* 142 (2), 626-641. doi: 10.1016/j.jclepro.2016.07.123
13. Babiceanu, R.F., & Seker, R. (2016). Big data and virtualization for manufacturing cyber-physical systems: a survey of current status and future outlook. *Computer in Industry*, 81, 128-137. doi: 10.1016/j.compind.2016.02.004
14. Mahonraj, T., Shankar, S., Rajsekar, R., Sakthivel, N.R., & Pramanik, A. (2020). Tool condition monitoring techniques in milling process – a review. *Journal of Material Research and Technology*, 9 (1), 1032-1042. doi: 10.1016/j.jmrt.2019.10.031

15. Zhang, X., Lu, X., Wang, S., Wang, W., & Li, W.D. (2018). A multi-sensor based online tool condition monitoring system for milling process. *Procedia CIRP*, 72, 1136-1141. doi: 10.1016/j.procir.2018.03.092
16. Rizal, M., Ghani, J.A., Nuawi, Z., & Haron, C.H.C. (2014). Research article a review of sensor system and application in milling process for tool condition monitoring. *Research Journal of Applied Sciences. Engineering and Technology*, 7 (10), 2083-2087. doi: 10.19026/rjaset.7.502
17. Babitsky, V.I., Kalashnikov, A.N., & Molodtsov, F.V. (2004). Autoresonant control of ultrasonically assisted cutting. *Mechatronics*, 14 (1), 91-114. doi: 10.1016/S0957-4158(03)00014-X
18. Altinas Y., & Aslan, D. (2017). Integration of virtual and on-line machining process control monitoring. *CIRP Annals*, 66 (1), 349-352. doi: 10.1016/j.cirp.2017.04.047
19. Zhu, K., & Zhang, Y. (2018). A cyber physical production system framework of smart CNC machining monitoring system. *IEEE/ASME Transactions on Mechatronics*, 23 (6), 2579-2586. doi: 10.1109/TMECH.2018.2834622
20. Manu, K.S.A., Adam, N., Taparelo, C., Avatollahi, G., & Heinzelmann, W. (2018). Energy-Harvesting Wireless Sensor Networks (EH-WSNs): A Review. *ACM Transactions on Sensor Networks*, 14 (2), 1-50. doi: 10.1145/3183338
21. Shaikh, F.K., & Zeadally, S. (2016). Energy-harvesting in wireless sensor networks: A comprehensive review. *ACM Transactions on Sensor Networks*, 55, 1041-1054. doi: 10.1016/j.rser.2015.11.010
22. Babayo, A.A., Anjsi, M.H., & Ali, I. (2017). A review on energy management schemes in energy harvesting wireless sensor networks. *Renewable and Sustainable Energy Review*, 76, 1176-1184. doi: 10.1016/j.rser.2017.03.124
23. Yadav, S., & Yadav R.S. (2016). A review on energy efficient protocols in wireless sensor networks. *Wireless Networks*, 22, 335-350. doi: 10.1007/s11276-015-1025-x
24. Aznoli, F., & Navimipour, N.J. (2017). Deployment strategies in the wireless sensor networks: systematic literature review, classification and current trends. *Wireless personal communications*, 95, 819-846. doi: 10.1007/s11277-016-3800-0
25. Cansiz, M., Altinel, D., & Kurt, G.K. (2019). Efficiency in RF energy harvesting systems: A comprehensive review. *Energy*, 174, 292-309. doi: 10.1016/j.energy.2019.02.100
26. Kishore, R.A., & Priya S. (2018). A review on low-Grade Thermal Energy Harvesting: Materials, Methods and Devices. *Materials*, 11 (8), 1433. doi: 10.3390/ma11081433
27. Lau, D., Song, N., Hall, C., Jiang, Y., Lim, S., Perez-Wurfl, I., Ouyang, Z., & Lennon, A. (2019). Hybrid solar energy harvesting and storage devices: The promises and challenges. *Materials today Energy*, 13, 22-44. doi: 10.1016/j.mtener.2019.04.003
28. Vullers, R.J.M., Schaijk, R.V., Visser, H.J., Penders, J., & Hoof, C.V. (2013) Autonomous wireless sensor networks. *International Journal of Distributed Sensor Networks*, 2 (2), 29-38. doi: 10.1109/MSSC.2010.936667
29. Mohanty, A., Parida, S., Behera, R., & Roy, R. (2019). Vibration energy harvesting: A review. *Journal of Advanced Dielectrics*, 9 (4). doi: 10.1142/S2010135X19300019
30. Siang, J., Lim, M.H., & Leong, M.S. (2018). Review of vibration-based energy harvesting technology: Mechanism and architectural approach. *International Journal of Energy Research*, 42 (5), 1866-1893. doi: 10.1002/er.3986
31. Wie, C., & Jing, X. (2017). A comprehensive review on vibration energy harvesting: Modelling and realization. *Renewable and Sustainable Energy Reviews*, 74, 1-18. doi: 10.1016/j.rser.2017.01.073

32. Li, H., Tian, C., & Deng, Z.D. (2014). Energy harvesting from low frequency applications using piezoelectric materials. *Applied physics reviews*, 1 (4), 1-20. doi: 10.1063/1.4900845
33. Moheimani, S.R., & Fleming, A.J. (2006). *Piezoelectric transducers for vibration control and damping*. London: Springer-Verlag.
34. Kim, H.S., Kim, J.H., & Kim, J. (2011). A review of piezoelectric energy harvesting based on vibration. *International Journal of Precision Engineering and Manufacturing*, 12, 1129-1141. doi: 10.1007/s12541-011-0151-3
35. Sarker, M.R., Julai, S., Sabri, M.F.M., Said, S.M., Islam, Md.M., & Tahir, M. (2019). Review of piezoelectric energy harvesting system and application of optimization techniques to enhance the performance of the harvesting system. *Sensors and Actuators, A: Physical*, 300 (1), 111634. doi: 10.1016/j.sna.2019.111634
36. Liu, H., Zhong, J., Lee, C., Lee, S.W., & Lin, L. (2018). A comprehensive review on piezoelectric energy harvesting technology: Materials, mechanisms, and applications. *Applied Physics Reviews*, 5 (4). doi: 10.1063/1.5074184
37. Chen, T., Lius, S., Liu, W., & Wu, C. (2017). Study on longitudinal-torsional ultrasonic vibration system with diagonal slits. *Advances in Mechanical Engineering*, 9 (7), 1-10. doi: 10.1177/1687814017706341
38. Shuyu, L. (1997). Sandwiched Piezoelectric Transducers of Longitudinal-Torsional Compound Vibrational Modes. *IEEE Transactions on Ultrasonics, Ferroelectrics, and Frequency Control*, 44 (6), 1189-1197. doi: 10.1109/58.656619
39. Zheng, J. (2012). Realization of longitudinal-torsional complex vibration by conical compound horn under single acoustic excitation. *Key engineering materials*, 522, 251-255. doi: 10.4028/www.scientific.net/KEM.522.251
40. Harkness, P., Lucas, M., & Cardoni, A. (2012). Couplind and degenerating modes in longitudinal-torsional step horns. *Ultrasonics*, 52 (8), 980-988. doi: 10.1016/j.ultras.2012.05.002
41. Chuanshoa, L., Haoqiong, W., & Amoei, L. (2013). Design of longitudinal-torsional vibration stepped horn with multiple diagonal slits. *Applied Mechanics and Materials*, 312, 51-54. doi: 10.4028/www.scientific.net/AMM.312.51
42. Liu, S., Shan, X., Cao, W., Yang, Y, & Xia, T. (2017). A longitudinal-torsional composite ultrasonic vibrator with thread grooves. *Ceramics International*, 43 (1), 214-220. doi: 10.1016/j.ceramint.2017.05.305
43. Liu, S., Shan, X., Guo, K., & Xia, T. (2016). Design and fabrication of a skew-typed longitudinal-torsional composite ultrasonic vibrator for titanium wire drawing. *IEEE Access*, 4, 6749-6756. doi: 10.1109/ACCESS.2016.2614516
44. Pang, Y., Feng, P., Zhang, J., Ma, Y., & Zhang, Q. (2020). Frequency coupling design of ultrasonic horn with spiral slots and performance analysis of longitudinal-torsional machining characteristics. *International Journal of Advanced Manufacturing Technology*, 106, 4093-4103. doi: 10.1007/s00170-019-04898-2
45. Ostasevicius, V., Jurenas, V., Markevicius, V., Gaidys, R., Zilys, M., Cepenas, M., & Kizauskiene, L. (2016) Self-powering wireless devices for cloud manufacturing applications. *International Journal of Advanced Manufacturing Technology*, 83, 1937-1950. doi: 10.1007/s00170-015-7617-x
46. Ostasevicius, V., Markevicius, V., Jurenas, V., Zilys, M., Cepenas, M., Kizauskiene, L., & Gyliene, V. (2015). Cutting tool vibration energy harvesting for wireless sensor applications. *Sensors and Actuatos, A: Physical*, 233, 310-318. doi: 10.1016/j.sna.2015.07.014

47. Chung, T.K., Yah, P.C., Lee, H., Lin, C.M., Tseng, C.Y., Lo, W.T., Wang, C.M., Wang, W.C., Tu, C.J., Tasi, P.Y., & Chang, J.W. (2016). An attachable Electromagnetic Energy Harvester Driven Wireless Sensing System Demonstrating Milling Process and Cutter Wear/Breakage Condition Monitoring. *Sensor*, 16 (3), 1-20). doi: 10.3390/s16030269
48. Ostasevicius, V., Jurenas, V., Augustinaitis, V., Gaidys, R., Cesnavicius, R., Kizauskiene, L., & Dundulis, R. (2017). Monitoring the condition of the cutting tool using self-powering wireless sensor technologies. *International Journal of Advanced Manufacturing Technology*, 88, 2803-2817. doi: 10.1007/s00170-016-8939-z
49. Saffar, R.J., Razfar, M.R., Zarei, O., & Ghassemiah, E. (2008). Simulation of three-dimensional cutting force and tool deflection in the end milling operation based on finite element method. *Simulation Modelling practice and Theory*, 16 (10), 1677-1688. doi: 10.1016/j.simpat.2008.08.010
50. Thanongsak, T.,& Ozel, T. (2015). Finite Element Process Simulation of Micro-end Milling Ti-6Al-4V Titanium Alloy: Experimental Validation on Chip Flow and Tool Wear. *Journal of Materials Processing Technology*, 221, 128-145. doi: 10.1016/j.jmatprotec.2015.02.019
51. Hu, F., & Li, D. (2012). Modelling and simulation of milling forces using an arbitrary Langrangian-Eulerian Finite Element Method and support vector regression. *Journal of Optimization Theory and Applications*, 153, 461-484. 10.1007/s10957-011-9927-y
52. Li, H., & Shin, C.Y. (2006). A comprehensive dynamic end milling simulation model. *Journal of Manufacturing Science and Engineering*, 128 (1), 86-95. doi: 10.1115/1.2035694
53. Cao, Y., Liu, X., Fu, L., & Bai, Y. (2016). Thermo-mechanical coupled simulation analysis of solid end mill on milling process. In *Proceedings of the 4th International Conference on Information Systems and Computing Technology, 22-23 December 2016, Shanghai, China.*
54. Haglund, A.J., Kishawy, H.A., & Rogers, R.J. (2008). An exploration of friction models for the chip-tool interface using Arbitrary Lagrangian-Eulerian finite element model. *Wear*, 265 (3-4), 452-460. doi: 10.1016/j.wear.2007.11.025
55. Gao, Y., Ko, J., & Lee, H. (2018). Eulerian Finite Element Modelling of End Milling. *Materials*, 12 (13). doi: 10.3390/ma12132070
56. Choi, Y., Park, L., Hong, Y., Kim, K., Lee, S., & Choi, H. (2013). Effect of ultrasonic vibration in grinding; horn design and experiment. *International Journal of Precision Engineering and Manufacturing*, 14, 1873-1879. doi: 10.1007/s12541-013-0253-1
57. Nad, M. (2010). Ultrasonic horn design for ultrasonic machining technologies. Applied and Computational Mechanics. *Applied and Computational Mechanics*, 4 (1), 79-88.
58. Pang, Y., Feng, P., Zhang, P., Ma, Y., & Zhang, Q. (2020). Frequency coupling design of ultrasonic horn with spiral slots and performance analysis of longitudinal-torsional machining characteristics. *International Journal of Advanced Manufacturing Technology*, 106, 4093-4103. doi: 10.1007/s00170-019-04898-2
59. Zhao, B., Bie, W., Wang, X., Chen, F., & Chang, B. (2019). Design and experimental investigation on longitudinal-torsional composite horn considering the incident angle of ultrasonic wave. *International Journal of Advanced Manufacturing Technology*, 105, 325-341. doi: 10.1007/s00170-019-04220-0

60. Zhang, C., Zhao, B., & Niu, Y. (2018). Design, simulation and adjustment of the longitudinal-torsional composite integrated ultrasonic variable amplitude system. *Advances in Mechanical Engineering*, 10 (10). doi: 10.1177/2F1687814018804739
61. Xuan, Y., Wang, A., & Zhang, N. (2019). Design and simulation of piezoelectric ultrasonic transducer with sandwich composite horn. In *2018 4th International Conference on Mechanical Engineering and Automation Science (ICMEAS 2018), 12-14 October 2018, Beijing, China.* IOP Conference Series: Materials Science and Engineering.
62. Rani, M.R., & Rudramoorthy, R. (2019). . Computational modeling and experimental studies of the dynamic performance of ultrasonic horn profiles used in plastic welding. *Ultrasonics*, 53 (3), 763-772. doi: 10.1016/j.ultras.2012.11.003
63. Shu, K., & Chen, J. (2015). The design of acoustic horns for ultrasonic aided tube doubled side flange making. *International Journal of Mechanical, Aerospace, Industrial, Mechatronic and Manufacturing Engineering*, 9 (5), 904-907.
64. Choi, K., Park, Y., Hong, Y., Kim, K., Lee, S., & Choi, H. (2012). Design of ultrasonic horn for grinding using finite element method. *Advanced Materials Research*, 565, 135-141. doi: 10.4028/www.scientific.net/AMR.565.135
65. Fakhzan, M.N., & Muthalif, A.G.A. (2013). Harvesting vibration energy using piezoelectric material: Modeling, simulation and experimental verifications. *Mechatronics*, 23 (1), 61-66. doi: 10.1016/j.mechatronics.2012.10.009
66. Fakhzan, M.N., & Muthalif, A.G.A. (2011). Vibration Based Energy Harvesting using Piezoelectric Material. In *2011 4th International Conference on mechatronics (ICOM), 17-19 May 2011, Kuala Lumpur, Malaysia.* IEEE.
67. Taylor, P., Ramesh, R., & Ebenezer, D. (2011). Analysis of axially polarized piezoelectric ceramic rings. *Ferroelectrics*, 323 (1), 17-23. doi: 10.1080/00150190500308454
68. Elvin, A., & Elvin, N. (2009). A general equivalent circuit model for piezoelectric generators. *Journal of Intelligent Material Systems and Structures*, 20 (1), 3-9. doi: 10.1177/2F1045389X08089957
69. Sivakumar, N., Kanagasabapthy, H., & Srinath, H. (2018). Analysis of perforated piezoelectric sandwich smart structure cantilever beam using COMSOL. *Materials Today: Proceedings*, 5 (5), 12025-12034. doi: 10.1016/j.matpr.2018.02.177
70. Niu, J., Ding, Y., Geng, Z., Zhu, L., & Ding, H. (2018). Patterns of Regenerative Milling Chatter under Joint Influences of Cutting Parameters, Tool Geometries and Runout. *Journal of Manufacturing Science and Engineering*, 140 (12). doi: 10.1115/1.4041250
71. Bayly, P., Metzler, S., Schaut, A., Young, K. (2001). Theory of torsional chatter in twist drills: model, stability analysis and composition to test. *Journal of Manufacturing Science and Engineering*, 123 (4), 526-561. doi: 10.1115/1.1381399
72. Barandas, M., Folgado, D., Fernandes, L., Santos, S., Abreu, M., Bota, P., Schultz, T., & Gamboa, H. (2020). TSFEL: Time Series Feature Extraction Library. *SoftwareX*, 11. doi: 10.1016/j.softx.2020.100456
73. Ostasevicius, V., Jurenas, V., Karpavicius, P., Bubulis, A., Eidukynas, D., Cesnavicius, R., & Cepenas, M. Wireless sensor to assess the quality of rotating tools. Patent Application number LT2009:553.

LIST OF AUTHOR'S PUBLICATIONS

Indexed in the Web of Science with Impact Factor

1. Ostasevicius, Vytautas; **Karpavicius, Paulius;** Paulauskaite-Taraseviciene, Agne; Jurenas, Vytautas; Mystkowski, Arkadiusz; Cesnavicius, Ramunas; Kizauskiene, Laura. A machine learning approach for cutter wear monitoring by self-powereing wireless sensor nodes // Sensors. Basel : MDPI. ISSN 1424-8220. 2021, vol. 21, iss. 9, art. no. 3137, p. 1-26. DOI: 10.3390/s21093137. [Science Citation Index Expanded (Web of Science); Scopus; DOAJ] [IF: 3,275; AIF: 3,581; IF/AIF: 0,914; Q1 (2019, InCites JCR SCIE)] [M.kr.: T 007, N009, T 009]. [Contribution: 0,142]
2. Ostasevicius, Vytautas; **Karpavicius, Paulius**; Jurenas, Vytautas; Cepenas, Mindaugas; Cesnavicius, Ramunas; Eidukynas, Darius. Development of universal wireless sensor node for tool condition monitoring in milling // International journal of advanced manufacturing technology. London : Springer. ISSN 0268-3768. eISSN 1433-3015. 2020, vol. 110, iss. 3-4, p. 1015-1025. DOI: 10.1007/s00170-020-05812-x. [Science Citation Index Expanded (Web of Science); Scopus] [IF: 2,633; AIF: 3,749; IF/AIF: 0,702; Q2 (2019, InCites JCR SCIE)] [M.kr.: T 009]. [Contribution: 0,166]
3. Ostaševičius, Vytautas; Jūrėnas, Vytautas; **Karpavičius, Paulius**; Baskutienė, Jolanta. Self-powered wireless sensor system application for cutting process control // Mechanika. Kaunas : KTU. ISSN 1392-1207. eISSN 2029-6983. 2017, vol. 23, no. 3, p. 456-461. DOI: 10.5755/j01.mech.23.3.17957. [Science Citation Index Expanded (Web of Science); Scopus; Academic Search Complete] [IF: 0,529; AIF: 2,663; IF/AIF: 0,198; Q4 (2017, InCites JCR SCIE)] [M.kr.: T 009]. [Contribution: 0,250].
4. Ostaševičius, Vytautas; **Karpavičius, Paulius**; Janušas, Giedrius; Balevičius, Gytautas. Design and implementation of uniform light guide based, force and deflection measurement device // Mechanika. Kaunas : KTU. ISSN 1392-1207. eISSN 2029-6983. 2016, vol. 22, no. 4, p. 279-284. DOI: 10.5755/j01.mech.22.4.15414. [Science Citation Index Expanded (Web of Science); Scopus; Academic Search Complete] [IF: 0,382; AIF: 2,419; IF/AIF: 0,157; Q4 (2016, InCites JCR SCIE)] [M.kr.: T 009]. [Contribution: 0,250]

IEEE database

5. Ostasevicius, Vytautas; Mystkowski, Arkadiusz; **Karpavicius, Paulius**; Jurenas, Vytautas. Investigation of piezoelectric transducer application for vibrational energy harvesting in milling operation // Mechatronic Systems and Materials: IEEE proceedings of the 15th international conference – MSM 2020, Bialystok, Poland, 1-3 July, 2020, p. 30. [Contribution: 0.250]

In peer-reviewed conference proceedings

1. Ostasevicius, Vytautas; Jurenas, Vytautas; **Karpavicius, Paulius**. Feasibility investigation and design of a piezoelectric self-powered sensor for monitoring the tool condition during milling // Mechanika 2017: proceedings of the 22nd international scientific conference, May 2017, Kaunas University of Technology, Lithuania. [Contribution: 0.333]
2. Ostasevicius, Vytautas; Jurenas, Vytautas; Eidukynas, Darius; **Karpavicius, Paulius**. Reverse ultrasonic actuator for efficient machining // Mechanika 2018: proceedings of the 23rd international scientific conference, May 2018, Kaunas University of Technology, Lithuania. [Contribution: 0.250]

3. **Karpavicius, Paulius**; Ostasevicius, Vytautas; Jurenas, Vytautas; Eidukynas, Darius; Cepenas, Mindaugas; Cesnavicius, Ramunas. Development of real time wireless milling tool condition monitoring system // 9-th Junior Scientist Conference, March 2019, The Lithuanian Academy of Sciences. [Contribution: 0.200]
4. Ostasevicius, Vytautas; Jurenas, Vytautas; Eidukynas, Darius; **Karpavicius, Paulius**. Possibilities of milling process monitoring in cloud manufacturing applications // Mechanika 2019: proceedings of the 24th international scientific conference, May 2019, Kaunas University of Technology, Lithuania. [Contribution: 0.250]
5. Ostasevicius, Vytautas; Mystkowski, Arkadiusz; **Karpavicius, Paulius**; Jurenas, Vytautas. Investigation of piezoelectric transducer application for vibrational energy harvesting in milling operation // Mechatronic Systems and Materials: 15th international conference – MSM 2020, Bialystok, Poland, 1-3 July, 2020. [Contribution: 0.250]
6. Ostasevicius, Vytautas; Jurenas, Vytautas; **Karpavicius, Paulius**. Research and development of the universal wireless sensor for cutting tool condition monitoring // Mechanika 2021: proceedings of the 25th international scientific conference, May 2021, Kaunas University of Technology, Lithuania. [Contribution: 0.333]

SL344. 2021-07-08, 18,25 eidyb. apsk. l. Tiražas 14 egz. Užsakymas 180.
Išleido Kauno technologijos universitetas, K. Donelaičio g. 73, 44249 Kaunas
Spausdino leidyklos „Technologija“ spaustuvė, Studentų g. 54, 51424 Kaunas